Microplastic Entrainment in Ice Formations and Their Electrochemical Removal from Water

Zhikun Chen

A Thesis
In the Department
of
Building, Civil and Environmental Engineering

Presented in Partial Fulfillment of the Requirements
for the Degree of
Doctor of Philosophy (Civil Engineering) at
Concordia University
Montreal, Quebec, Canada

October 2024

CONCORDIA UNIVERSITY
SCHOOL OF GRADUATE STUDIES

This is to certify that the thesis prepared

By: Zhikun Chen

Entitled:

and submitted in partial fulfillment of the requirements for the degree of

DOCTOR OF PHILOSOPHY (Civil Engineering)

Complies with the regulations of the University and meets the accepted standards with respect to originality and quality.

Signed by the final examining committee:

______________________________________Chair
Dr. Michel Trudeau
______________________________________External Examiner
Dr. Hui Peng
______________________________________Examiner
Dr. Zhi Chen
______________________________________Examiner
Dr. Fuzhan Nasiri
______________________________________Examiner
Dr. Xianming Zhang
______________________________________Co-Supervisor
Dr. Maria Elektorowicz
______________________________________Supervisor
Dr. Chunjiang An

Approved by ______________________________________
Dr. Po-Han Chen, Graduate Program Director

Month/day/year ______________________________________
Dr. Mourad Debbabi, Dean
Gina Cody School of Engineering and Computer Science

Abstract

Microplastic Entrainment in Ice Formations and Their Electrochemical Removal from Water

Zhikun Chen, Ph.D.

Concordia University, 2024

Sea ice can act as a temporary sink for microplastics (MPs), which also function as secondary sources and transport mediums for MPs. While field investigations have confirmed the widespread presence of MPs in ice, knowledge about their environmental fate in cold regions remains limited. This study investigates the entrainment of MPs during ice formation processes and how freezing alters their behavior in water. Additionally, an electrochemical removal technology was developed to separate MPs from water, addressing the issue at its source.

The study first explored the effects of various MP properties and environmental conditions on the entrainment and enrichment of MPs in ice under different turbulence scenarios. Results revealed that high turbulence in freshwater significantly increased the entrainment of hydrophobic MPs in ice, due to the combined influence of frazil ice and air bubbles. The hydrophobic nature of MPs led them to concentrate at the water/air or water/ice interface. However, in saline water, high turbulence inhibited the entrainment of all MP types, as loose ice structures allowed for the exchange of MPs between ice and water, resulting in rapid expulsion. In calm saline conditions, MP enrichment factors were higher compared to calm freshwater.

Next, the study examined the interactions between aquatic organic matter and MPs, focusing on how these interactions influence MP behavior during ice formation. A 28-day experiment evaluated the effects of dissolved organic matter on MP properties under UV and dark conditions. Findings revealed that aquatic organic matter adhered to MPs, with varying impacts on different MP types. Surface damage caused by physical abrasion and UV radiation improved the entrapment of MPs in ice, highlighting the critical role of MP properties in their environmental behavior.

As temperatures fluctuate, MPs stored in ice can be released, and freezing conditions can alter their properties, affecting their fate in the environment. Freezing in freshwater led to MP aggregation through physical compression, increasing particle size upon release. This aggregation enhanced buoyancy, accelerating the settling or rising velocity of MPs in water. In contrast, the presence of salt mitigated freezing effects due to the formation of a brine network within the ice structure, reducing pressure on entrapped MPs.

To address the issue of MP release into the environment via wastewater, this study developed an electrosorption (ES) technology using graphite felt electrodes to remove MPs from water. Preliminary experiments investigated the effects of flow rate, applied voltage, and electrolyte concentration on MP removal efficiency. Under optimal conditions, 96.9% of MPs were removed after 150 minutes. By analyzing the factors influencing MP removal efficiency and the underlying mechanisms using DLVO theory, this study provides a foundation for future advancements in ES technology for MP removal, with potential for real-world applications in complex environments.

.

Acknowledgments

I would like to express my sincere gratitude to everyone who supported and guided me throughout my PhD journey. First, I am deeply grateful to my supervisor, Dr. Chunjiang An. His support, feedback, and encouragement were invaluable to my research. I also thank my co-supervisor, Dr. Maria Elektorowicz. Her comments, advice, and support were vital in shaping this work. I would also like to thank my committee members: Dr. Michel Trudeau, Dr. Hui Peng, Dr. Zhi Chen, Dr. Fuzhan Nasiri, Dr. Xianming Zhang, Dr. Maria Elektorowicz, and Dr. Chunjiang An. Their comments and suggestions greatly improved my work.

I would like to acknowledge the financial support provided by the Gina Cody School of Engineering and Computer Science Graduate Scholarship, which is generously funded by a donation from Dr. Gina Cody. I would also like to express my gratitude to the Fonds de recherche du Québec for recognizing my research and awarding me the Relève Étoile Louis-Berlinguet Award.

My heartfelt thanks go to my colleagues and friends who accompanied me on my five-year Ph.D. journey. Your camaraderie, support, and shared experiences have been invaluable. I would also like to thank our dedicated lab techs: Guan Hong, Mazen Samara, Luc Demers, and Dmytro Kevorkov. Their support and help were invaluable.

Lastly, I deeply thank my family. Their support and understanding were unwavering throughout this long, transformative journey. To my parents, your endless encouragement and profound understanding have been the quiet strength behind every step I've taken. Without your love, this achievement would not have been possible. To my partner, Xuelin Tian, your faith in me has been my anchor in the storm. Your patience, especially in hard times, helped most. You have been my unwavering support during every high and low, and for that, I hold deep gratitude.

Table of Contents

List of Tables

List of Figures

List of Abbreviations

ANOVA	Analysis of variance
CFD	Computational fluid dynamics
CV	Cyclic voltammetry
DI	Deionized water
DLVO	Derjaguin, Landau, Verwey, and Overbeek
DOM	Dissolved organic matter
EDS	Energy dispersive X-ray spectroscopy
EIS	Electrochemical impedance spectroscopy
FWHM	Full width at half maximum
FTIR	Fourier transform infrared
GF	Graphite felt
HA	Humic acid sodium
LD	laser diffraction
PE	Polyethylene
PMMA	Polymethylmethacrylate
PSU	Practical salinity units
PTFE	Polytetrafluoroethylene
PU	Polyurethane
RDA	Redundancy analysis
NaCl	sodium chloride
SA	Sodium alginate

SE	Standard error
SEM	Scanning electron microscope
WCA	Water contact angle
XRD	X-ray diffraction

Chapter 1. Introduction

1.1. Background

Plastic pollution is a growing concern in terms of the threat it poses to ecosystems, organisms, and even public health (Amelia et al., 2021). With long-term weathering through physical abrasion, and chemical and biological degradation, microplastics (MPs) can be released from large pieces of plastic waste (Wang et al., 2021c; Wang et al., 2022b). In addition, MPs can be directly emitted from anthropogenic activities; these small polymer particles having seen intensive use in commercial and industrial products such as paints, cosmetics, and cleaning products (Weithmann et al., 2018; Yuan et al., 2022). The marine environment has been identified as an important sink for plastic waste. MPs are widely detected in the global ocean, even in some remote regions such as the Arctic Ocean (Kanhai et al., 2020). The fate and transport of MPs in the marine environment is a complex process and has attracted increasing attention from the research community in recent years. MPs are present in the various environmental media of the ocean, such as the intertidal zone, sediment, and seawater (Yang et al., 2022a). Understanding the mobility and exchange between these media can be highly challenging, though, since the environmental behaviour of MPs is subject to a range of factors such as their physical and chemical natures and the variability of natural features.

Sea ice can serve as a temporary sink for MPs, and thus it too can function as a secondary source of, and transport medium for, MPs. Recent studies have observed MP enrichment in sea ice, and have found MPs to be significantly more concentrated in sea ice than in open water (Kelly et al., 2020; Peeken et al., 2018). In another study, the contribution of atmospheric input to MPs in sea ice was found to be less than 1%, suggesting marine MPs are the main source of ice-trapped MPs

(Kim et al., 2021). Indeed, it has been estimated that the total mass of MPs accumulated in seasonal sea ice is comparable to that of the MP stock floating in global oceans (Kim et al., 2021).

The entrapment of MPs in water bodies has also been widely observed in freshwater ice formations within rivers and lakes (Liu et al., 2023). During the winter seasons in cold regions, the entrainment of MPs into ice can result in seasonal fluctuations in MP concentration within the water columns. A notable drop in MP abundance in winter has been documented during ice-cover periods, both in river and lake environments, owing to the enrichment of MPs within the ice matrix. Environmental sampling in Lake Ulansuhai, China, for instance, revealed that the MP abundance in ice-free periods was 4.5–11.3 times higher than during the ice-cover periods, and that the abundance in ice was 2.74–8.14 times higher than that in the underlying water (Liu et al., 2023). Similarly, sampling of an urban river in Beijing, China, showed that MP abundance was doubled after thawing of the ice (Zhang et al., 2022).

Some studies have hypothesized that ice algae might be responsible for transporting MPs to sea ice, given the high exchange of ice algae between sea ice and underlying water. In this regard, Hoffmann et al. (2020) found that while ice algae does not enhance MP enrichment in sea ice, the extracellular polymeric substances (EPS) produced by ice algae can affect the surface characteristics of MPs. Pradel et al. (2021b) investigated the distribution pattern of MPs and nanoplastics in ice and water, using a cold finger to simulate the sea ice formation. The results revealed that MPs can become trapped in ice more easily than nanoplastics, and that the process can be affected by EPS and salinity. Geilfus et al. (2019) conducted a microcosm experiment to determine MP distributions and effects on sea ice properties, observing that MP enrichment was occurring, and concluding that a high concentration of MPs can affect sea ice properties such as salinity and albedo.

These studies contributed to the understanding of the enrichment and entrainment of MPs in ice and explained some of the factors that influence this process. However, all these studies were implemented in calm water, whereas water convection and turbulence can be critical factors affecting the behavior of suspended particulate matter in water. Flowing water can enhance the suspension of particles; moreover, their hydrophobic nature causes some MPs to attach to the air bubbles or ice crystals that form in water under high turbulence (Smedsrud, 2001). These can be favorable conditions for the entrainment of MPs in ice. For instance, Kempama et al. (1989) demonstrated that the turbulent flow can be a crucial factor in the formation of 'dirty ice' caused by sediment entrainment.

The behavior of MPs is highly dependent on their physicochemical properties and surface characteristics, which can be significantly impacted by aging and the presence of organic matter on their surfaces. Aquatic dissolved organic matter (DOM) includes various functional groups that can provide diverse sites for the adsorption of environmental contaminants including MPs (Chen et al., 2023a; Chen et al., 2022b). Aquatic DOM can strongly interact with MPs, potentially altering their characteristics and mobility (Yang et al., 2022b). Moreover, aquatic DOM can also affect the aging of MPs. DOM like humic acid and fulvic acid can generate reactive oxygen species (ROS) during their photolysis to accelerate the photoaging of MPs (Qiu et al., 2022). Aquatic DOM can also act as the ROS scavengers and light-shielding effect to inhibit the photoaging of MPs. The role of aquatic DOM in the aging of MPs may depend mainly on the chemical structure of the plastic and its ability to adsorb DOM, which can either accelerate or inhibit the aging process (Cao et al., 2022). The aquatic DOM can also alter the surface properties of MPs such as zeta potentials and hydrophobicity by adsorbing on their surface (Chen et al., 2023a). The presence of large amounts of DOM in the natural environment can affect the behavior of MPs in cold regions, especially their entrapment in sea ice.

With changing temperatures, MPs stored in ice can be released back into the environment, while freezing conditions can alter the properties of MPs, ultimately affecting their fate in the environment. Freezing conditions can physically compress the MP particles to increase their particle size or cause them to integrate with other substances in the water (Alimi et al., 2021). In addition, it has been observed that freezing conditions can accelerate the degradation of MPs as a result of the enhanced generation of free radicals due to the freezing-induced aggregation and extrusion of MPs (Lv et al., 2023; Tian et al., 2022).

Recently, various technologies have been developed to reduce MPs at their sources by facilitating their removal from water. Electrosorption (ES) is an electrochemical method that removes ions or organic compounds from water by adsorbing them onto conductive electrodes using an external electric potential, without the need for additional chemicals. This technique has been widely used for deionizing water and removing heavy metal through capacitive deionization. In water, MPs are often stably dispersed as colloidal particles carrying surface charges, which create electrostatic repulsive forces that stabilize them and lead to prolonged suspension. Thus, these charged particles can theoretically be removed through ES. Research on the removal of colloidal particles using ES dates back to (Hall et al., 1987; Tobias et al., 1987), who used a flow-through ES cell with porous carbon electrodes to effectively remove carboxylated polystyrene and suspended aluminum nanoparticles. ES presents a promising technology for removing MPs, addressing the challenge of low removal efficiency for smaller MPs in traditional wastewater treatment facilities. It offers high removal efficiency, minimal chemical usage, and potential for electrode regeneration (Fdez-Sanromán et al., 2024).

1.2. Research Objectives

The study aims to thoroughly investigate the environmental behavior and fate of MPs in cold regions, considering the influence of polymer physicochemical properties and environmental conditions. Additionally, it seeks to develop an advanced electrochemical treatment technology for the removal of MPs from water. To achieve these goals, the following objectives are outlined:

- Investigate the impact of MP properties and environmental conditions on the entrainment and enrichment of MPs in ice.
- Examine the interaction between aquatic DOM and MPs, and the role of DOM in MP entrainment during ice formation.
- Assess the influence of freezing conditions on the environmental fate of MPs in aquatic environments.
- Evaluate the feasibility of using ES technology for MP removal from water.

1.3. Thesis Outline

This thesis comprises seven chapters, and a brief summary of each chapter is outlined as follows:

- Chapter 1 provides an overview of the research background, outlines the objectives, and presents the structure of the thesis.

- Chapter 2 offers a comprehensive literature review, summarizing recent studies on the sources of MPs, their entrainment in ice, and advancements in water treatment techniques for MP removal.
- Chapter 3 presents a laboratory batch test investigating the entrainment and enrichment of MPs with different physicochemical properties during ice formation under various environmental conditions. This chapter provides insights into how different factors influence MP behavior during ice formation.
- Chapter 4 examines the interaction between MPs and DOM under UV irradiation and dark conditions, focusing on how these interactions impact the entrainment of weathered MPs in ice. It also explores MP entrainment under diverse environmental scenarios.
- Chapter 5 investigates the effects of freezing on the properties and behavior of MPs, characterizing MPs before and after freezing to assess how freezing influences MP behavior across various polymer types and environmental conditions.
- Chapter 6 explores the interactions between electrochemical parameters and their effects on MP removal efficiency. Potential removal mechanisms are also examined through MP characterization and theoretical calculations.
- Chapter 7 summarizes the major findings and contributions of this research, providing recommendations for future studies.

Chapter 2. Literature Review

2.1. Presence of MPs in Aquatic Environments

MPs are defined as plastic debris measuring less than 5 mm in size. The marine environment has become a significant repository of plastic waste. Despite the ban on discharging plastics from at-sea vessels since 1988, the input of terrestrial-sourced plastics into the marine environment is growing rapidly due to the increasing consumption of plastic products (Jambeck et al., 2015). Plastic wastes with improper management can eventually enter marine environment through wastewater discharges, inland waterways, and transported by wind and tides. The sources of MPs in aquatic environments are summarized in Figure 2-1. It was estimated that 4.8 to 12.7 million tonnes plastics waste entered ocean in 2010 (Jambeck et al., 2015). With long-term weathering through physical abrasion, and chemical and biological degradation, MPs can be released from large pieces of plastic waste (Wang et al., 2021c; Wang et al., 2022b). In addition, MPs has been also widely used as additives in cleaning product, paints, sandblasting media and cosmetics (Jambeck et al., 2015).

MPs, owing to their small size, can be ingested by lower trophic organisms, including small marine invertebrates. Ingested microplastics pose not only physical risks but also chemical ones, as they can leach plastic additives such as plasticizers and flame retardants (Wang et al., 2021a). Furthermore, microplastics can act as carriers for hydrophobic contaminants due to their hydrophobic nature (Malli et al., 2022), which can lead to the bioaccumulation of the contaminants in higher trophic levels of the food chain. Therefore, the accumulation of MPs in the marine environment poses a serious threat to both marine ecosystems and human health.

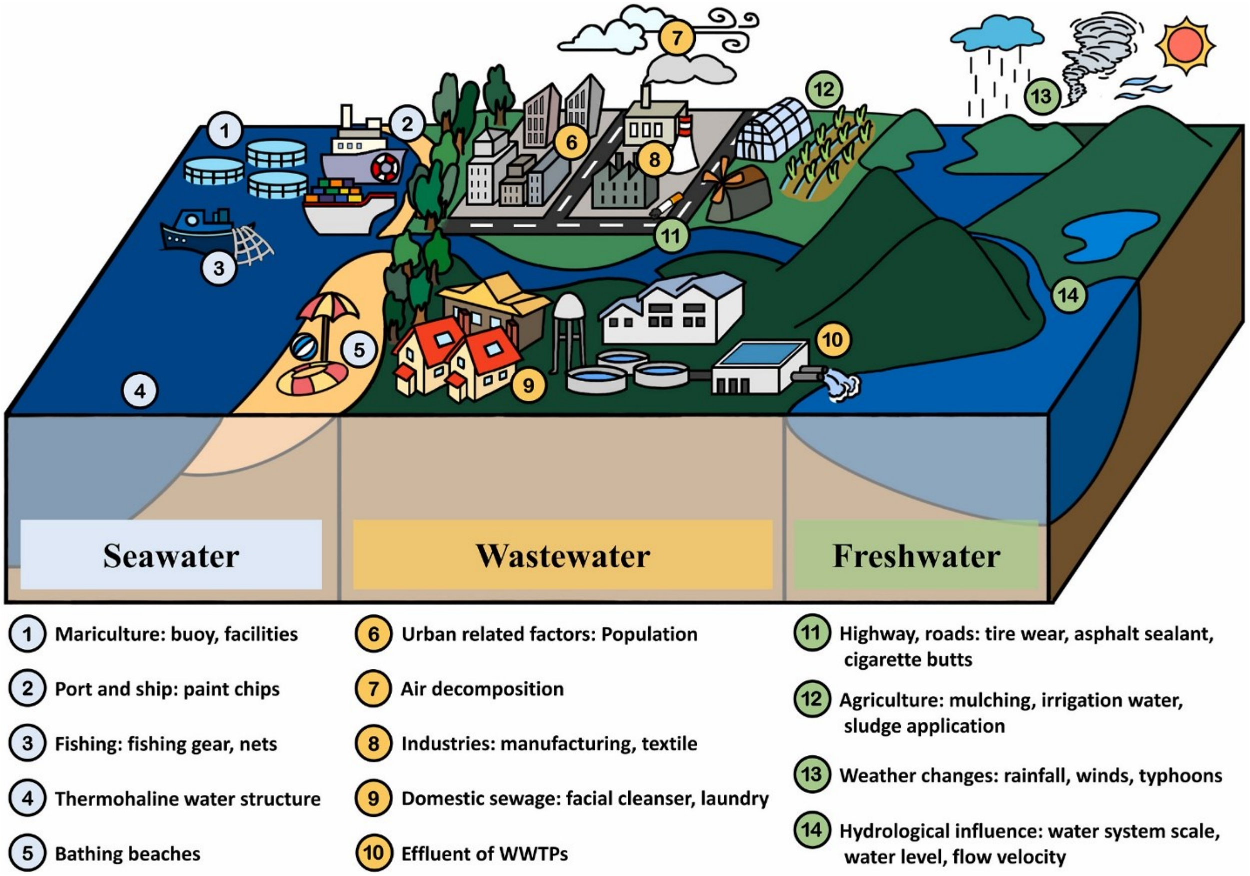

Figure 2-1. Sources of MPs in aquatic environments (Kye et al., 2023).

The abundance of MPs in marine environments varies significantly depending on location and is positively correlated with population density. Generally, higher concentrations of MPs are observed in coastal areas and estuaries compared to open ocean waters. Semi-enclosed seas, such as the Black Sea, Bohai Sea, and Yellow Sea in China, tend to have even higher concentrations due to limited water exchange with the broader ocean (Kye et al., 2023; Zhang et al., 2020). The average MP concentrations were 1.2 × 10^3 particles/m3 in November of 2014 and 0.6 × 10^3 particles/m3 in February of 2015 in Black Sea (Aytan et al., 2016). The MP concentration in Bohai Sea and Yellow Sea is 0.33 ± 0.34 and 0.13±0.20 particles/m3 (Sun et al., 2018; Zhang et al., 2017).

The presence of MPs in freshwater environments has been studied less extensively than in marine ecosystems, despite the fact that freshwater systems play a critical role in the transport of MPs. The occurrence of MPs in freshwater is closely linked to urban areas and industrial activities. In urban environments, sources of MPs include particles from tire wear, fabric fibers from clothing, and plastic microbeads found in personal care products (Sommer et al., 2018). Additionally, weathered plastic waste, such as cigarette butts, plastic products, and disposable masks, contributes to the issue (Wang et al., 2021c). These plastic particles can enter freshwater systems through urban runoff or be released following treatment at sewage plants. The environmental fate of MPs in rivers and lakes is influenced by their physicochemical properties. Larger particles tend to either float on the surface or settle on the riverbed, depending on their density, while smaller particles are more likely to persist over the long term and be transported through water systems into marine environments (Liu et al., 2019).

2.2. Entrainment of MPs in Sea Ice

For a long time, people ignored the presence of plastic and microplastics in polar regions due to the absence of significant human settlements or pollution sources. However, in recent years, some studies and field sampling have revealed the widespread occurrence of microplastics in some polar oceans, with concentrations even comparable to those found in densely populated areas (Kelly et al., 2020). MPs can be long-distance transported from heavily populated areas to remote regions by ocean currents, winds, and even sea ice (Figure 2-2) (Obbard, 2018). Ocean and atmospheric transports of contaminants have been relatively well studied, but the potential of sea ice transport in cold regions was recognized later (Pfirman et al., 1995). Sea ice formation is effective in capturing suspended particulate matter present in the water column, especially in cases where the particles have irregular shapes. The entrapment of sediment within the sea ice has been extensively observed in both laboratory experiments and field sampling (Kempama et al., 1989). However, sediment particles with a higher density require an additional turbulent flow to remain suspended in the water column, allowing them to be captured by the growing ice crystals through a process known as "suspended freezing" (Barber et al., 2021; Ito et al., 2019; Smedsrud, 2001). Due to their lower density, most polymers are easier to capture than sediment particles such as sand and silt. In particular, polymers such as polyethylene (PE) and polystyrene (PS) are lighter than seawater and can float due to their buoyancy, making them especially susceptible to being captured by sea ice. As a result, MPs are much more likely to be entrapped by sea ice than by sediment (Obbard, 2018).

In recent years, many researchers have studied microplastics in sea ice in cold regions through sampling Chubarenko et al. (2022) studied the microplastics in the first-year sea ice formed in the Novik Bay in the Peter the Great Bay, Sea of Japan. Four ice cores with around 40 cm length were sampled in February and March of 2020 to investigate the MP types, concentrations, salinity and their vertical distribution in the sea ice cores. The authors analyzed MPs within the size range of 25–5000 µm and discovered that non-fiber MPs made up 81% of the total number of MPs ranging from 25–300 µm within the sea ice. Furthermore, they found that microplastics with sizes between 0.3–5 mm contributed to 99.6% of the total mass of MPs.

Kim et al. (2021) sampled two sea ice floes drifting in the northern part of the Chukchi Sea. The total MPs concentration in these two ice floes were 103 ± 267 and 5.05 ± 4.75 mg m^{-3} respectively. However, the MPs in the snow above the sea ice floes were 18.5 ± 16.2 and 2.09 ± 4.48 mg m^{-3}. It suggested that the contribution from atmospheric input to MPs in seasonal sea ice in western Arctic Ocean was less than 1%.

von Friesen et al. (2020) explored MPs in sea ice and seawater in Svalbard and revealed that the MPs stored in seasonal sea ice could potentially be a primary source of water in Svalbard. They found that the concentration of MPs (ranging from 50 µm to 5 mm) in the sea ice of Rijpfjorden was two orders of magnitude greater (158 items/L) than that in seawater (7.4 items/L). The researchers also confirmed the release of MPs from seasonal sea ice based on their particle morphology. The non-fiber MPs dominated in sea water in the areas of melting sea ice, while the fiber MPs normally dominated in sea water. Significant amounts of sea ice originate from the Siberian shelves. Depending on the drift patterns of each ice floe, they traverse various regions within the Central Arctic Ocean, but eventually end up being transported through the Transpolar Drift and into the Fram Strait.

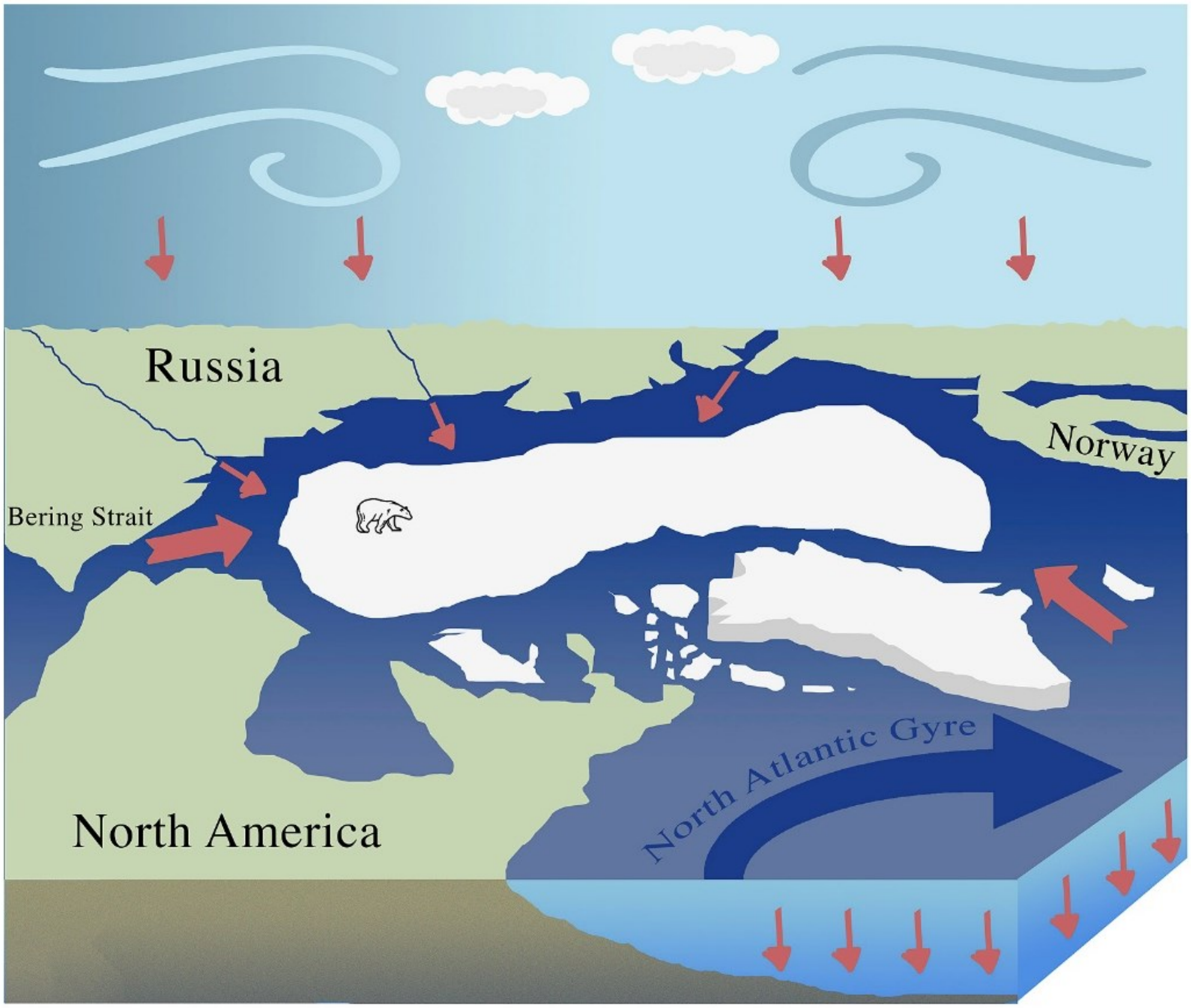

Figure 2-2 Long-range transport of MPs to Arctic regions (Obbard, 2018).

Peeken et al. (2018) investigated the MPs in sea ice cores sampled in Farm Strait and Central Arctic and tracked the sources of the sea ice using low-resolution ice drift and concentration products from passive microwave satellites (Serreze et al., 1989). The highest MPs concentration (excluding rayon and fibers) in sea ice was found in the pack ice and land-fast ice of Fram Strait, which were $(1.2 \pm 1.4) \times 10^{7}$ and $(4.1 \pm 2.0) \times 10^{6}$ items/m^3. The research has demonstrated that any source of contamination originating from remote Arctic areas will inevitably reach the specific region of the Fram Strait through the sea ice transport though the length of time can be different by the locations of contaminant sources.

Recent studies have shown that MPs have also been observed entrained in Antarctic sea ice in addition to the northern hemisphere cryosphere, although only a few studies have reported on this. Kelly et al. (2020) investigated the MPs in east Antarctic sea ice and the MPs concentration was 11.71 items/L in the land-fast ice core. Although the concentrations of plastic in the Southern Ocean are lower than those found in the Arctic Ocean, it is noteworthy that the Southern Ocean is further away from major sources of plastic production and use. Additionally, the region experiences less ship traffic around the continent than Arctic waters (Obbard, 2018).

2.3. Factors Affecting MPs Entrainment in Sea Ice

Although the entrainment of MPs in sea ice was widely observed in global cold oceans but few studies have investigated the how the MPs were entrapped by growing sea ice and the potential influencing on this process using laboratory experiments. Geilfus et al. (2019) using mesocosm experiment to investigate the distribution patterns of MPs in the sea ice the potential impacts of

MPs on the sea ice. Different size (63 to >1400 μm) of polypropylene, polyvinyl chloride, and polyethylene terephthalate were mixed to simulate the MPs in the marine environment. 23 cm thickness of sea ice layer was frozen within 17 days experiment, and it was found that the MPs with large particle (>500 μm) was mainly distributed in the surface layer of the ice (0 to 1 cm). This can be occurred as the underlying seawater was depleted in large microplastic particles due to their inclusion within the ice structure during early sea ice growth. In addition, the highest MPs were found at the interface between sea ice and atmosphere and the MPs on the surface was not included in the ice structure. Although the study found that high concentrations of MPs increased the albedo of sea ice, it is unlikely that the concentrations of MPs present in the natural environment would have a significant impact on sea ice albedo.

Hoffmann et al. (2020) conducted batch tests to examine the potential interactions between ice algae, *Fragillariopsis cylindrus*, and PS MP with diameter of 0.5 μm in sea ice. They discovered that the presence of ice algae, did not have a significant impact on the entrainment of PS MP in sea ice. However, they did observe a significant decrease in the number of algae cells in the sea ice when it was incubated with MP. Furthermore, a positive correlation was observed between the salinity of sea ice and the entrapment of MP within it. As the salinity of the sea ice increased from 10 to 20 PSU, the percentage of MP within the sea ice also increased from 10% to 50%, but ice algae did not affect the process as well. The study also revealed that the presence of ice algae can effectively reduce the amount of MP that adhere to the beaker wall, because the EPS produced by the algae can alter the surface properties of the MP (Peeken et al., 2018).

Pradel et al. (2021b) investigated the distribution pattern of MPs and nanoplastics in ice and water, using a cold finger to simulate the sea ice formation. The batch tests evaluated the potential effects of salinity, size and shape of MPs, and natural organic matters. The results revealed that MPs were easier to be entrapped by the growing sea ice in comparison to nanoplastics. Nanoplastics can be gradually expulsed with time due to its colloidal behaviors, but MPs with larger particle size can be entrapped by the growing ice front. Microplastics, being relatively larger in size, are primarily influenced by gravity and water advection. However, in this experimental setup, the only significant factor affecting movement is water convection caused by differences in salinity and temperature, which is negligible compared with the turbulent conditions in natural environment. The authors summarized the behaviors of MPs and nanoplastics in the ice as shown in Figure 2-3.

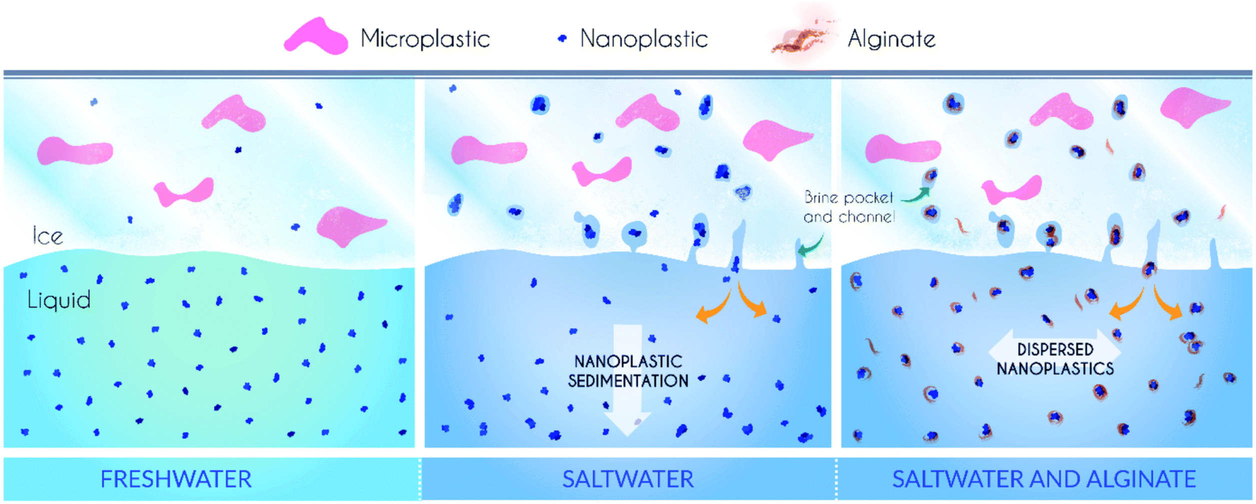

Figure 2-3. Nanoplastic and microplastic behaviors at the water/ice interface as a function of water composition (Pradel et al., 2021b)

These studies contributed to the understanding of the enrichment and entrainment of MPs in ice and explained some of the factors that influence this process. However, all these studies were implemented in calm water, whereas water convection and turbulence can be critical factors affecting the behavior of suspended particulate matter in water. Flowing water can enhance the suspension of particles; moreover, their hydrophobic nature causes some MPs to attach to the air bubbles or ice crystals that form in water under high turbulence (Smedsrud, 2001). These can be favorable conditions for the entrainment of MPs in ice. For instance, Kempama et al. (1989) demonstrated that the turbulent flow can be a crucial factor in the formation of 'dirty ice' caused by sediment entrainment. Sea ice plays a critical role in the global microplastic cycle as a temporary sink for these particles. However, there is a significant knowledge gap in understanding the factors that influence the entrainment of microplastics in ice.

2.4. Removal of MPs

MPs produced through human activities can enter the environment via wastewater systems. For instances, microbeads intentionally added to products like toothpaste and facial cleansers, as well as microfibers released during laundry, can be directly discharged into drains and subsequently enter the wastewater stream. While wastewater treatment plants (WWTPs) can partially remove MPs, the effectiveness of this removal varies depending on the treatment processes used.Unfortunately, a significant quantity of MPs still ends up in the environment through WWTP effluent (Prata, 2018). Studies have shown that the abundance of MPs in the effluent water from WWTPs can range from 0 to 447 particles per liter (Sun et al., 2019). However, there is a lack of specific regulations governing the discharge of MPs in wastewater, as well as efficient treatment methods to control their release in many regions around the world (Khan et al., 2022).

The removal efficiency of MPs in typical treatment procedures in WWTPs are summarized in Figure 2-4. Primary treatment processes in WWTPs, such as filtration, screening, and sedimentation, have been effective in removing larger MPs ranging from 1 to 5 mm (Prata, 2018).

Additionally, methods like air flotation and flocculation have proven efficient for MP removal (Sun et al., 2019; Talvitie et al., 2017). However, these techniques primarily target larger MPs, leaving smaller particles inadequately removed (Prata, 2018). Smaller MPs are particularly concerning because they can be transported over long distances and more easily enter the food chain, leading to heightened environmental impact and potential health risks (Forte et al., 2016). Studies examining MPs in WWTP effluent have shown that smaller particles constitute the majority of those present. Over 90% of MPs in WWTP outlet water are less than 500 μm in size, with approximately 60% being smaller than 100 μm. This underscores the challenge of effectively removing smaller MPs with current treatment processes (Mintenig et al., 2017; Sun et al., 2019).

Various efforts have been made to develop technologies for the removal of MPs from water using chemical, physical and biological methods. MPs can be physically separated from water through techniques such as filtration, adsorption, coagulation, and magnetic separation (Rajala et al., 2020; Wang et al., 2020). Chemical degradation methods include advanced oxidation processes and photolysis, which aim to break down MPs into small molecules or facilitate mineralization (Kim et al., 2022; Shi et al., 2022). Additionally, biodegradation of MPs has been studied using bacteria, fungi or insects capable of degrading plastics (Paço et al., 2017). However, electrochemical treatment approaches, commonly used in water treatment, have rarely been explored for their potential in MPs removal except the electrocoagulation (Chen et al., 2022a).

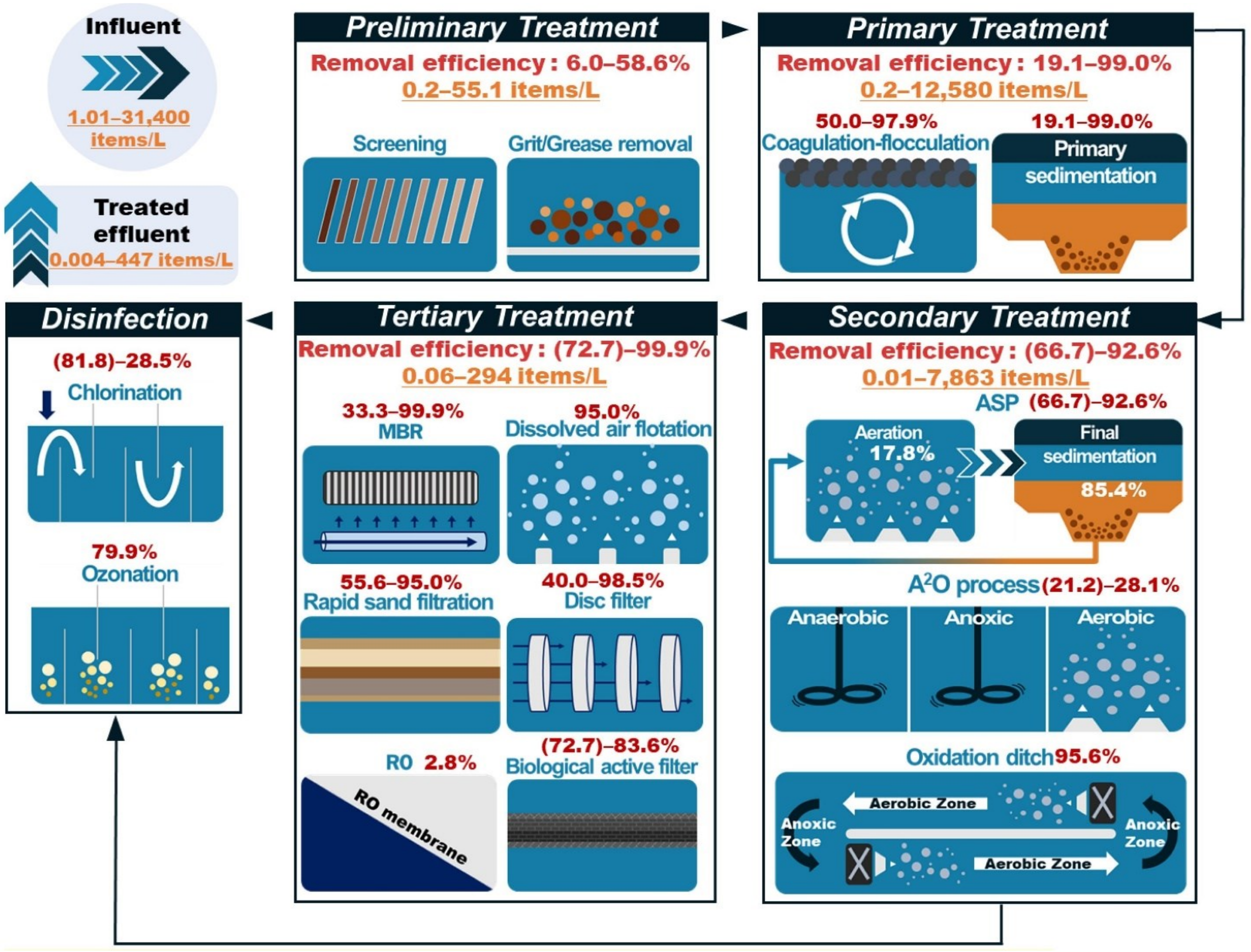

Figure 2-4. Removal efficiency of MPs in typical treatment procedures in WWTPs (Cheng et al., 2021).

Chapter 3. Entrainment and Enrichment of Microplastics in Ice Formation Processes: Implications for the Transport of Microplastics in Cold Regions

3.1. Materials and Methods

3.1.1. Chemicals and Materials

Because the physical and chemical properties of plastics have a dominant role in the environmental behavior of MPs, three different plastic materials each in two different mean particle size ranges were used in this experiment. Polyethylene (PE) with mean particle sizes ranging from 8.0 to 10.0 µm (PE-1) and from 20.0 to 25.0 µm (PE-2) were obtained from Micro Powder Inc. (New York, USA). Polytetrafluoroethylene (PTFE) with mean particle sizes of 6.0 to 9.0 µm (PTFE-1) and 20.0 µm (PTFE-2), and Polymethylmethacrylate (PMMA) with mean particle sizes of 6.0 µm (PMMA-1) and 15.0 µm (PMMA-2) were obtained from Goodfellow Cambridge Ltd. (Huntingdon, UK). Other chemicals needed for the experiment, including Tween 20 and sodium chloride (NaCl), were obtained from Millipore Sigma (Oakville, Canada).

A dispersion of 10 mg/L MP was prepared by adding 15 mg of MPs to 1.5 L deionized water (DI) in a 1.8 L beaker. Next, a 150 µL tenfold dilution of Tween 20 solution was added to achieve 0.001% v/v concentration to prevent the MPs from agglomeration. To avoid the possible influence of natural particles present in seawater on the measurement of MPs in the water, the salinity levels were controlled by adding NaCl instead of sea salt. Three salinity levels were considered in this

---

Reprinted with permission from *Environmental Science & Technology* 2023, 57, 8, 3176–3186.

study: 0, 10, and 34 practical salinity units (PSU). The mixtures were homogenized at 13000 rpm for 20 min using an ULTRA-TURRAX High-Speed Homogenizer (IKA, Germany). The prepared dispersion was immediately dispensed into small beakers for subsequent experimentation.

3.1.2. Ice Formation Experiment

A 175 mL sample of water containing a 10 mg/L MPs dispersion was added to a 250 mL beaker. The side walls and bottom of the beakers were covered by foam rubber insulation to prevent ice forming on the walls. Turbulence was simulated using a magnetic stirrer, with the ice formation being simulated under different stirring speeds (0, 250, 500, 750, 1000, and 1250 rpm). Various modeling approaches have been used for exploring environmental issues (Schuster-Wallace et al., 2022; Wang et al., 2022c; Yao et al., 2022). A computational fluid dynamics (CFD) simulation was implemented to calculate the energy dissipation rates (ε) in beakers at different rotation speeds of the magnetic stirrer (representing varying levels of turbulence intensity in the natural environment). Ansys CFX (Ansys, US) was employed to conduct the simulation. A 3D model was built to simulate the turbulence conditions in the beakers used in batch experiments. The inner diameter of beaker is 64.0 mm. The length and width of magnetic bar are 30.0 and 7.0 mm respectively. The height of the modeling area is equal to the water surface and ensures a total water volume of 175 mL. The simulation was based on standard k-ε model. The rotation area of magnetic bar was set as the rotating domain and the wall of beaker was set as stationary domain. The boundary condition of top surface of the modeling area was set as open boundary with atmospheric pressure. The wall and bottom of the beaker were set as non-slip boundary condition. Frozen rotor approach was used for the interface of stationary and a rotating domain. The size of time step is 0.1 s and total time step is 50 in this simulation. The energy dissipation rate at different rotation speeds in beakers was simulated using CFD, with the results presented in Figure 3-1and Table 3-1.

The beakers and magnetic stirrers were placed in an EPL-2H Platinous Series Temperature Humidity Chamber (ESPEC, Japan) at -10 °C for 3 h to simulate the ice formation process. After 3 h of freezing, the ice that had formed and the remaining water were carefully separated into different beakers. The beakers were then sealed and stored at room temperature (20 °C) for 12 h to allow them to reach ambient temperature prior to measurement. Each experimental condition was repeated twice. The volume concentration of MPs was measured using laser in situ scattering and transmissometry (LISST-200X, Sequoia Scientific, Bellevue, USA), which is capable of measuring particles in the size range of 1 to 500 μm. The enrichment factor of MPs (EF_{MP}) could thus be determined using the measured MP concentrations in ice (C_{ice}) and water (C_{water}) by employing the following equation: $EF_{MP} = C_{ice}/C_{water}$.

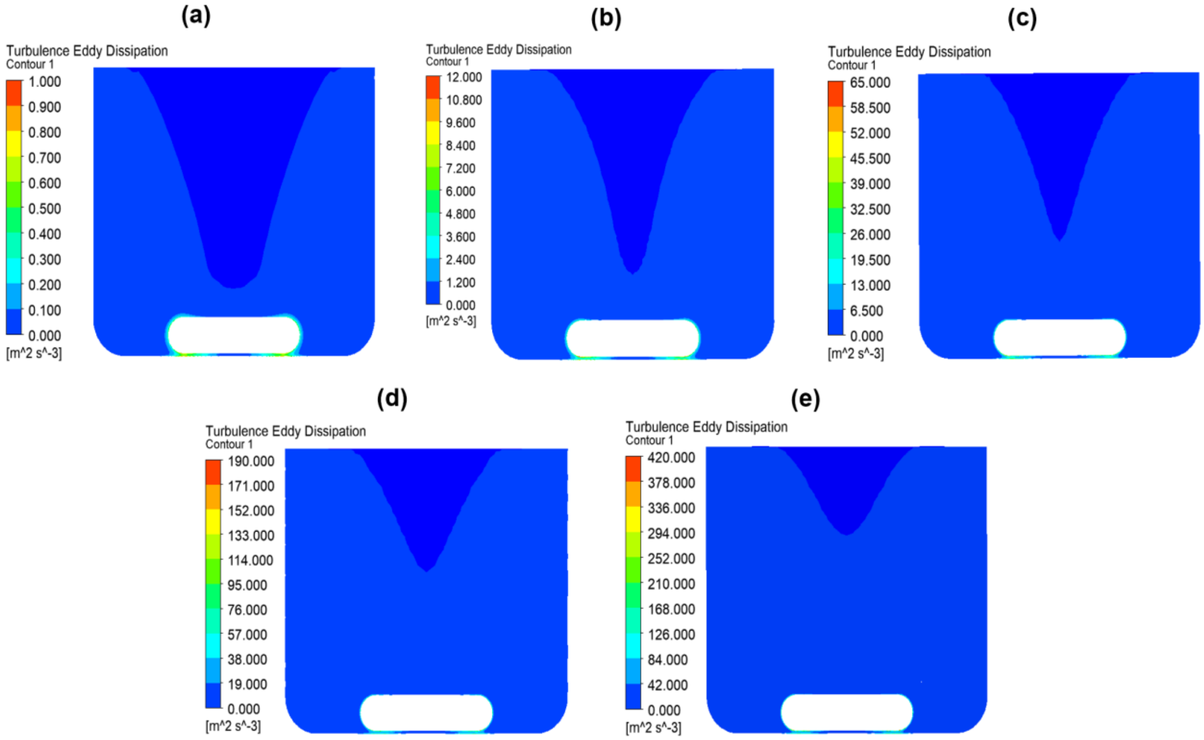

Figure 3-1. The distribution of energy dissipation rate at (a) 250, (b) 500, (c) 750, (d) 1000, and (e) 1250 RPM.

Table 3-1. Rotation speed and corresponding energy dissipation rate in beakers.

Rotation speed (rpm)	Energy Dissipation Rate, ε (m^2/s^3)		
	Average	Maximum	Minimum
250	2.45×10^{-3}	1.17	4.09×10^{-8}
500	1.81×10^{-2}	14.92	4.61×10^{-7}
750	6.08×10^{-2}	67.88	1.95×10^{-6}
1000	0.15	200.83	5.64×10^{-6}
1250	0.27	444.31	7.97×10^{-6}

3.1.3. MP Characterization

The water contact angle (WCA) of the MPs, meanwhile, was measured using an AST video contact angle system (Billerica, USA) to assess the wettability of the MPs. The MP powder was fixed on the glass slide using double-sided tape, and a 5 μL DI water was then dropped on the surface of the solid sample. The embedded software was able to automatically fit an ellipsoid to the curve of the sessile water droplet and determine the contact angles. The respective mean particle size and particle size distribution of the MPs in water and ice were also measured, employing the LISST-200X and using the laser diffraction method. The zeta potentials of the prepared MP dispersions were measured using a Malvern Zetasizer Nano ZS (Malvern, UK). For each measurement, the MP dispersion was fully homogenized (by shaking and ultrasonic bath) prior to reading. Standard deviation was used to describe all error bars appearing in the enclosed figures of this study.

3.1.4. Statistical Analysis

An unpaired *t*-test was used to compare the enrichment factors and mean particle sizes of the two groups of samples to determine whether there was a significant difference. Meanwhile, a paired *t*-test was implemented to identify the variation in mean particle size between water and ice. Spearman correlation analysis was performed to identify the relationship between entrainment behavior of MPs and plastic properties and environmental factors. It should be noted that Spearman's rank correlation coefficient, ρ, nonparametrically measures the strength and direction of a relationship between two variables. Redundancy analysis (RDA), meanwhile, was used to study the relationship between environmental variables and MPs entertainment in ice.

3.2. Results and Discussion

3.2.1. Microplastic Entrainment and Enrichment during Ice Formation

The entrainment and enrichment of MPs in ice in the cold ocean have been reported. Some studies have explored the potential mechanisms underlying such process, but there is still relatively little known about these phenomena. In addition, seasonal ice can function as an important transport medium and temporary sink for MPs in the freshwater environment as well. For rivers, lakes, or estuaries in densely populated areas, the enrichment of MPs in the ice can be an important environmental process concerning the fate of MPs, and to the authors' knowledge ours is the first study to investigate it. The entrainment of different MPs in the calm freshwater as observed in our study are shown in Figure 3-2a. As can be seen, the enrichment factor was not significantly affected by the particle size of the MPs in the cases of PE and PTFE. The enrichment factors of PE-1, PE-2, PTFE-1, and PTFE-2 were found to be 0.79 (± 0.20), 0.77 (± 0.32), 1.79 (± 0.17), and 1.76 (± 0.56), respectively. In fact, for both PE and PTFE, the difference in the plastic materials had a greater effect on the ice entrainment in the calm freshwater than did the particle size. However, for PMMA, the sample with a larger particle size showed a higher enrichment in ice in comparison to the sample with a smaller particle size. The enrichment factors were 1.64 (± 0.16) and 3.82 (± 1.88) for PMMA-1 and PMMA-2, respectively.

The difference in the ice entrainment of different types of MPs in calm water can be explained by their respective colloidal behavior. Pradel et al. (2021b) investigated the transport behaviors of polystyrene nanoplastics and microplastics in freezing saltwater. They found that nanoplastics were expelled much more rapidly from ice over time compared to larger-sized microplastics. The difference can be attributed to the stability of the dispersion system; non-colloidal particles can more easily become entrapped by the growing ice front. The zeta potential of the dispersions with different MPs was shown in Figure 3-2b. The zeta potentials of PE-1 and -2 dispersion were -50.5 (± 4.2) and -42.8 (± 11.2) mV, respectively, indicating physical stability of the dispersion. In comparison, the zeta potentials of PTFE-1, PTFE-2, PMMA-1, and PMMA-2 were -24.5 (± 0.8), -16.1(± 0.7), -20.0 (± 0.7), and -16.6 (± 3.0), respectively, showed unstable systems. As can be seen, these zeta potentials followed a similar trend to the rate of MP enrichment in ice. The relatively high zeta potentials of PE dispersion resulted in low MP enrichment.

The particle size distribution and mean particle size of MPs in water and ice are presented in Figure 3-2c and Figure 3-2d. Although the enrichment factor for PE and PTFE were not significantly affected by the particle size, a different particle size distribution in water versus in ice was observed for both PE-2 and PTFE-2. Interestingly, the particle size changes of these two MPs in ice and water after freezing were exactly opposite. The mean particle size of PE-2 in ice and water was 24.0 (± 0.2) and 17.9 (± 1.4) μm, respectively, whereas the corresponding values for PTFE-2 were 15.3 (± 1.0) and 20.2 (± 0.5) μm, respectively. The results demonstrated that larger-sized PE particles and smaller-sized PTFE particles were more prone to being entrapped by ice formed under calm water conditions. However, for the other MPs, there was not a significant difference in the particle size of the MPs in ice and compared to the MPs in water. These behaviors are largely governed by the properties of MPs. For instance, the sinking/floating of MPs can be controlled by various factors, such as particle size, wettability, and density. Although

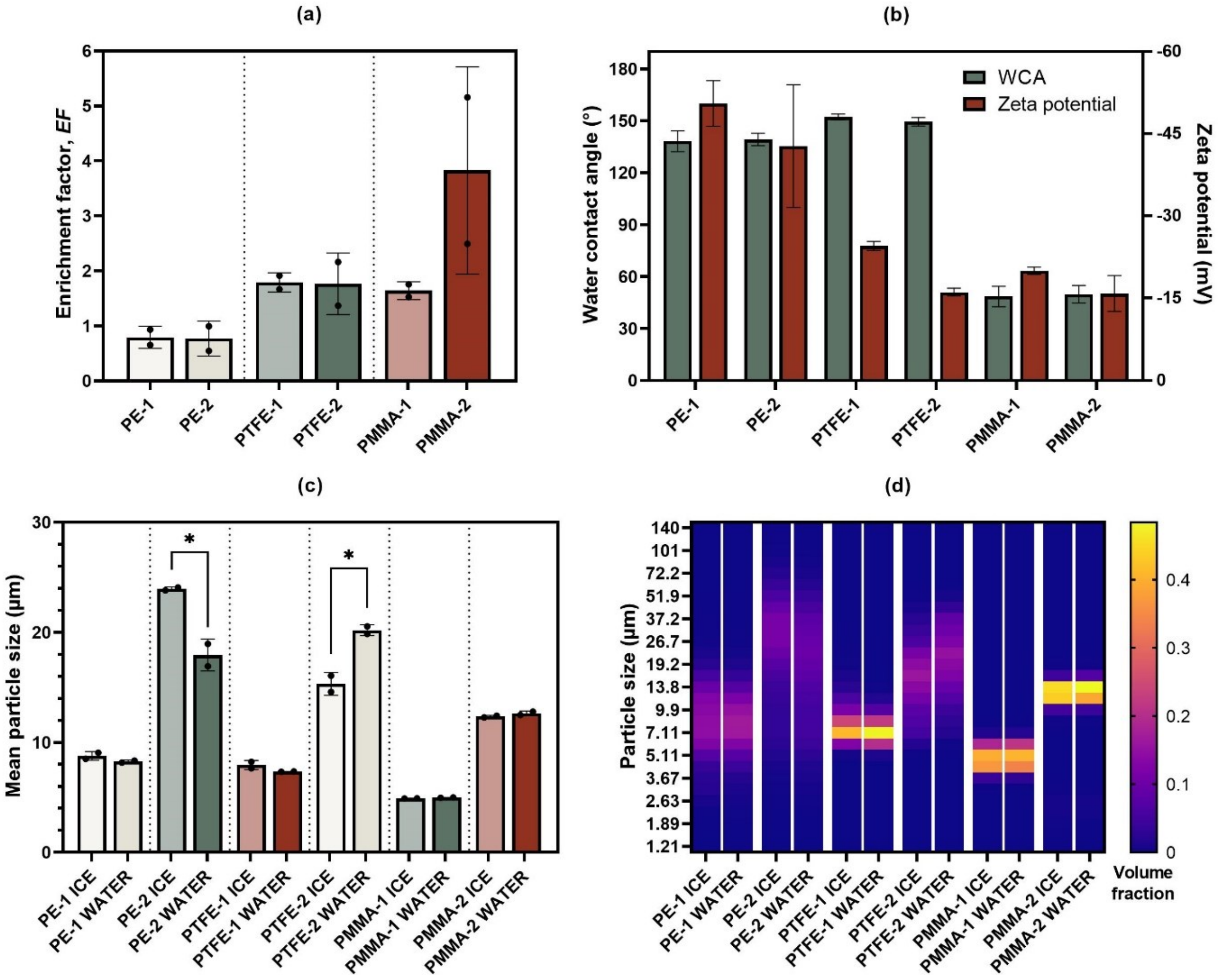

Figure 3-2. (a) Enrichment factors of MPs in ice formed in calm freshwater. (b) WCA and Zeta potential of MPs dispersion. (c) Mean particle size and (d) particle size distribution of MPs in ice and water. '*' represented the significant difference with $p < 0.05$ between two groups.

PTFE has a density higher than that of water, its relatively small particle size means this MP can remain in suspension for a longer period of time than the MP with larger particle size. In addition, its strong hydrophobicity causes PTFE to tend to adsorb at the water–air interface. As shown in Figure 3-2b, PTFE has the strongest hydrophobicity among the three polymers considered in this study. The WCAs of PTFE-1 and PTFE-2 were found to be 152.2° (± 1.8°) and 149.5° (± 2.4°), respectively. On the other hand, the behavior of particles with larger particle sizes in water is more easily controlled by gravity (Khatmullina and Isachenko, 2017). These factors combine to result in smaller mean particle size of PTFE in ice than in water. Similarly, the larger particle size of PE-2 means that the behavior of this MP in water is largely governed by the weight. In other words, the low density of PE (0.97 g/cm^3) makes it easier for larger particles to float to the water surface and become trapped by ice.

3.2.2. Role of Turbulence Intensity in Microplastic Entrainment during Ice Formation

Turbulence intensity plays a critical role in the ice entrainment of suspended particles during the ice formation process. The previous section discussed the ice entrainment behaviors of MPs under calm water. However, the level of turbulence in natural water bodies can vary and is often influenced by variable weather conditions (Oziel et al., 2019; Voermans et al., 2019). Field sampling and laboratory studies have demonstrated that turbulence is an essential condition under which for "suspension freezing" to form sediment-laden ice (Barber et al., 2021; Ito et al., 2019; Smedsrud, 2001). In our study, the effect of turbulent flows on ice entrainment of MPs was investigated by simulating different turbulence intensities in laboratory microcosm beakers. The energy dissipation rate, ε, was the indicator used to measure turbulence intensity. The energy dissipation rate at different rotation speeds in beakers was simulated using CFD, with the results presented in Figure 3-1 and Table 3-1. As can be seen, the average energy dissipation rates at rotation speeds of 250, 500, 750, 1000, and 1250 rpm were found to be 2.4×10^{-3}, 1.81×10^{-2}, 6.08×10^{-2}, 0.15, and 0.27 m^2/s^3, respectively. Turbulence in the surface layer of ocean is caused by the wind, wave breaking, buoyancy forcing, interactions between waves and turbulence, and Langmuir circulation (Ardhuin and Jenkins, 2006). The turbulence intensity in ocean ranges from 10^{-10} to 10^{-1} m^2/s^3 depending on the weather and location (Iyer et al., 2021). This implies that the turbulence intensity simulated by the magnetic stirrer in this study was reasonably representative of the conditions typical of natural water bodies.

The enrichment factors of MPs under different turbulence intensities are demonstrated in Figure 3-6. It was found that the entrainment behavior of MPs was significantly influenced by the turbulence intensity, with the trend varying depending on the type of MP. The two hydrophobic MPs—PE and PTFE—had similar trends, although the enrichment factors were different. In specific, the enrichment factors were overall positively correlated with turbulence intensity for both PE and PTFE. The enrichment factor of PE-1 was relatively stable (ranging from 0.79 to 1.00) at rotation speeds of 0 to 750 rpm, but increased dramatically at rotation speeds beyond this threshold. For instance, the enrichment factors at 1000 and 1250 rpm were 1.70 (± 0.03) and 2.82 (± 0.14), respectively. A similar trend was observed for PTFE-1, although the enrichment factors were higher overall than in the case of PE-1. The enrichment factors of PTFE-1 at 1000 and 1250 rpm were 2.86 (± 1.10) and 4.69 (± 1.06), respectively. An interesting finding was that, at high turbulence intensity, both PE-2 and PTFE-2 were more strongly enriched in ice than were PE-1 and PTFE-1. The enrichment factors of PE-2 and PTFE-2 were 7.14 (± 0.04) and 16.92 (± 1.44), respectively.

This finding underscores the importance of particle size for the entrainment of MPs in ice forming under high turbulence.

The enrichment factors of PE-1 and PE-2 were significantly different at 250 rpm versus at 500 rpm, whereas a disparity at different rotation speeds was not observed in the case of PTFE MP. This, too, can be attributed to the difference in density between these two polymers. In calm water, the low density of PE made it easier for relatively large particles to float on the surface compared to smaller particles. However, the presence of turbulence made it difficult for these larger MP particles to stay afloat by buoyancy (and thus also to be captured by ice forming at the water surface). This results in a lower enrichment factor for PE-2 at low turbulence intensity (250 and 500 rpm) relative to the calm water.

The two hydrophobic MPs—PE and PTFE—had a high enrichment factor at both 1000 rpm and 1250 rpm. The formation of frazil ice was also observed at these rotation speeds, as shown in Figure 3-3c and 3-3f) suggesting a correlation between the entrainment of these hydrophobic MPs and frazil ice. Frazil ice, it should be noted—which is the collection of randomly oriented ice crystals in the form of small disks, dendrites, or needles—can form in turbulent open water (Figure 3-4 and Figure 3-5). The ice crystals forming at the water surface due to heat loss can become vertically mixed in the turbulent flow, overcoming their buoyancy. The frazil ice forming in supercooled and turbulent water can thus be a very important medium for the removal of suspended particulate matter from the water column. Ice crystals can attach to particles and carry them to the surface by buoyancy. The entrapment of sediment by frazil ice has been widely reported and proven by field sampling, laboratory experiments, and model simulation (Dethleff and Kempema, 2007; Smedsrud, 2001, 2002). With respect to our study, it was also observed that a large amount of air bubbles became frozen into the ice at high turbulence (Figure 3-3f). Given that air bubbles forming at high turbulence can capture and carry hydrophobic MPs to the surface through enhanced buoyancy, the combined effect of air bubbles and frazil ice significantly increased the enrichment of hydrophobic MPs in the ice under high turbulence.

PMMA, as a hydrophilic plastic material, has a completely different entrainment behavior than the two hydrophobic plastics studied as ice forms under turbulent flows. In our study, both PMMA-1 and PMMA-2 showed higher enrichment factors in calm water compared to in flowing water, whereas high turbulence intensity significantly enhanced the enrichment for the two hydrophobic MPs (as described above). The enrichment factors for PMMA-1 and PMMA-2 at 0 rpm were 1.64 (± 0.16) and 3.82 (± 1.88), respectively, while at rotation speeds ranging from 250 to 1250 rpm, the enrichment factors ranged from 0.42 to 0.87 and from 0.67 to 1.27, respectively. Moreover, larger particle sizes of PMMA showed a higher rate of ice entrainment at both 0 and 250 rpm compared to smaller particle sizes of PMMA. These findings strongly indicate that MP characteristics such as particle size, density, and hydrophobicity play important roles in the entrainment and enrichment of MPs in ice.

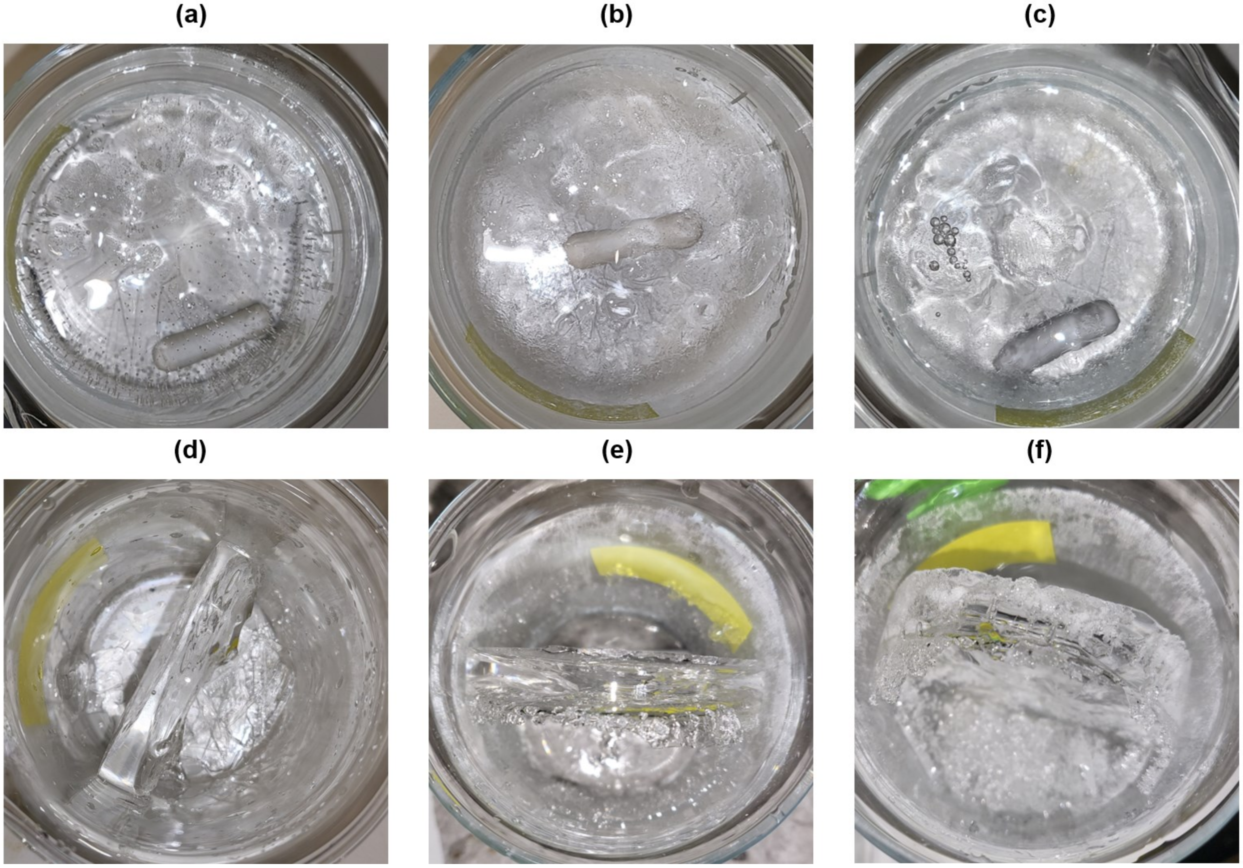

Figure 3-3. Ice formed by freshwater at (a, d) 0, (b, e) 500, and (c, f) 1000 RPM.

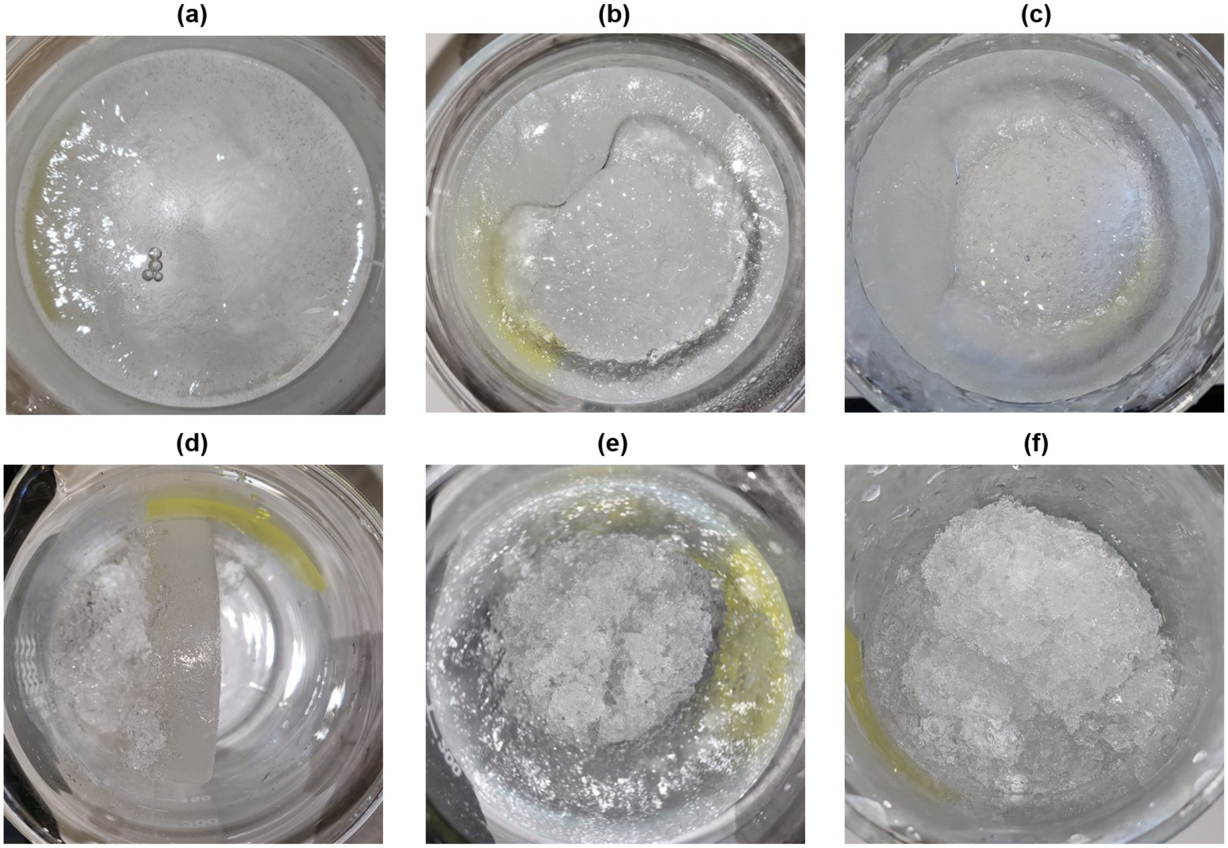

Figure 3-4. Ice formed by 10 PSU saline water at (a, d) 0, (b, e) 500, and (c, f) 1000 RPM.

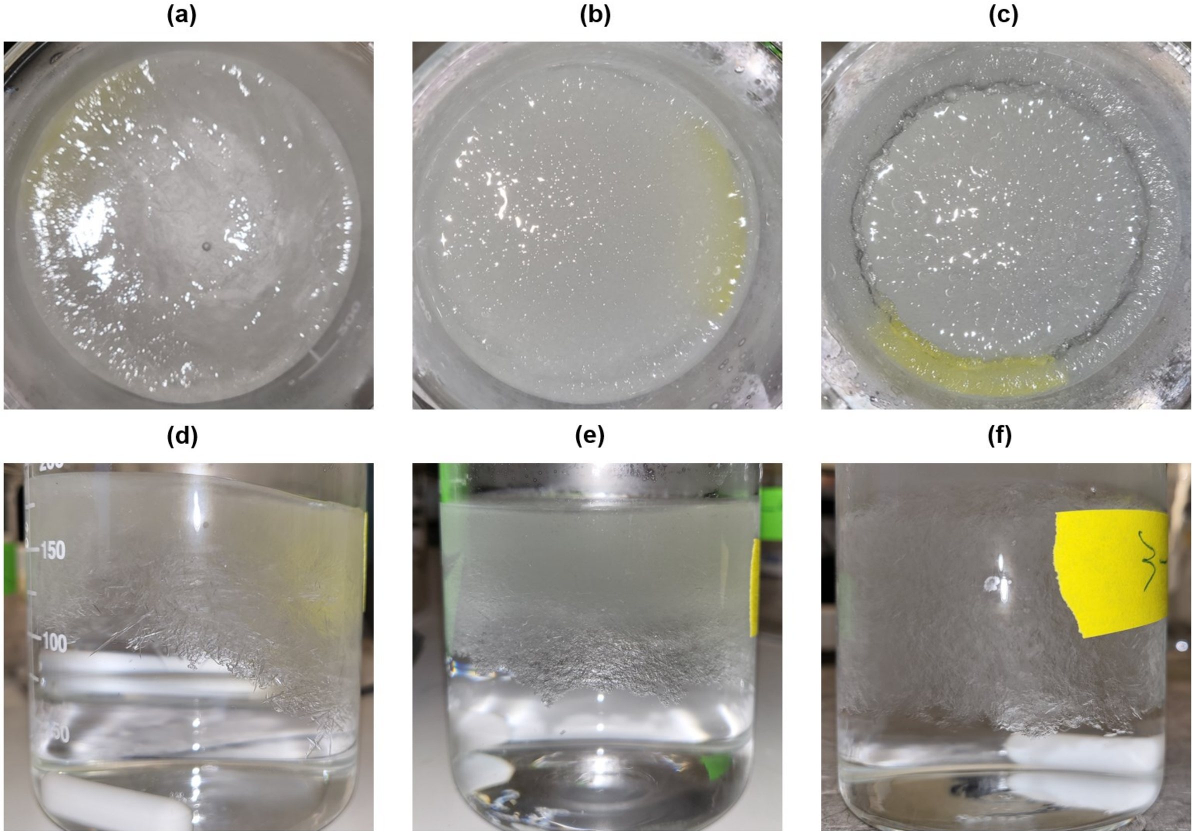

Figure 3-5. Ice formed by 34 PSU saline water at (a, d) 0, (b, e) 500, and (c, f) 1000 RPM.

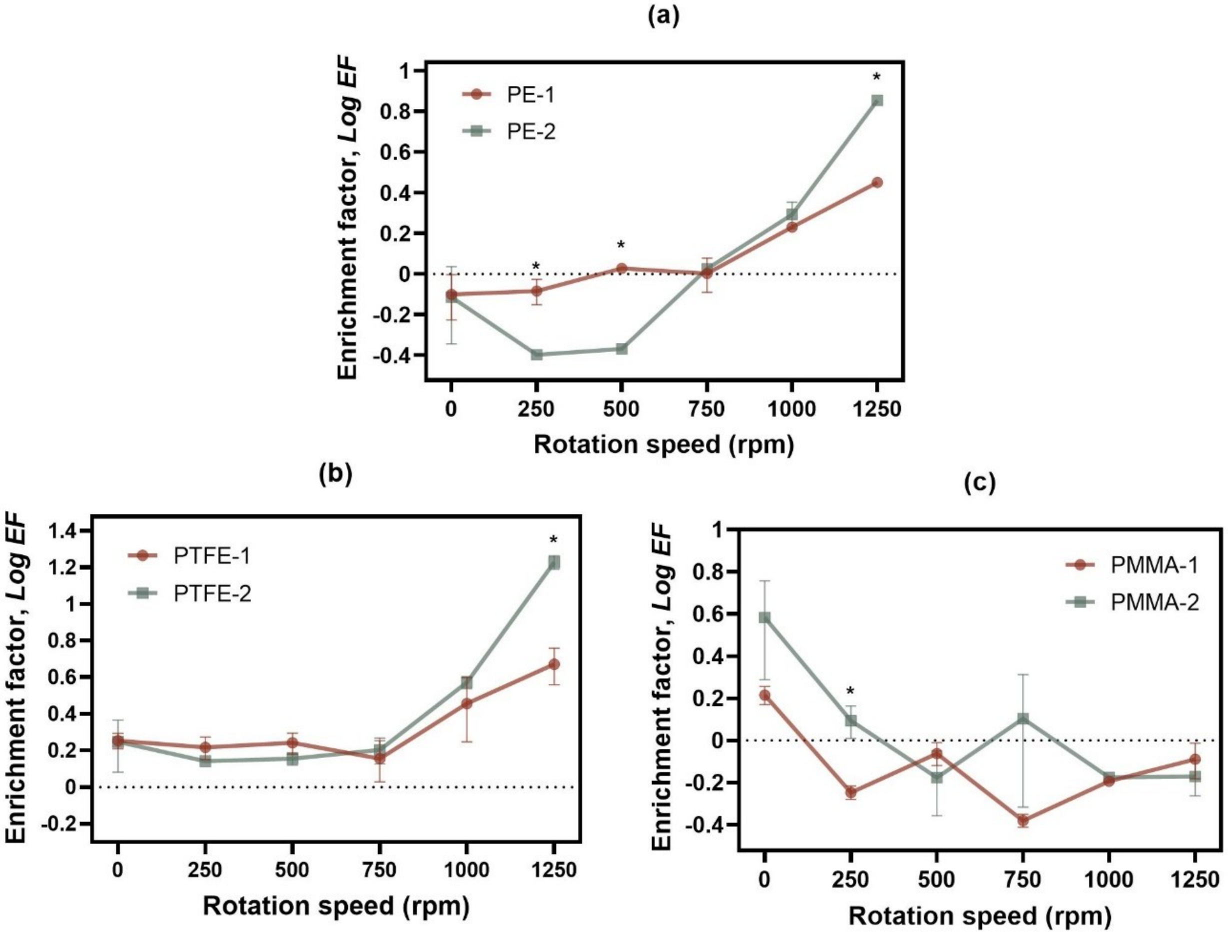

Figure 3-6. Enrichment factor of (a) PE, (b) PTFE, and (c) PMMA, in ice under different turbulence intensities. '*' represented that the difference in enrichment factor between two MPs was significant (*p* < 0.05) at corresponding rotation speed.

3.2.3. Effect of Salinity

Salinity can be highly variable in the marine environment, especially in estuaries, where freshwater mixes with seawater to create brackish water, leading to a salinity gradient whereby salinity can range from 0.5 to 34 PSU. The salinity in estuary water can also vary due to daily tides, weather conditions, and other factors (Telesh and Khlebovich, 2010). Variations in the salinity of water can result in different behaviors of MPs. For instance, a difference in salinity can slightly alter the density of the water, thus affecting the buoyancy of the MPs (Malli et al., 2022). The increase in ionic strength also destabilizes and accelerates the settling of MPs as they enter the saline water (Feng et al., 2022b). In addition to changing the behavior of MPs, the salinity in water can affect the formation of ice. For instance, salinity can lead to changes in the texture of formed ice due to brine rejection. The ice naturally rejects salty water when the water freezes, and the brine water drains through narrow brine channels that weave through the ice. The difference in the ice structure can significantly affect the entrainment of MPs. Therefore, this study explored the effects salinity on the ice entrainment of MPs under different turbulences. Three saline levels—0, 10, and 34 PSU—were simulated by adding NaCl to DI water. The results are shown in Figure 3-7.

As the results show, salinity can have opposite effects on MP enrichment depending on the rotation speed. The salinity increased the enrichment factors for all MPs in calm water (although the difference was not statistically significant for some MPs). Changing salinity also affects ice formation and MP behavior, leading to an increase in enrichment factors. As has been noted in the literature, the increased density and surface tension of water due to salinity can be favorable conditions for the buoyancy of MPs (Malli et al., 2022). In our study, ice crystals formed below the ice cover in the calm saline water, whereas this phenomenon was not observed in freshwater, as shown in Figure 3-3a and Figure 3-5d. The concentrated brine with high density and low temperature were expelled from the ice, creating ice crystals when contacting the surrounding water. Moreover, the brine channel and brine pockets forming due to brine rejection led to sea ice having a porous and permeable structure. In our study, as shown in Figure 3-3, Figure 3-4, and Figure 3-5, the ice forming in calm saline water was less transparent in comparison to that forming in freshwater due to the formation of a brine network in the former case. As noted in the literature in this regard, MPs in ice tend to be pushed into brine channels due to their hydrophobic nature; in this manner, the brine channels can temporarily trap the particles until further redistribution during freeze/thaw cycles (Chubarenko, 2022).

Brine networks present in sea ice facilitate the exchange of MPs between ice and water. In this regard, batch experiments conducted in calm seawater as part of a recent study have suggested that the MPs in sea ice can be gradually expulsed from ice and transferred to water (Pradel et al., 2021b). MPs of a larger particle size exhibit a lower expulsion rate, suggesting that larger MPs are more prone to becoming stuck in the brine channels in sea ice. The electrostatic screening effects of salt lead to the agglomeration of MPs, thus hindering the expulsion of MPs from the brine channels of sea ice (Peydayesh et al., 2021).

However, the enrichment factor in saline water was reduced with the introduction of turbulent flows for all of the MPs studied, as shown in Figure 3-7. At the same time, a large amount of frazil ice was observed in the flowing saline water. Contrary to the results in the freshwater environment, in the case of saline water the formation of frazil ice was not accompanied by enhanced entrainment of hydrophobic MPs. This is attributable to the different characteristics of frazil ice in saline water and compared to in freshwater. In this study, the formation of frazil was observed with the introduction of rotation, although the frazil ice generated differed in structure at different salinities and rotation speeds. The formation of frazil ice was observed at high turbulence (1000 and 1250 rpm) in freshwater. Only clear columnar ice was generated in calm water and water with a low rotation speed. At a high rotation speed, meanwhile, frazil ice was generated below the columnar ice. The ice crystals adhered to one another and attached to the ice cover, as shown in Figure 3-3c. The formation of frazil ice was more readily observed in saline water. A large amount of frazil ice was generated when the rotation speed exceeded 500 rpm at both 10 and 34 PSU. This was presumably due to the favorable effect of salinity on the generation of frazil ice (Ushio and Wakatsuchi, 1993). However, as noted in the literature, frazil ice forming in saline water has lower adhesiveness and cohesiveness than that produced in freshwater, meaning that the ice crystals forming in flowing saline water tend to remain a loose collection of crystals rather than congealing (Barrette, 2021). In our study, the loose structure of the frazil ice in saline water allowed for the exchange of MPs between ice and water. The entrained MPs were expelled, leading to the low enrichment factors of MPs in both the 10 and 34 PSU samples under high turbulence (compared to in the freshwater samples).

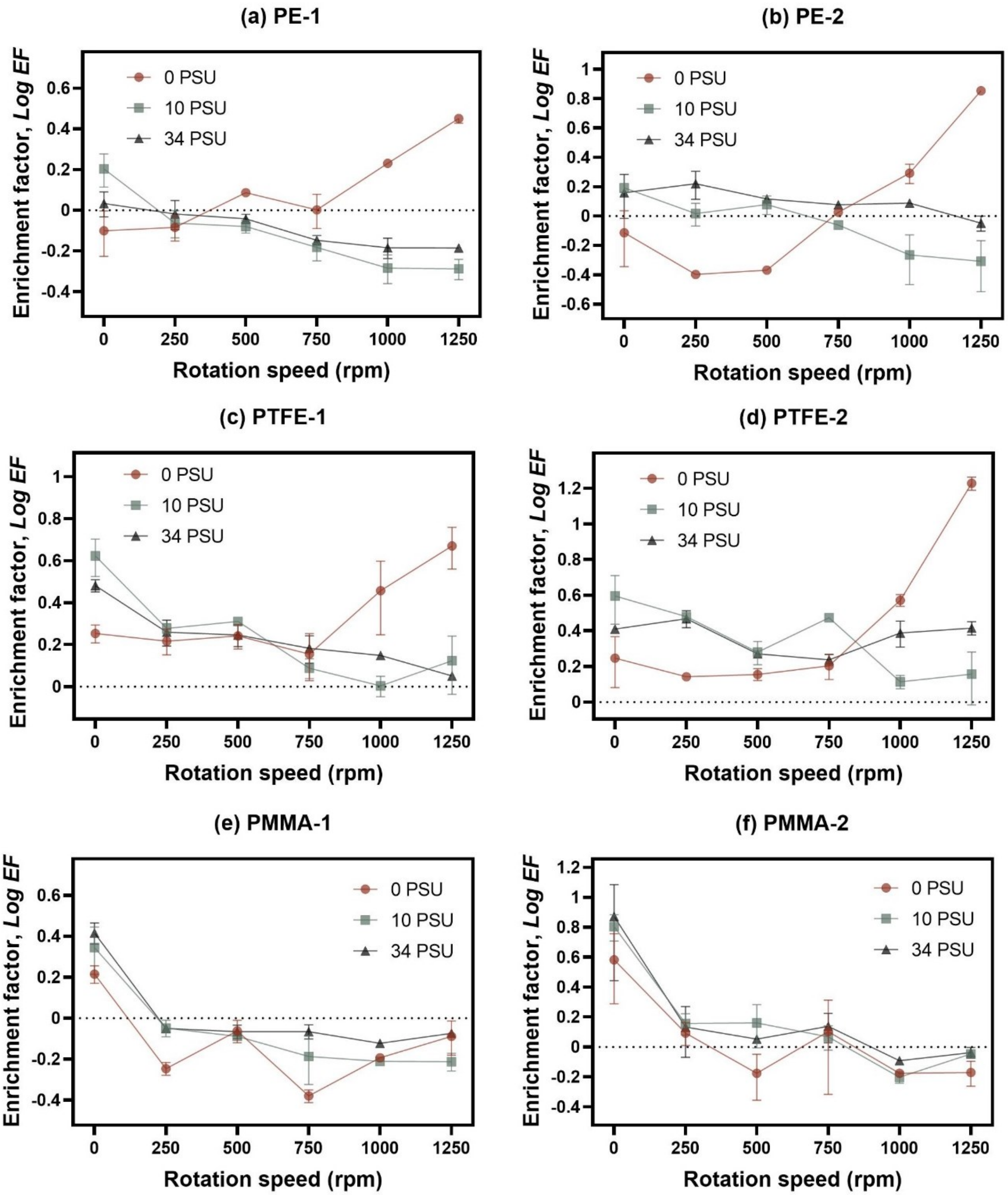

Figure 3-7. The enrichment factors of (a) PE-1, (b) PE-2, (c) PTFE-1, (d) PTFE-2, (e) PMMA-1, and (f) PMMA-2 in ice with different turbulence intensities.

3.2.4. Effect of Microplastics Properties

Effect of wettability

MP characteristics are the primary determinant of an MP's environmental behavior and of its fate in water. The results of this study demonstrate that the entrainment and enrichment in ice of the MPs under study varied considerably depending on the properties of the given MP. PTFE has a density of 2.20 g/cm^3 and is considered non-buoyant in water. In contrast, PE has a density of 0.97 g/cm^3, and is relatively buoyant in water. However, the enrichment factor of PTFE was found to be significantly higher than that of PE MPs of a similar particle size and at the same rotation speed, even in calm water, as shown in Figure 3-6. Ideally, PTFE MPs will sink to the bottom in a calm water due to the effects of gravity and non-buoyancy and will not become entrapped by the ice forming on the water surface. However, due to their high hydrophobicity and low surface free energy, suspended MPs at the water surface can be held there by surface tension (Anderson et al., 2018).

In calm water and under freezing temperature conditions, columnar ice forms at the water surface and gradually grows downward due to heat diffusion. Therefore, the dissolved gas in water cannot be expelled to the ambient environment during the process of ice formation, but instead forms air bubbles in the freshwater ice, as shown in Figure 3-3a. However, the air bubbles were not observed in the ice formed by saline water. It has been reported in the literature that the entrainment of MPs in ice is associated with the air bubbles in ice because the hydrophobicity and icephobicity of the MPs cause them to be pushed out into the air bubbles (Chubarenko, 2022). Meanwhile, it has also been noted that air bubbles in the water are more likely to be attracted to more hydrophobic MPs (Wang et al., 2021b). The higher enrichment of PE-2 and PTFE-2 in calm water compared to under low rotation speeds (250 and 500 rpm) observed in our study could be attributable to this phenomenon. In other words, flowing water carried away the gas and prevented the formation of gas bubbles in the ice. As shown in Figure 3-3b, there were no air bubbles visible in the ice that formed at 500 rpm. The hydrophobic MP particles lacked the air bubbles for attachment at 250 and 500 rpm, which may have led to their entrapment in the ice being inhibited.

However, the hydrophilic MP, PMMA, exhibited a different behavior under the influence of turbulence, this being attributable to the hydrophilic surface of PMMA. Hydrophobicity of particles in water, it should be noted, can be a critical factor in ice nucleation, which is the beginning of the ice formation process (Fitzner et al., 2015). The lower energy barrier means that ice crystals can more easily nucleate on hydrophilic surfaces compared to on hydrophobic surfaces (Alizadeh et al., 2012; Zhao et al., 2020). Accordingly, ice crystals are able to grow on the hydrophilic surface of PMMA, in turn leading to PMMA becoming highly enriched in ice forming in calm water as shown in Figure 3-7e and Figure 3-7f. In this regard, Liu et al. (2017) used fluoroalkyl silane samples with different fluorine concentrations to modify the surface of different materials in order to study the effect of wettability on ice growth patterns. Their results showed that the ice crystal growth pattern changed from on-surface growth to off-surface growth when the WCA of the smooth surface was larger than 32.5° (Liu et al., 2017). Their finding suggests that ice crystals may not adhere strongly enough to the PMMA surface under strong water advection conditions. This could explain the decrease in the enrichment factor of PMMA observed in our study when the rotation was introduced during the ice formation process.

Effect of particle size

The entrainment and enrichment behaviors of MPs can also be influenced by the particle size. In our study, the PE and PTFE samples of larger particle size showed significant increases in the enrichment factor under high turbulence (1250 rpm), while PMMA-2 exhibited higher enrichment in calm water than in turbulent water. The relationship between entrainment behavior and particle size in ice has been observed in other studies. Nano-size plastics can have more significant colloidal behaviors in water, whereas MPs of a larger particle size are more susceptible to the effects of gravity and water advection (Pradel et al., 2021b).

The high concentration of air bubbles present in highly turbulent water is also more likely to entrain these larger particles (Yuan et al., 2022). Moreover, a study on the interaction between air bubbles and MPs showed that larger particle size can lead to a higher removal rate of MPs through air flotation (Swart et al., 2022). Another study evaluating the froth flotation of MPs similarly demonstrated that MPs of a larger particle size and higher density exhibit a higher flotation rate (Zhang et al., 2021). This further explains the differences in enrichment factors for different particle sizes of PE and PTFE observed in our study.

The difference in mean particle size of MPs in ice versus in water can be used to demonstrate the effect of particle size on MP entrainment. The mean particle sizes in ice versus in water of the different MPs under study in our experiments at 0, 10, and 34 PSU are shown in Figure 3-8. As can be seen, the mean particle size of the MPs entrained in ice was significantly larger than that of the MPs remaining in the water for all of the samples except the PTFE-2 at 0 PSU, the PMMA-1 at 0 PSU, and the PMMA-2 at all salinities.

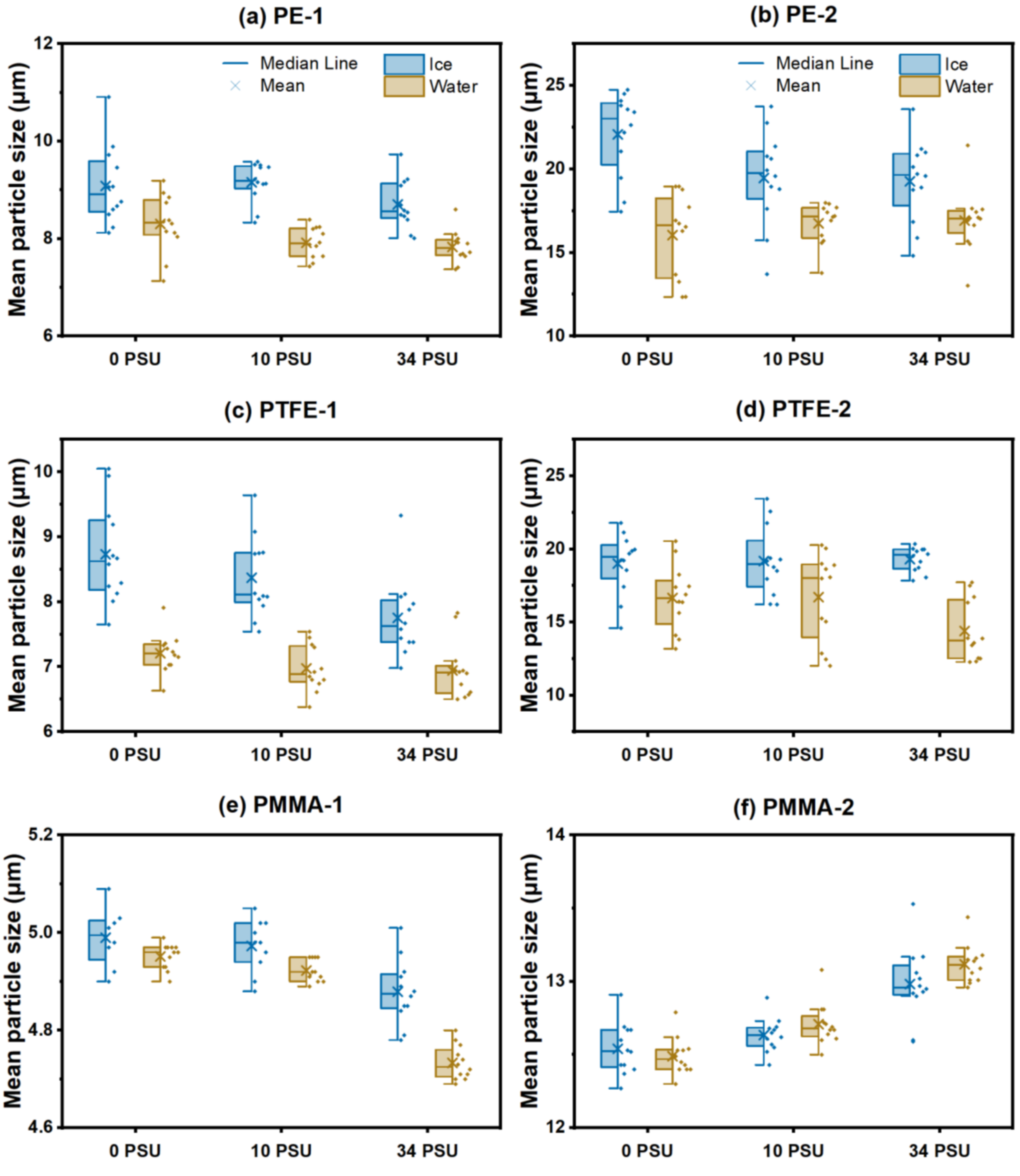

Figure 3-8. Box plots showing mean particle size of MPs in ice and water for (a) PE-1, (b) PE-2, (c) PTFE-1, (d) PTFE-2, (e) PMMA-1, and (f) PMMA-2 at 0, 10 and 34 PSU.

This suggests that the particles of a larger size more easily became trapped in the ice. In addition to the effect of air bubbles in water, the formation of frazil ice can be another important factor leading to the increase in mean particle size of MPs entrained in ice. Frazil ice can aggregate with suspended particles and transport them to the surface through buoyancy. Compared with the two hydrophobic MPs, the hydrophilic PMMA had no significant difference in mean particle size between ice and water. These results suggest that the entrainment of MPs in ice was governed by these polymer properties acting in concert.

3.2.5. Correlation and Redundancy Analysis of Factors Influencing MP Enrichment in Ice

Correlation analysis and RDA were implemented to further explore the significant factors affecting MP entrainment in ice, with the results presented in Figure 3-9. In addition to enrichment factor, particle size ratio, defined as the ratio of mean particle size in ice to that in water for the purpose of this study, was considered in investigating the difference in particle size in ice versus in water. The results of the correlation analysis show that the characteristics of MPs had a significant effect on both particle size ratio and enrichment factor. The enrichment factor was positively correlated to the mean particle size, WCA, and density of MPs, with ρ-values of 0.33 ($p < 0.001$), 0.53 ($p < 0.001$), and 0.37 ($p < 0.001$), respectively. Meanwhile, particle size ratio was positively correlated to rotation speed, mean particle size, and WCA of MPs, with ρ-values of 0.14 ($p < 0.05$), 0.21 ($p < 0.01$), and 0.54 ($p < 0.001$), respectively. Similarly, the RDA showed that WCA, density, mean particle size, and rotation speed contributed to 60.4%, 15.9%, 10.0%, and 9.5% of explained variations, respectively, but that the proportion of variations explained by salinity was not statistically significant ($p > 0.05$). This is attributable to the fact that the influence of salinity on entrainment behavior can vary depending on the type of MP.

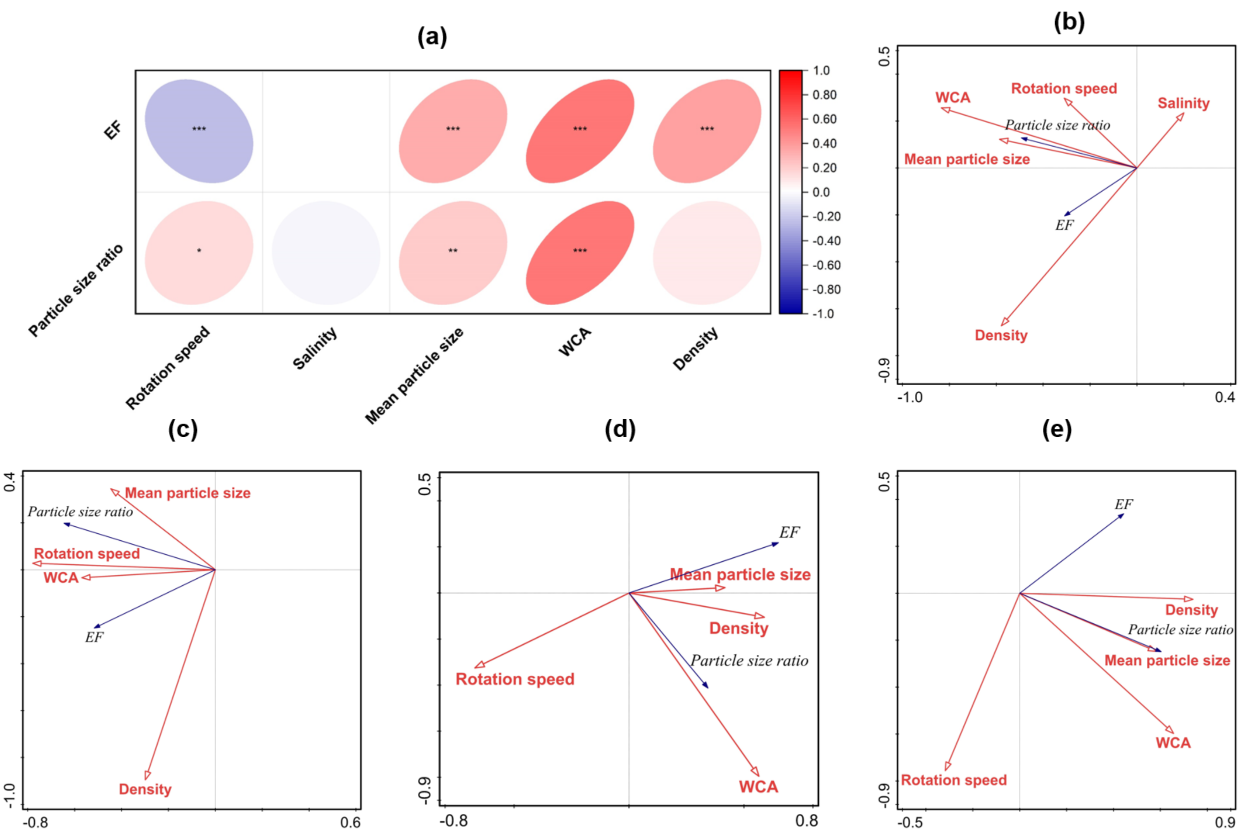

Figure 3-9. (a) Correlation analysis of MPs entrainment in ice and environmental and MPs characteristics (‘*’: $p < 0.05$; ‘**’: $p < 0.01$; ‘***’: $p < 0.001$). (b) The ordination plot showing the relationship between MPs entrainment behaviors in ice (blue arrows) and environmental and MPs characteristics (red arrows) based on RDA analysis. (c, d, e) The ordination plots with selected samples at 0, 10, and 34 PSU.

RDA was implemented for 0, 10, and 34 PSU in order to observe various environmental factors in terms of the responses at different salinity levels. The ordination plots are provided to present the results of the RDA as shown in Figure 3-9(c, d, e). The arrows in the ordination plots of RDA indicate the direction of the steepest increase of the corresponding parameter. The projection of the response arrow onto the line that is overlaid by the environmental variables arrow can roughly explain the correlation between environmental factors and response; the further the projection point is from the coordinate origin, the stronger the correlation is between the two variables. (Chen et al., 2021) Both rotation speed and WCA were found to be positively correlated to enrichment factor and particle size ratio at 0 PSU, with these two variables accounting for 52.9% and 28.3%, respectively, of total explained fitted variation. WCA and rotation speed were also the two most significant variables at 10 PSU, with these two factors accounting for 40.9% and 35.1%, respectively, of total explained fitted variation. However, the effects were completely different at 0 PSU. WCA was positively correlated to particle size ratio, but there was no discernible relationship between WCA and enrichment factor at 0 PSU; in reference to Figure 3-9d, the angle between the two arrows is almost a right angle. In addition, the enrichment factor was negatively associated with rotation speed at 10 PSU, which was the opposite of what was observed at 0 PSU. Moreover, compared to at 10 PSU, particle size ratio was more positively related to mean particle size at 34 PSU. Density, mean particle size, and rotation speed explained 41.5%, 27.1%, and 21.4%, respectively, of total explained fitted variation. The results of these statistical analyses demonstrate that the entrainment and enrichment of MPs in ice were governed by the MP properties and environmental factors acting in concert. In other words, the same MPs can exhibit completely different entrainment behaviors under different environmental conditions (e.g., salinity, turbulence intensity). For example, the entrainment of PE and of PTFE in ice was enhanced by salinity in calm water but was inhibited by salinity when turbulent flows were introduced.

3.2.6. Environmental Implications

Low temperatures can cause plastics to become more mechanically brittle, and ice formation and motion can pose mechanical impacts on plastics; both of these factors accelerate the fragmentation of plastics (Chubarenko, 2022). The transport of MPs in cold regions can be a critical pathway affecting their fate. The strong enrichment of MPs in sea ice has been observed in global cold regions, but there is a gap in the literature with respect to the possible mechanisms. This study explored the effects of MP properties and environmental factors on the entrainment and enrichment of MPs in ice, in particular considering the effects of turbulent flows, which have been proven to be an important condition for the entrainment of sediment during ice formation. Frazil ice forming in turbulent and supercooled conditions can aggregate with suspended particulate matter and carry it to the water surface through buoyancy. In our study, it was found that the effect of turbulence on the entrainment of MPs can vary considerably depending on the type of MP and the environmental conditions. High rotation speed in freshwater distinctively enhanced the entrainment of hydrophobic MPs in ice, this being attributable to the combined effects of frazil ice and air bubbles. The hydrophobic nature of these MPs caused them to attach to the water/air or water/ice interface. Thus, the MPs moved to the water surface due to enhanced buoyancy and were captured by growing ice. However, in saline water, high turbulence inhibited the entrainment of all MP types under study. The ice crystals formed a loose structure in saline water instead of congealing, and this allowed the exchange of MPs between ice and water, leading to the rapid expulsion of MPs from the ice. The enrichment factors of all the MPs under study increased in calm saline water compared to in calm freshwater. Ice formed in nearshore environments with high concentrations of MPs may serve as a carrier for transport of microplastics, temporarily storing and transporting them to remote areas. The entrapped MPs in ice may result in their redistribution in the marine environment and affect their interaction with marine biota. For example, MPs entrained in ice may interact with ice algae present in sea ice (Hoffmann et al., 2020). The production of EPS by ice algae can change the surface properties of MPs and affect how they become entrained in ice.

MPs can undergo a variety of physical and chemical aging phenomena in the natural environment that alter their surface properties. The surface properties of MPs can also be changed by biofilm caused by microbial colonization and natural organic matter. It should also be noted that this study only considered MP distribution in the early stages of ice formation. The ice-trapped MPs may be redistributed through various means, including brine networks in sea ice or the freeze-thaw cycle. These can be important factors influencing the behavior of MPs in ice. Overall, the entrainment and enrichment of MPs in ice can be critical pathways affecting their fate in cold regions, but knowledge in this field is limited at present, and thus further exploration is warranted.

Chapter 4. Role of Aquatic Dissolved Organic Matter in the Entrainment of Microplastics under Freezing Conditions

4.1. Materials and Methods

4.1.1. Chemicals and Materials

In the present study, two different types of polymer materials, polyethylene (PE) with a density of 0.97 g/cm^3 and polymethylmethacrylate (PMMA) with a density of 1.19 g/cm^3, were employed, representing the hydrophobic and hydrophilic MPs, respectively. PE samples with average particle sizes spanning from 8.0 to 10.0 μm (PE-1) and from 20.0 to 25.0 μm (PE-2) were acquired from Micro Powder Inc. (New York, USA). PMMA samples with mean particle sizes of 6.0 μm (PMMA-1) and 15.0 μm (PMMA-2) were obtained from Goodfellow Cambridge Ltd. (Huntingdon, UK). Humic acid sodium (HA) purchased from Sigma-Aldrich (Oakville, Canada) was used to simulate the effects of aquatic DOM. To eliminate the potential effects of any insoluble impurities in HA, on the measurement of MPs, the HA was dissolved in deionized (DI) water and then filtered using a 0.45 μm filter paper. The resulting solution was then subjected to a vacuum oven at 30 °C to prepare the HA solid used for the further experiments. Additional chemicals required for the study, such as Tween-20 and sodium chloride (NaCl), were likewise procured from Sigma-Aldrich (Oakville, Canada).

Reprinted with permission from *ACS EST Water* 2024, 4, 1, 256–267.

4.1.2. Interaction Experiment of Aquatic DOM and MPs

500 mg of MPs were combined with 200 mL of a 20 mg/L HA solution to create a mixed sample of MPs and HA. To explore the interactions between aquatic DOM and MPs under light and dark conditions, these prepared samples were subjected to UV radiation and dark conditions respectively. The samples that interacted with HA under UV radiation were accommodated in a UV chamber. This chamber was calibrated to emit UV light at a wavelength of 302 nm, with an intensity of 20 mW/cm^2, radiating from a position 5 cm above the liquid surface. In order to compensate for evaporation during the process, the samples in the UV chamber were periodically topped up with DI water, and also manually shaken twice a day. In parallel, identical samples were placed in a shaker under dark conditions, with the shaker set to a speed of 250 rpm. After different interaction durations (7, 14, and 28 days), the samples were removed from their respective environments. The samples taken out at 7, 14, and 28 days in the UV chamber were labeled as UV7, UV14, and UV28, respectively. The samples subjected to the dark conditions were labeled as HA7, HA14, and HA28. MP samples after interaction experiments were isolated from the mixture by passing them through a 0.45 µm filter paper. Subsequently, the filtered samples underwent multiple rinses with DI water. To eliminate any remaining moisture, the obtained MPs were subjected to a vacuum oven set at 30°C and left overnight. The weathered MPs samples were stored in a light-proof sealed glass containers prior to characterization and ice formation experiments.

Reprinted with permission from *ACS EST Water* 2024, 4, 1, 256–267.

4.1.3. Ice Formation Experiment

MP stock solutions were created by combining 30 mg of MPs with 1 L of DI water and a 30 μL solution of Tween 20 diluted tenfold. This was done to achieve a concentration of 0.0003% V/V (3 ppm), which improves the dispersion of the MPs. The MP stock solution was thoroughly mixed for 15 minutes using a high-speed blender. The MP concentration in all batch tests was 10 mg/L. To prepare a 10 mg/L dispersion of MPs, 50 mL of the MPs stock solution was combined with different amounts of 100 g/L NaCl and 500 mg/L HA stock solutions to regulate the salinity and DOM concentrations of the MP dispersion. DI water was then added to the mixture, bringing the total volume up to 150 mL in a beaker.

To inhibit the development of ice on the walls and base of the beakers, butyl sponge insulation was wrapped around 250 mL beakers that held 150 mL of the MP dispersion. Subsequently, the beakers and magnetic stir bars were relocated to an environmental chamber equipped with temperature control. They were subjected to a temperature of -10 °C for a duration of 150 minutes to mimic the process of ice formation. To achieve a uniform dispersion of MPs in each container at the start of the ice formation experiment, magnetic stirring was utilized at 500 rpm for 10 minutes. Following a 150-minute freezing period, the dispersion underwent an additional 5 minutes of homogenization using magnetic stirring. This step was taken to ensure that any MPs that were not entrapped by ice remained dispersed in the water and could be completely separated from the formed ice. After carefully separating the ice and residual water into separate beakers, they were sealed and left at room temperature overnight before taking measurements. The procedure of the ice formation experiment was modified from our previous study by Chen et al. (2023c). The MP concentration in ice and water was measured with LISST-200X (Sequoia Scientific, USA) using laser diffraction principles. The volume of melt ice (V_{ice}) was determined using a 50 mL graduated cylinder, and the volume of residual water after the ice formation experiments (V_{water}) was calculated. The enrichment factor of MPs (EF_{MP}) could thus be determined by measuring MP concentrations in ice (C_{ice}) and water (C_{water}) and employing the following equation:

$$EF_{MP} = \frac{C_{ice}}{C_{water}} \tag{1}$$

Additionally, the percentage of MPs entrapped in ice was calculated as:

$$P_{MP,ice} = \frac{C_{ice}V_{ice}}{C_{ice}V_{ice} + C_{water}V_{water}} \times 100\% \tag{2}$$

It is possible that some MPs were not recovered in the measurement due to flotation, settling, or adhesion to container walls. Therefore, the MP concentration of stock solution (C_{stock}) was measured before all tests to calculate the MP recovery rate using the following equation:

$$R_{MP} = \frac{C_{ice}V_{ice} + C_{water}V_{water}}{C_{stock}V_{stock}} \tag{3}$$

where, V_{stock} refers to the volume of MP stock solution used for each sample, which was 50 mL. All experimental conditions were replicated in triplicate to ensure accuracy. The standard error (SE) was then calculated to determine the variability and precision of the data, which was visually represented by incorporating error bars in the figures. One-way analysis of variance was implemented to identify whether the factor has significant impacts on the entrainment behavior of MPs in ice. Additionally, the statistically significance between two specific groups was identified using unpaired t-test.

4.1.4. MPs Characterization

The pristine and aged MPs underwent comprehensive characterization to investigate the influence of DOM on MP entrainment within ice. The mean particle size and size distribution of MPs were determined using the LISST-200X based on laser diffraction principles. Prior to measurement, MP dispersions were effectively homogenized through shaking and an ultrasonic bath. During the measurement process, the LISST collected data at a frequency of one measurement per second. Once the readings stabilized, a total of 20 measurements were taken to ensure accuracy and reliability. To evaluate the zeta potential of MP dispersions, a Malvern Zetasizer Nano ZS (Malvern, UK) was employed. The water contact angle (WCA) of pristine and weathered MPs was measured using an optical contact angle goniometer (AST Product, USA) to evaluate changes in the wettability of MPs after interacting with DOM. The crystal characteristics of MPs was assessed using a Philips X'pert Multipurpose X-ray diffraction (XRD) system (Philips Analytical, Netherlands). The full width at half maximum (FWHM) of characteristic peaks in XRD spectra was calculated using Origin (OriginLab, USA) and crystallite size was calculated using Scherrer equation accordingly. The alteration of the surface chemistry of MPs was measured using a Bruker INVENIO-S Fourier transform infrared (FTIR) spectroscopy (Bruker, USA). The surface morphology of MPs was observed using a Hitachi S-3400N scanning electron microscope (SEM; Hitachi, Japan).

4.2. Results and Discussion

4.2.1. Effects of Salinity on MP Entrainment

Previous studies have shown that ice formed in seawater contains a significantly higher amount of particle inclusions due to the formation of brine channels, which provide space for entrained particles (Barber et al., 2021; Smedsrud, 2001). However, the impact of salinity levels on the entrainment of different MPs has not been thoroughly investigated. Exploring the effects of varying salinity levels on MP behavior is of great importance, particularly in waters with salinity gradients, such as estuary areas. The indicators included enrichment factors, percentage of MP incorporated into the ice, mean particle size in both water and ice, as well as MP recovery rate. Figure 4-1 illustrates the influence of salinity levels on these indicators.

Similar trends in enrichment factors were observed for the same MP with different particle sizes under varying salinity levels. However, notable differences were observed in the entrainment behaviors between PE and PMMA MPs. The enrichment factors of PE MPs exhibited a sudden increase from 0.64 to 1.71 for PE-1 and from 0.88 to 2.12 for PE-2 when the salinity level was increased from 0 to 2 practical salinity unit (PSU). However, further increases in salinity did not lead to additional enhancement in PE entrapment within the ice. In fact, a slight decline in the enrichment factors was observed. Despite PE MPs being buoyant and naturally floating on the water surface, which facilitates their capture by ice, the absence of brine pockets in freshwater ice leads to the expulsion of MP particles from growing ice crystals.

Higher salinity led to denser brine networks, and the loose ice structure facilitated the expulsion of hydrophobic PE MP from the ice. This expulsion of PE MP can be the main factor contributing to a slight decline in enrichment factors when increasing salinity from 2 PSU for both PE-1 and PE-2. However, the enrichment factors for PMMA MP gradually increased with the increasing salinity from 0 to 35 PSU. It can be caused by the hydrophilic surface of PMMA MP which demonstrates a greater affinity for ice surface compared with hydrophobic PE (Lee, 2019). In the presence of high salinity, an increased number of brine channels is formed, offering additional opportunities for PMMA entrapment rather than expulsion like hydrophobic PE.

The enrichment factors of PMMA at varying salinity levels were all much lower than PE, which can be contributed to the difference in density. PMMA is a non-buoyant polymer with density of

1.2 g/cm^3. However, plastic particles with buoyancy, such as PE, that are not initially trapped in ice tend to accumulate at the interface between the ice and water beneath the ice cover. The buoyant forces exerted on these particles push them towards the advancing ice fronts, increasing the likelihood of their incorporation into the freezing ice (Mountford and Morales Maqueda, 2021; Yemmou et al., 1991).

Additionally, the effects of particle size on the entrainment factors of PE and PMMA were found to be opposite. For PE, the enrichment factors of PE-2, which had a larger mean particle size, were all higher than those of PE-1 at varying salinity. However, for PMMA, PMMA-1 had higher enrichment factors than PMMA-2 across the salinity range of 2 to 35 PSU. The critical velocity was used to define the speed of ice front growth at which foreign particles can be entrapped (Lipp et al., 1990). Generally, larger particle sizes can reduce the critical velocity, indicating that larger particles have a higher probability of being entrapped by the growing ice front (Asthana and Tewari, 1993; Körber et al., 1985). However, in the case of PE and PMMA, the difference in buoyancy between the two materials resulted in contrasting effects of particle size on the enrichment factors.

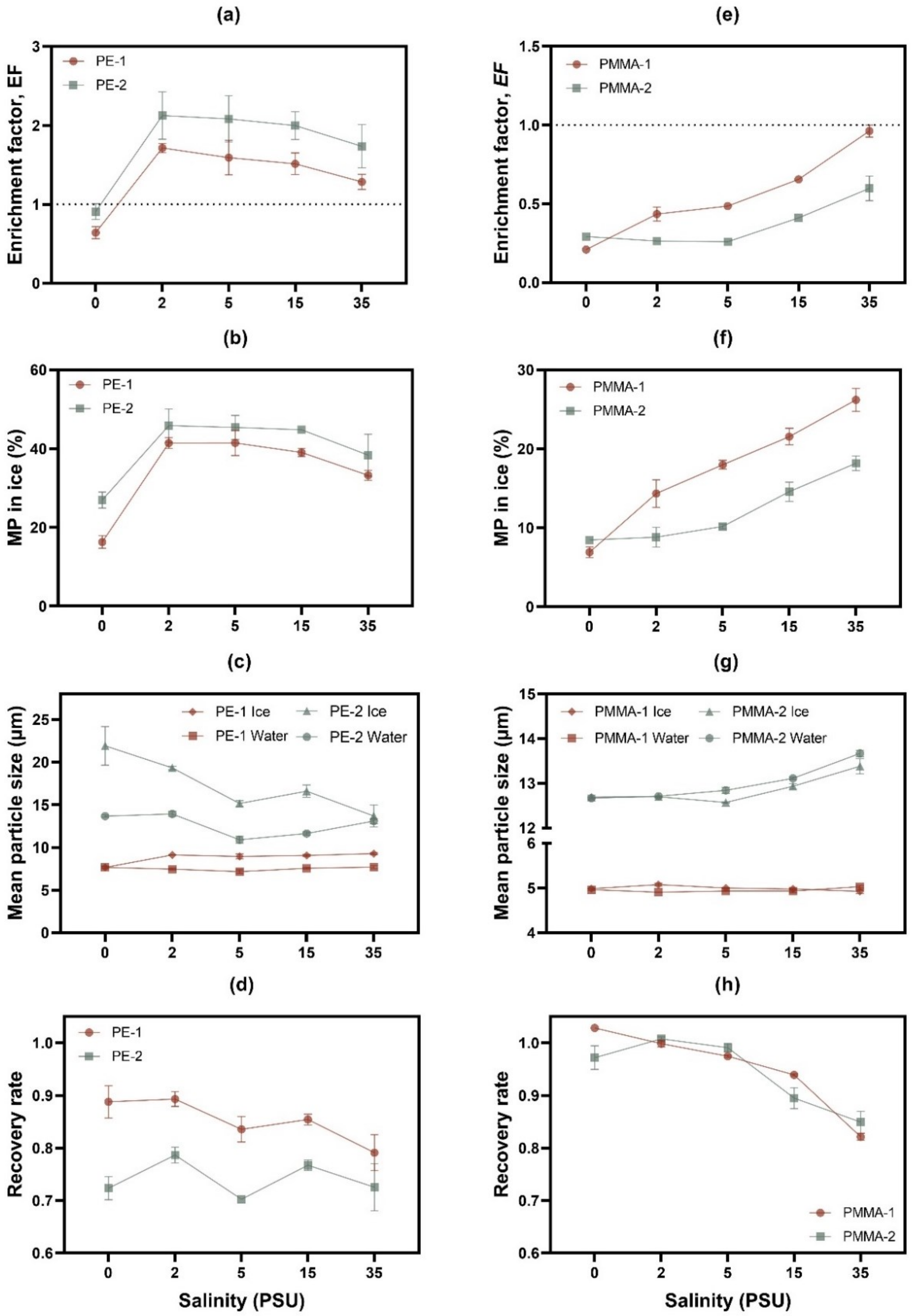

Figure 4-1. Effects of salinity on enrichment factors, percentage of MP in ice, mean particle size, and recovery rate for PE (a–d) and PMMA MPs (e–h). The dashed lines in (a) and (e) denote an enrichment factor of 1, indicating that the MP concentration is the same in both ice and water.

The higher sedimentation speed of non-buoyant PMMA particles with larger sizes makes it more difficult for them to be trapped in the ice grown from the surface, in contrast to smaller particles which can remain suspended for a longer period (Andral et al., 1999). By observing the mean particle size in ice and water (Figure 4-1c and 4-1g), both PE-1 and PE-2 had larger mean particle sizes in ice than in water. However, the mean particle size in water was relatively larger for PMMA-2. The MPs with larger particle size in water were more affected by buoyant force. Therefore, the non-buoyant PMMA-2 had a larger mean particle size in water than in ice, while the opposite was true for PE, which has buoyancy.

Regarding the effect of salinity on the mean particle size, both PE-1 and PMMA-2 showed an increase in mean particle size with increasing salinity levels. This can be attributed to the elevated ionic strength, which leads to the compression of the electric double layer and subsequently destabilizes the dispersion system (Feng et al., 2022b). As a result, particle aggregation occurs, leading to an overall increase in the mean particle size. A decrease in recovery rate was also observed for them with the increased salinity. Destabilized particles exhibited accelerated settling, floating, or adherence to the walls of the beaker, consequently leading to a decrease in the recovery rate (Figure 4-1d and 4-1h) (Yang et al., 2022b).

While the salinity level had no significant impact on the mean particle size of PMMA-1 in both ice and water, a decrease in the recovery rate of PMMA-1 was still observed. Additionally, the disparity in mean particle size between ice and water was not significant, attributable to the relatively small and uniform particle size of PMMA-1. PMMA exhibits a higher overall recovery rate compared to PE MPs due to its hydrophilic nature. The hydrophobic interaction of PE makes them more prone to aggregation and adhesion to the walls of the beaker (Sharma et al., 2021). Furthermore, the MP dispersion prepared using PE-2, which has larger particle sizes, presents challenges in achieving uniform distribution. The larger particles tend to float out of the system, making it difficult to recover them during quantification measurements.

4.2.2. Effects of Aquatic DOM on MP Entrainment

DOM is extensively found in aquatic ecosystems, encompassing both marine and freshwater environments (Hashemi Safaei et al., 2022). It consists of a complex mixture derived from the decomposition products of plants, bacteria, and algae (Khadanga et al., 2022). In freshwater environments, humic substances are predominant components, accounting for approximately 50–90% of DOM. Their concentration typically ranges from 0.2 to 30 mg/L (Black et al., 1996). Additionally, the input of terrestrial DOM from rivers into the ocean makes humic acid an important fraction in estuarine and coastal environments. The presence of DOM in water can enhance the stability of suspended particles by reducing aggregation through electrostatic and steric effects (Philippe and Schaumann, 2014). DOM can significantly alter the environmental behaviors of MPs, depending on the concentration and composition of DOM (Abdurahman et al., 2020). Therefore, the study examined the effects of HA in both freshwater and 35 PSU saltwater conditions. The results of the investigation are illustrated in Figure 4-2.

The enrichment factors for both PE and PMMA in saltwater were significantly higher compared to freshwater, primarily due to the formation of brine channels, as discussed in the previous section. While the impact of HA on entrainment was not as pronounced as salinity, it still exerted influence on the entrainment of MPs in ice, especially for PE. Interestingly, the role of HA concentration in the enrichment of PE MP differed between freshwater and saltwater. In freshwater, the enrichment factor of PE-1 increased with higher HA concentrations. Without HA, the enrichment factor was

0.64 (SE: 0.08), whereas at a concentration of 20 mg/L HA, it increased to 0.83 (SE: 0.04). However, in 35 PSU saltwater, HA inhibited the entrainment of PE-1 in ice; the enrichment factor decreased from 2.09 (SE: 0.22) to 1.41 (SE: 0.1) when 2 mg/L HA was added.

Owning to large number of active functional groups, HA exhibits amphiphilic properties, allowing it to form pseudomicelles in aqueous solution (Urdiales et al., 2018; Von Wandruszka, 2000). Therefore, HA molecules adsorbed on the PE MP can decrease its hydrophobicity; the WCA of PE decreases with interaction with the HA solution over time, and this is further discussed in the following section. The decreased hydrophobicity enhances the affinity of the PE MPs for ice, making them easier to be embedded within the ice matrix (Chubarenko, 2022; Lipp et al., 1990). Therefore, the DOM increased the enrichment factor of PE in freshwater. In the case of MPs entrapped in ice formed in saltwater, they are primarily located within the brine channels. The high ionic strength within these channels can destabilize and aggregate the PE particles, facilitating their physical entrapment within the brine network (Pradel et al., 2021b). However, the addition of HA can counteract this effect by providing electrostatic repulsion and steric hindrance, thereby stabilizing the MPs during the ice formation process (Pradel et al., 2021a). This facilitates their expulsion from the ice structure. As the concentration of HA increases, the mean particle size of PE-1 in ice formed in saltwater with a salinity of 35 PSU decreases, and the recovery rate of MPs increases. For example, with an increasing HA concentration from 0 to 20 mg/L, the mean particle size of PE-1 in ice formed in saltwater decreased from 8.7 (SE: 0.09) to 8.0 (SE: 0.13).

Despite lacking statistical significance ($p>0.05$), there was a slight improvement observed in the enrichment factors for PMMA-1 when exposed to HA in both freshwater and 35 PSU saltwater. The enrichment factors for PMMA-1 were 0.21 (SE: 0.02) and 0.25 (SE: 0.03) at 0 and 20 mg/L

HA in freshwater, respectively, and 0.83 (SE: 0.02) and 0.87 (SE: 0.01) in saltwater. The primary reason for the enhanced entrainment of PMMA-1 by the increase in HA can be attributed to its stabilization effects on the non-buoyant PMMA MPs. The higher electrostatic repulsion force caused by HA results in a more stable colloidal system, leading to more entrapment of particles by the growing ice front (Chen et al., 2022c). Additionally, it can be found that the recovery rate for PMMA-1 in saltwater was significantly improved while increasing HA concentration.

Another interesting finding is that the mean particle size for PE-1 increased in the ice formed in freshwater with the addition of higher concentrations of HA. The mean particle size within the ice was measured at 7.67 (SE: 0.14) in the absence of HA, and it notably increased to 9.28 (SE: 0.12) at a HA concentration of 20 mg/L. The absence of porous brine networks in the freshwater ice resulted in the physical compression of HA and MPs, amplifying the formation of aggregate and contributing to the overall increase in particle size (Pradel et al., 2021b). Moreover, the larger particle size made them more prone to instability, leading to a reduction in the recovery rate of PE-1 in freshwater as the HA concentration increased. Similarly, Pradel et al. (2021b) assessed the influence of sodium alginate (SA) on the entrapment of nanoplastics and found that the addition of SA decreased the recovery of particles frozen in DI water due to the rapid sedimentation of the increased plastic particle size.

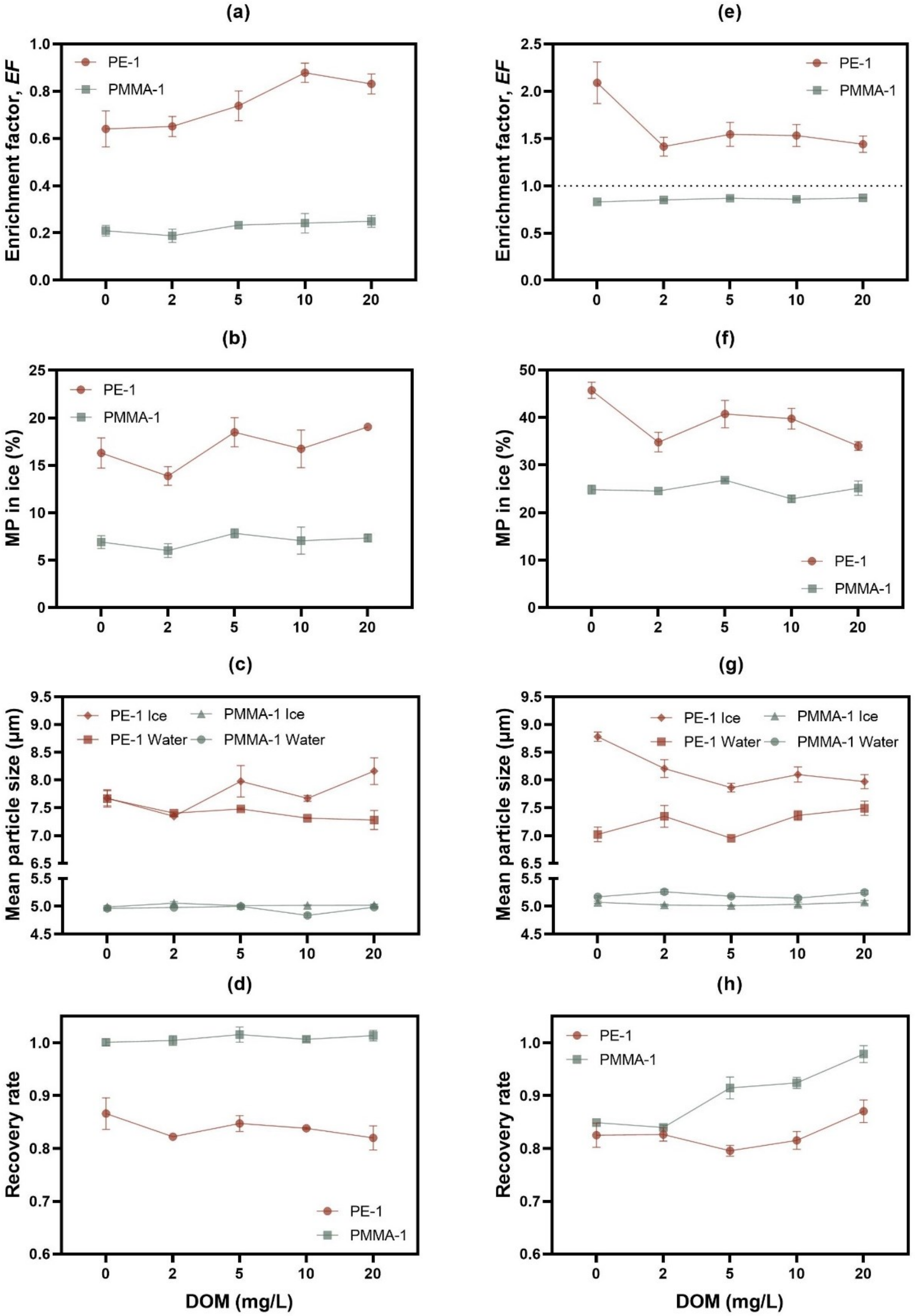

Figure 4-2. The effect of DOM on enrichment factors, percentage of MP in ice, mean particle size, and recovery rate of PE-1 and PMMA-1 at 0 (a–d) and 35 PSU (e–h).

4.2.3. Characterization of MPs after Interaction with Aquatic DOM

Various techniques were applied to characterize the physical and chemical characteristics of pristine MPs as well as MPs subsequent to the interaction with HA. The surface structure of both unaltered and aged MPs was examined using SEM (Figure 4-3). The PE MP, after 28 days of interaction with HA, exhibited smoother edges compared to the pristine and UV28 PE. This smoothening can be credited to physical abrasion caused by the shear force introduced by shaker (Feng et al., 2022a). However, the PE MPs in HA under UV exposure for 28 days did not show significant changes on the surface, as continuous shaking was not introduced in this scenario. These findings are consistent with prior research conducted by Feng et al. (2022a), which suggested that UV exposure not only fails to increase the surface roughness of MPs but also contributes to surface smoothing through chemical stripping.

FTIR analysis was conducted to investigate potential changes in chemical bonds and composition. The FTIR spectra of PE and PMMA MPs were demonstrated in Figure 4-4 and Figure 4-5. Following a 28-day interaction with HA under both dark and UV light conditions, PE-1 and PE-2 displayed no significant alterations in their FTIR spectra. However, weak peaks near 3700 cm^{-1} corresponding to O-H stretching were observed for UV28 PE-2, indicating the possibility of photodegradation occurring specifically in PE-2 (Cai et al., 2023; Lu et al., 2017). This observation can be attributed to the larger particle size of PE-2 compared to PE-1, as the reduced surface area makes the particles more susceptible to exposure under light.

In contrast, the FTIR analysis of PMMA MP exhibited the emergence of new peaks after exposure to the weathering conditions. All PMMA samples displayed new peaks at wavenumbers of 668, 1541, and 1558 cm^{-1}, although the absorbance levels varied among the samples. The emergence of these new peaks can be ascribed to the adherence of HA onto the surface of PMMA. The peak at 668 cm^{-1} can be caused by noise from gas-phase CO_2 or the O-H out of plane bending in C-OH alcoholic groups which are common functional groups found in HA (Wu et al., 2014; Yuan and Teja, 2011). Additionally, the peaks observed at 1541 and 1558 cm^{-1} can be linked to the aromatic C=C stretching vibrations in aromatic rings or other aromatic moieties present in HA (Stevenson, 1994).

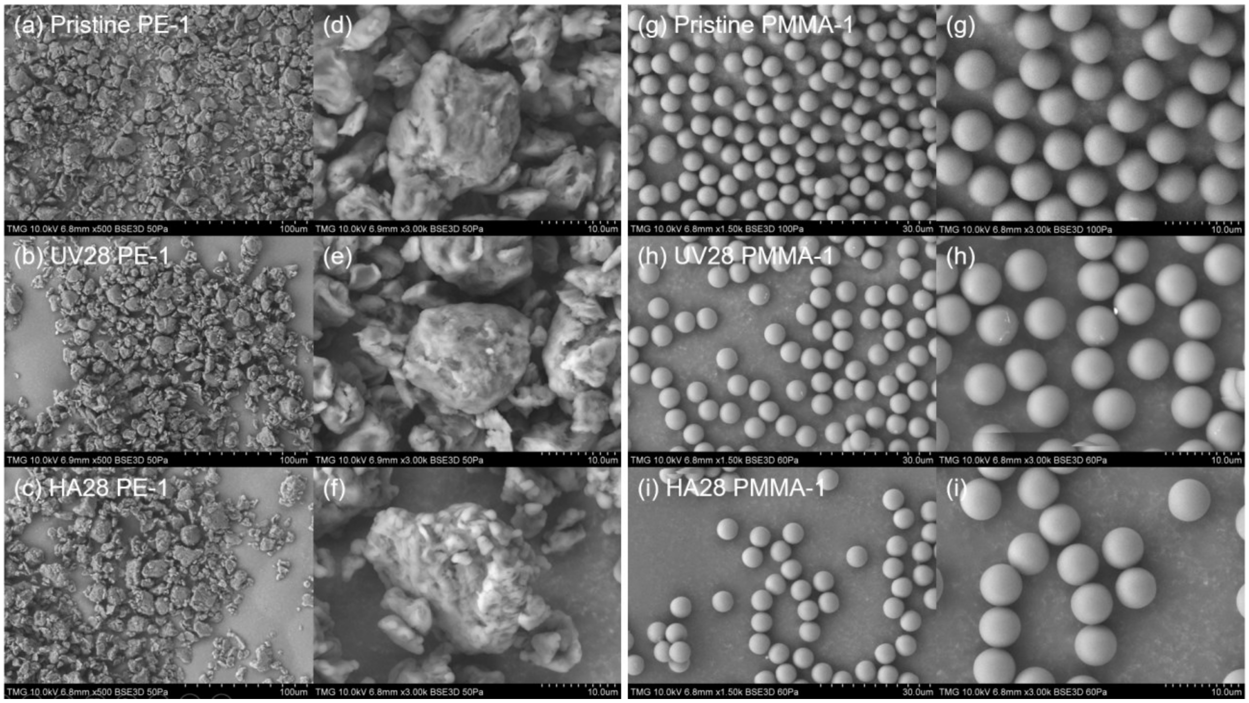

Figure 4-3. SEM images of (a–f) PE-1 and (g–i) PMMA-1 MP.

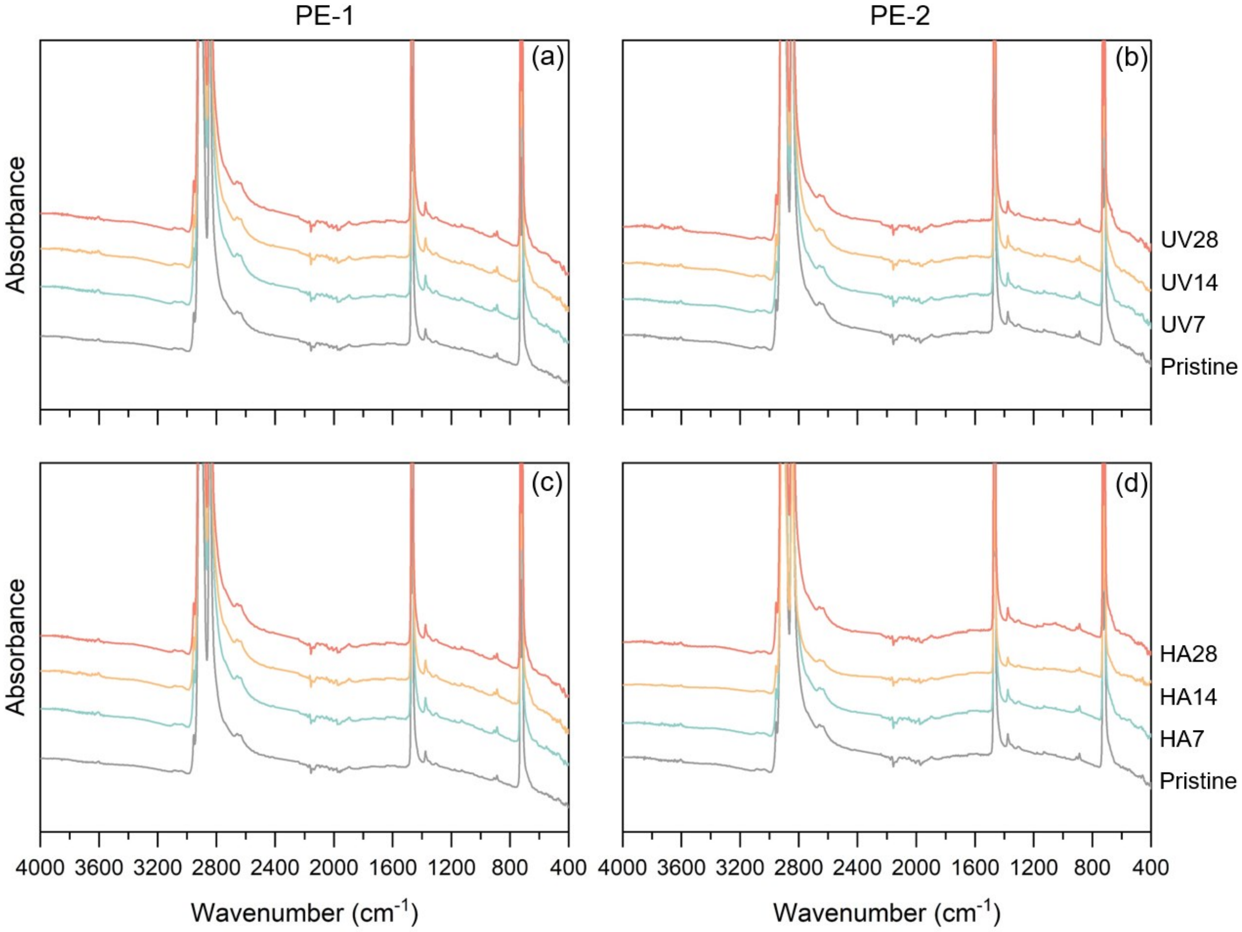

Figure 4-4. FTIR spectra of (a, c) PE-1 and (b, d) PE-2 after interaction experiments with HA under light and dark conditions.

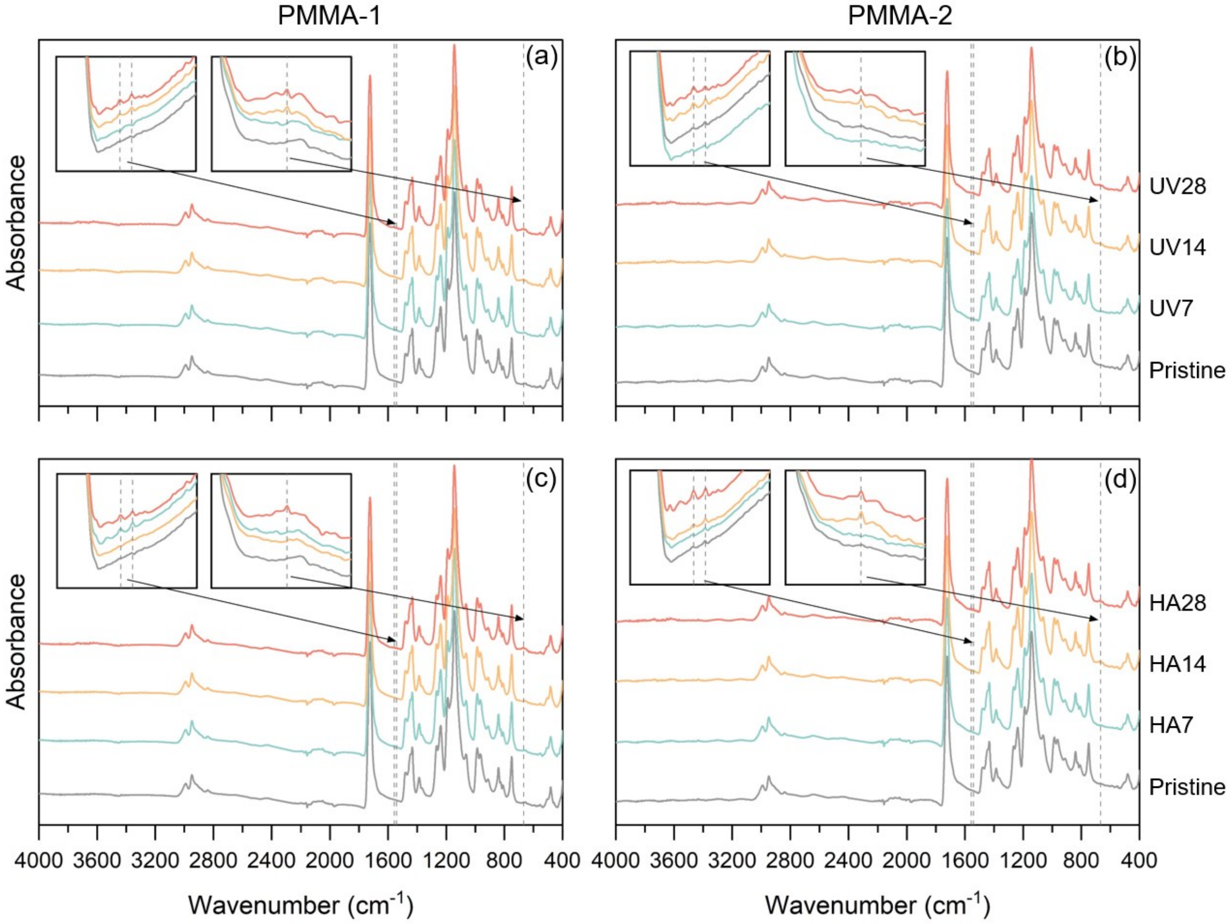

Figure 4-5. FTIR spectra of (a, c) PMMA-1 and (b, d) PMMA-2 after interaction experiments with HA under light and dark conditions.

XRD analysis was used to assess the crystalline structure of the polymer after 28-day interaction experiment and the results are shown in Figure 4-6. PE is a partially crystalline solid and PMMA is an amorphous polymer (Ruiz et al., 2011). Consequently, the XRD spectra of PE exhibit a distinct peak and a lower signal-to-noise ratio compared to PMMA. The FWHM is utilized to describe various characteristics of crystalline structures, including crystallite size and crystallographic parameters. The FWHM values for the primary peaks observed in the XRD spectra of PE ($2\theta = 21.3°$ and $23.7°$) and PMMA ($2\theta = 14.8°$ and $30.6°$) are presented in Figure 4-6b and 4-6d, respectively.

For PE, the XRD analysis revealed no noticeable differences between the UV28 PE and the pristine PE, but an increase in FWHM was observed for HA28 PE. This increase in FWHM suggests a reduction in crystallite size and an increase in lattice strain (Menzel et al., 2022). The physical abrasion resulting from the shaking process in HA28 introduced strain and disrupted the crystalline structure. The crystallite size of HA28 PE decreased from 13.79 nm to 12.86 nm at $2\theta = 21.3°$ and from 11.17 nm to 10.58 nm at $2\theta = 23.7°$. Similarly, the FWHM values of PMMA exhibited an overall increase following the interaction experiments. Specifically, the FWHM values for pristine, UV28, and HA28 PMMA at $2\theta = 14.8°$ were 6.63, 6.63, and 6.49, respectively. At $2\theta = 30.6°$, the FWHM values were 6.23, 6.36, and 6.65 for pristine, UV28, and HA28 PMMA, respectively.

Zeta potential measurements were employed as a technique to evaluate the dispersion stability of MPs. The same dispersion protocol used for the ice formation experiments was replicated to disperse the MPs, and zeta potential measurements were conducted in the absence of HA (Figure 4-7a) and 10 mg/L of HA (Figure 4-7b), respectively. The dispersion of pristine PE MPs exhibited relatively stable characteristics, with zeta potentials of −41.3 mV and −27.0 mV for PE-1 and PE-

2, respectively. In contrast, pristine polymethyl methacrylate PMMA MPs displayed lower absolute value of zeta potentials of −20.3 mV and −16.5 mV for PMMA-1 and PMMA-2, respectively, indicating a relatively less stable dispersion than PE MPs.

The absolute value of zeta potential of all MPs after HA28 treatment was significantly increased, which can be attributed to the increased electron density resulting from the adsorption of HA on the MPs surface (Luo et al., 2022). However, PMMA after UV28 treatment did not have the significant increase in the absolute value of zeta potential and UV28 PE-1 even showed a decline. UV radiation could eliminate the HA through the photodegradation, thus inhibiting the increase in surface charge due to HA adsorption (Kulovaara, 1996). Compared with HA28, the absolute values of zeta potential of MPs after UV28 treatment were significantly increased when adding 10 mg/L HA, suggesting that the surface is relatively unsaturated with sites for HA adsorption.

WCA was measured for the MPs after the weathering processes to evaluate the impact on the wettability. Pristine PE and PMMA are hydrophobic and hydrophilic polymer; the WCA of pristine PE-1, PE-2, PMMA-1, and PMMA-2 was 138.7°, 143.3°, 62.5°, and 51.9°, respectively. However, the PE and PMMA showed different impact after interacting with HA. The WCA of PE-1 and PE-2 was reduced to 126.3° and to 119.7° after UV28 interaction process. In contrast, the wettability of PMMA was changed from hydrophilic to hydrophobic for UV7, and the hydrophobicity was continued to be increased with treatment duration. The WCA of UV28 PMMA-1 and PMMA-2 was 122.4° and 120.2°. Similarly, the WCA of PE and PMMA decreased and increased respectively after HA28 treatment.

peaks.

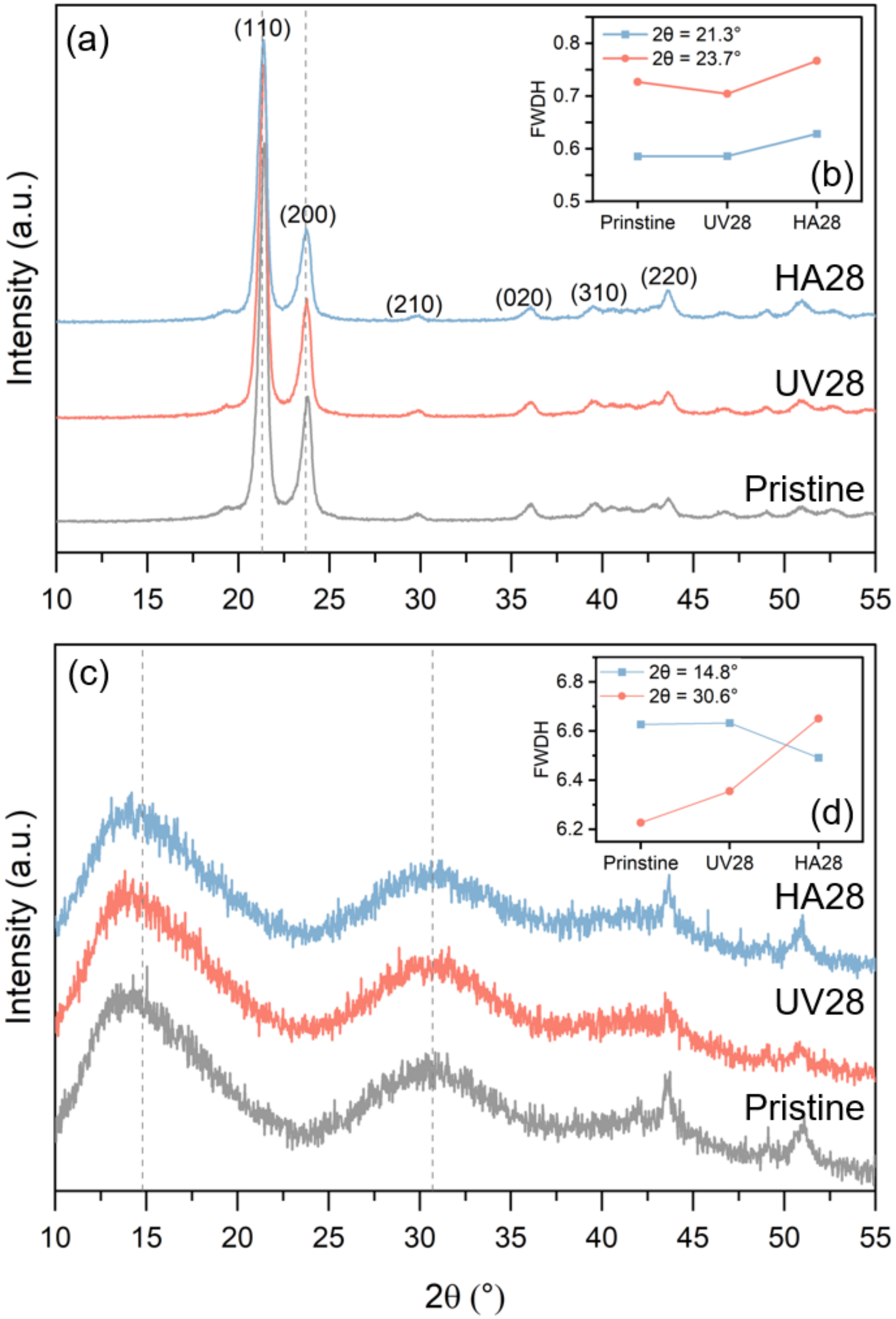

Figure 4-6. XRD spectra of (a) PE-1 and (c) PMMA-1 and (b, d) FWDH values of the characteristic peaks.

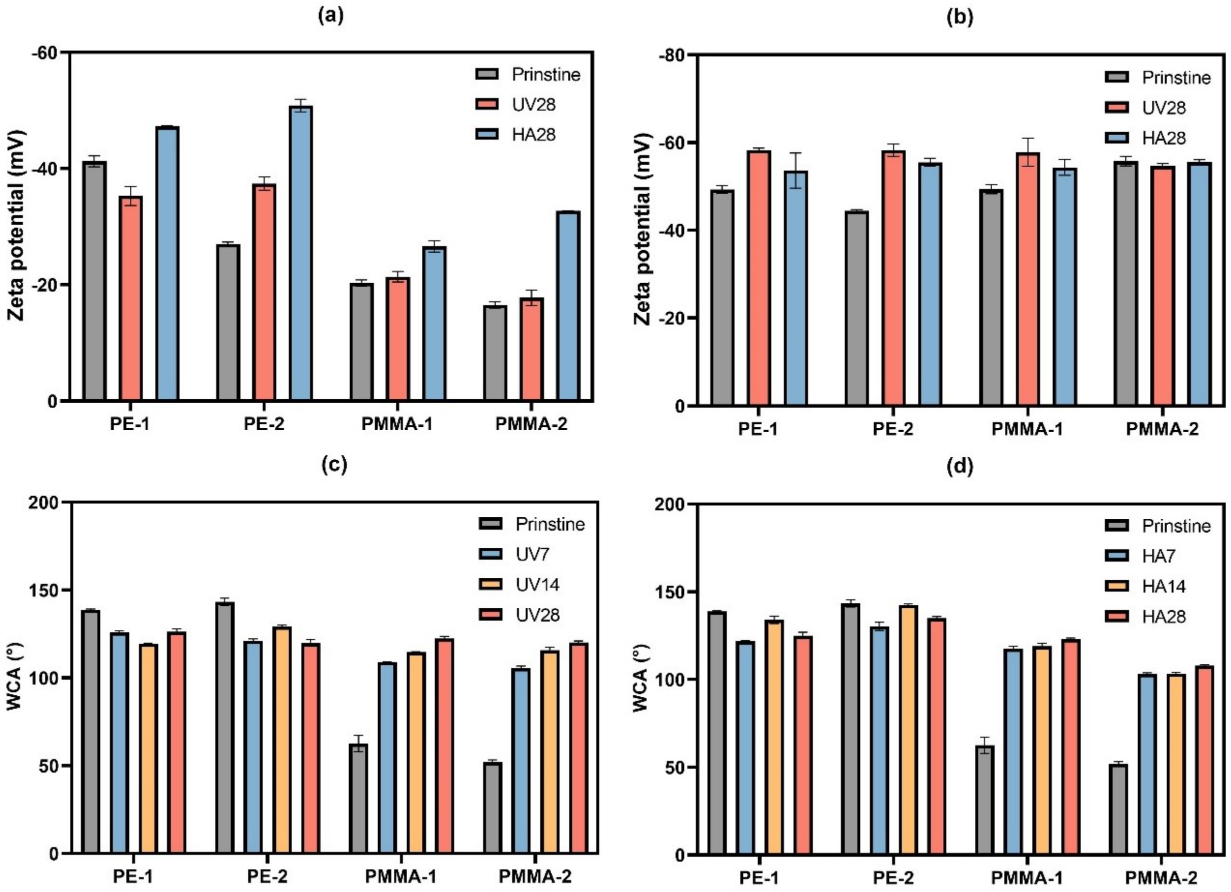

Figure 4-7. Zeta potential of MPs in DI water (a) and 10 mg/L HA (b). Changes in WCA of MPs after UV light exposure (c) and dark conditions (d).

The decrease in the hydrophobicity of hydrophobic MP due to DOM has been widely observed in previous studies. Chen et al. (2023a) evaluated the WCA of polystyrene (PS) MP with different sizes after interacting with DOM under dark and light conditions for 7 days and found that all MPs showed a decrease in the hydrophobicity. HA contains numerous hydrophilic groups such as carboxyl and phenolic groups. The adsorption of HA molecules on the PE surface after interaction experiment could be increase its affinity for water. Meanwhile, DOM can oxidize the MP surface, leading to the appearance of hydroxy groups. This has been observed in the FTIR spectra after the interaction experiment, although the changes in peaks depend on the MP and treatment (Figure 4-4 and Figure 4-5).

Relatively few studies have been conducted on the behavior of hydrophilic MP especially the interaction with DOM. Our findings highlight a distinct behavior of hydrophilic MPs, exemplified by PMMA, in contrast to hydrophobic PE when interacting with HA. Notably, the wettability of PMMA transitioned from hydrophilic to hydrophobic following exposure to HA. As an amphipathic substance, HA comprises both polar and non-polar moieties. Its adsorption onto hydrophilic particle can enhance the non-polar fractions on the surface, thereby reducing affinity of the materials for water (Volikov et al., 2016). This phenomenon of increased hydrophobicity in hydrophilic particles following HA adsorption is well-documented. For instance, Kholodov et al. (2018) discovered that HA adsorption onto clay particles, including kaolin and montmorillonite, significantly elevated the WCA, in other words, amplifying hydrophobicity.

The characterization of MPs after the interaction experiments, conducted under dark and UV light conditions, revealed modifications in their surface properties. These changes were primarily attributed to the adherence of humic acid to the surfaces of the MPs. Additionally, the interaction processes resulted in observable alterations in the physical properties of the MPs, such as physical damage and a reduction in crystallite size. However, no significant changes in the oxidation and chemical properties of the MPs were detected after the interaction with HA under both dark and UV light conditions.

4.2.4. Effect of the Interaction on MP Entrainment in Ice

In an effort to evaluate the impact of HA interaction on the entrainment of MPs within ice, a series of ice formation experiments were conducted. The results, as illustrated in Figure 4-8, indicate an enhancement in the enrichment factor and percentage in ice of PE MPs following interaction with HA under both experimental conditions—UV28 and HA28. Notably, the increase in enrichment factors was more pronounced for PE-2 compared to PE-1. Specifically, the enrichment factors of UV28 and HA28 in PE-1 increased by 7% and 21% respectively, relative to the pristine sample. For PE-2, these increases were even more substantial, with rises of 27% and 37% respectively. This differential response between PE-1 and PE-2 could be attributed to the larger particle size of PE-2, which results in a lower specific surface area. This in turn facilitates more extensive interaction with HA molecules compared to PE-1.

HA28 treatment showed a greater improvement in the entrainment of both PE-1 and PE-2 compared to UV28, although the results were not statistically significant. The physical abrasion caused by shaking in the HA28 treatment could potentially lead to more damage to the surface morphology of the PE, as depicted in Figure 4-3. Additionally, the enhancement on the ice entrapment of MP can result from an increase in the mean particle size of PE due to the formation of the aggregate after interacting with HA, both in the case of UV28 and HA28 treatments. Notably, PE MPs treated with HA28 exhibited a higher mean particle size compared to those treated with

UV28. Specifically, the mean particle sizes measured using LISST-200X for pristine, UV28, and HA28 treated PE-1 were 7.43 µm, 7.61 µm, and 8.38 µm, respectively. For PE-2, the corresponding values were 16.04 µm, 17.03 µm, and 18.58 µm, respectively. The increase in particle size can be attributed to the formation of a DOM layer on the surface of PE. Additionally, the adsorption of DOM onto the particles can introduce additional charges when they are in water. This leads to the stabilization of larger particles in suspension, preventing them from settling or floating, and consequently increasing the measured mean particle size. The photodegradation of HA due to UV light exposure in UV28, and the increased interaction with HA resulting from shaking in HA28, led to a greater increase in mean particle size in the HA28 treatment compared to UV28. Furthermore, the higher absolute value of the zeta potential observed in HA28-treated PE-1 and PE-2 also suggests the adsorption of more HA, which provides more electron density on PE. The influence of HA on the particle size of MP was observed by Chen et al. (2018b) as well. The formation of significantly widens the particle size distribution and increase the particle size of PS MP after interacting with HA.

Compared to PE MPs, the entrainment of PMMA-1 and PMMA-2 in ice after 28 days of interaction with HA did not show significant differences. The enrichment factor of pristine PMMA-1 was 0.84, while for UV28 and HA28 treated PMMA-1, it was 0.9 and 0.85, respectively. Similarly, for PMMA-2, the enrichment factor for pristine, UV28, and HA28 was 0.55, 0.55, and 0.54, respectively. Similarly, the mean particle size of PMMA MPs did not show the statistically significant differences after the 28-day interaction for both conditions. The increased electron density provided by HA contributes to the improved stability of non-buoyant PMMA particles in water. Additionally, minor surface damages on the particle surfaces may have played a role in the slight enhancement observed in the entrapment of PMMA MPs in ice after the treatment with UV.

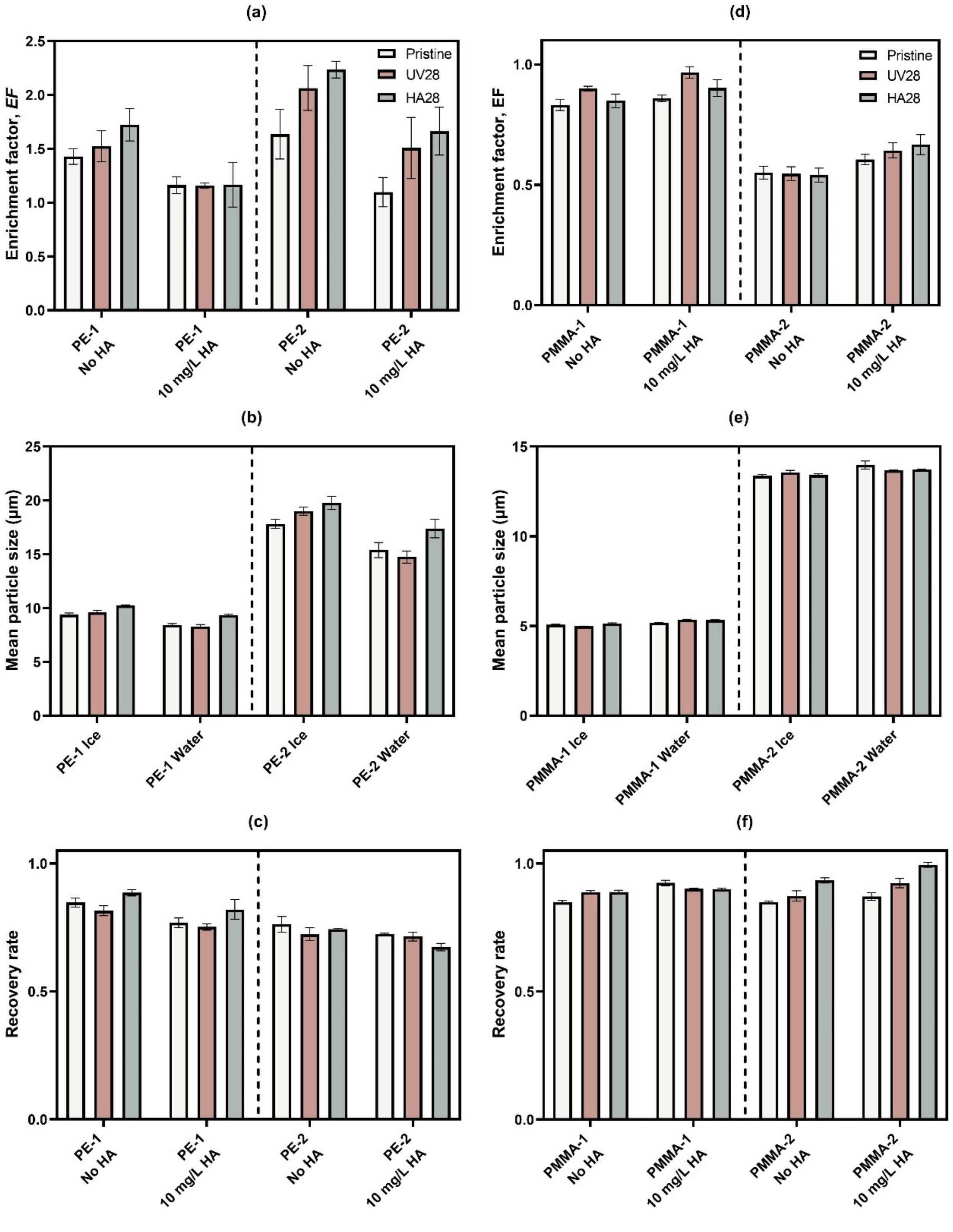

Figure 4-8. The enrichment factor, mean particle size and recovery rate of pristine, UV28, and HA 28 (a–c) PE and (d–f) PMMA.

The impact of DOM on the treated MPs was examined as well. Specifically, the entrainment behaviors of the MPs in ice were examined under two conditions: without HA and with 10 mg/L HA. The findings demonstrated the impact of HA on the treated MPs was similar to that observed for pristine MPs, as discussed in section 3.2. With the addition of 10 mg/L HA, both UV28 and HA28 PE exhibited a decrease in the enrichment factor and MP percentage in ice. In contrast, treated PMMA showed an increase in entrainment in ice when HA was added. In terms of the recovery rate, as depicted in Figure 4-8c, it was found that all PE MPs exhibited a decline in the recovery rate when 10 mg/L HA was added, suggesting the aggregation between PE MP and HA affected their stability. It was found that the sedimentation rate of hetero-aggregation increased significantly while nanoplastics aggregated with plastics particles (Chen et al., 2018a). However, further increasing the HA concentration to 20 mg/L showed a significant improvement in the recovery rate of pristine PE-1 and PE-2 as shown in Figure 4-8c. This may be attributed to higher surface charges provided by higher concentration of PE MPs, stabilizing the PE dispersions.

The recovery rate of PMMA MPs increases with the addition of HA, which is in contrast to PE MPs where the recovery rate declines. This difference can be attributed to the varying hydrophobicity of these two polymers. It has been observed that hydrophobic interactions are a major driving factor for the adsorption of DOM on MPs. The change in particle size between PE and PMMA after interaction experiments supports this observation: The mean particle size of PE significantly increases after interaction experiments, but there is no significant difference for PMMA. The stronger hydrophobic interaction between PE and the hydrophobic fraction of HA leads to more formation of hetero-aggregation, which in turn increases the mean particle size (Chen et al., 2018a; Chen et al., 2018b). On the other hand, the interaction between hydrophilic PMMA and HA does not form hetero-aggregation. The extra charges provided by HA increase the dispersion stability, which in turn increase the recovery rate of PMMA.

The notable variations in the enrichment factor and recovery rate observed in PMMA and PE following ice formation experiments, combined with the divergent impacts observed after their interaction with HA, highlight the critical role of the physicochemical properties of MPs in their fate within cold aquatic environments.

4.2.5. Environmental Implications

The escalating quantities of plastic waste discharged into marine ecosystems have inevitably led to the increase in MPs found in the cold regions, including ice and water bodies. A particularly alarming trend is the strikingly high concentration of MPs in Arctic sea ice, the levels of which have been observed to be two orders of magnitude greater than in the sub-ice water. MPs undergo a series of natural weathering processes in the environment, including physical abrasion and exposure to UV irradiation. These processes significantly alter the surface properties of MPs, thereby affecting their behavior within the environment. Indeed, various studies have found that the presence of aquatic DOM can either accelerate or inhibit the aging of MPs, acting as ROS generators or scavengers and having a light-shielding effect. It should be noted that the impact of aquatic DOM on the aging process of MPs is highly dependent on the properties and types of both aquatic DOM and MPs involved. This interaction can significantly influence MPs' behavior in colder regions, an area of research that has, thus far, received insufficient attention.

Our study investigated the effects of HA on the properties of MPs through a 28-day interaction experiment conducted under both UV and dark conditions. The implications of the alteration in

MPs properties on their incorporation into ice were also explored in an ice formation experiment. No significant oxidation was observed in MPs after the interaction experiments under either condition. However, the presence of HA on the MPs after the interactions was confirmed. The HA provided additional surface charges, leading to an increase in zeta potentials for all MPs tested after the interaction experiment. The interaction with HA had different impacts on the two types of MPs used in our study, PE and PMMA. PE exhibited an increase in mean particle size after the interaction experiments, presumably due to aggregation with HA through a hydrophobic effect. However, no change in particle size was observed in PMMA. The presence of HA also reduced the recovery rate of PE MPs during the ice formation experiment which was caused by the instability of dispersion due to increased particle size. Additionally, the wettability showed a different alteration for PE and PMMA after the interaction experiments. The hydrophobic MP—PE experienced a decrease in its WCA, indicating the increased hydrophilicity. In contrast, PMMA displayed an opposite behavior, with its WCA significantly increasing and transitioning from hydrophilic to hydrophobic. Furthermore, the entrapment of MPs in ice was noted improved post their interaction with HA, due to surface damage caused by physical abrasion and UV radiation.

These findings underscore the critical role that the inherent properties of MPs play in determining their environmental behavior. These properties can significantly impact their interactions with other natural components in the environment, thereby influencing their behavior in the cold environment. Beyond the influence of aquatic DOM, MPs can engage in interactions with a multitude of natural substances and microorganisms, such as adsorption, aggregation, and colonization processes. Additionally, the growing ice crystals exert pressure that might cause MPs to combine with other particles or dissolved substances, altering their behavior once they are released. These interactions can induce noteworthy modifications in the properties and environmental behaviors of MPs, thus underscoring their intricate role within various environmental contexts.

Chapter 5. Revealing the Freezing-induced Alteration in Microplastic Behavior and its Implication for the Microplastics Released from Seasonal Ice

5.1. Materials and Methods

5.1.1. Chemicals and Materials

Three different types of polymer particles were employed to represent MPs with different properties in the environmental context. High-density polyethylene (PE), with a density of 0.97 g/cm³, and aliphatic polyurethane (PU), having a density of 1.05 g/cm³, were obtained from Micro Powder Inc. (New York, USA). The PE particles ranged in mean size from 8.0 to 10.0 µm, while the PU ranged in mean size from 6.0 to 9.0 µm. Polytetrafluoroethylene (PTFE) powder, characterized by a density of 2.20 g/cm³, and a mean particle size of 6.0–9.0 µm, was obtained from Goodfellow Cambridge Ltd. (Huntingdon, UK). 67% of MPs found in the Arctic sea ice were distributed in sizes less than 11 µm. Therefore, MPs with a mean particle size ranging from 6.0 to 10.0 µm were used in this study (Peeken et al., 2018). Additionally, Tween 20, used to enhance the dispersion of MPs, and sodium chloride, employed for adjusting the salinity of the water, were acquired from Sigma-Aldrich (Ontario, Canada).

5.1.2. Freezing Experiment

The MP stock solutions were prepared by adding 60 mg of MP to 1.5 liters of deionized (DI) water, supplemented with 60 µL of a tenfold Tween 20 solution. The resulting mixture was subjected to

---

Reprinted with permission from *Environmental Science & Technology.* 2024, 58, 30, 13529–13539.

homogenization at 13000 rpm using a high-speed homogenizer for a duration of 20 min. Subsequently, the prepared MP stock solution underwent magnetic stirring at 1000 rpm to eliminate air bubbles introduced during the homogenization process and to maintain uniform suspension of the MPs prior to implementation. Samples of 200 mL of a 10 mg/L MP dispersion, featuring various salinity levels, were prepared by combining the corresponding volumes of the MP stock solution, 100 mg/L NaCl solution, and deionized (DI) water in beakers. The detailed experimental design is provided in Table 5-1.

These beakers, containing the MP samples, were tightly sealed with Parafilm and placed in a freezer set at −15 °C for a duration of 24 h to ensure complete freezing of the samples. The frozen samples were then removed from the freezer and allowed to thaw completely (to an ambient temperature of 20 °C) before proceeding with subsequent measurements and characterizations. Simultaneously, two control groups were established to assess the impact of freezing on MP behavior. One control group was subjected to measurements immediately after the MP dispersions (Control-1). The other control group was stored in a refrigerator at 4 °C for 24 h and then removed at the same time as the freezing group for comparison purposes (Control-2). All samples within the control groups were subjected to the same magnetic stirrer homogenization process as the experimental groups prior to measurement. All experiments were replicated three times, and the error bars in all figures of this study represent the standard error (SE).

Table 5-1. Experimental design

No.	Polymer type	Prepared MP concentration (mg/L)	Salinity (PSU)	Standing time (min)	Replicate	Research objectives
1	PE	10	0	0	3	Effects of freezing
2	PTFE	10	0	0	3	
3	PU	10	0	0	3	
4	PE	10	0	0	3	Effects of salinity under freezing
5	PE	10	5	0	3	
6	PE	10	10	0	3	
7	PE	10	20	0	3	
8	PE	10	35	0	3	
9	PTFE	10	0	0	3	
10	PTFE	10	5	0	3	
11	PTFE	10	10	0	3	
12	PTFE	10	20	0	3	
13	PTFE	10	35	0	3	
14	PU	10	0	0	3	
15	PU	10	5	0	3	
16	PU	10	10	0	3	
17	PU	10	20	0	3	
18	PU	10	35	0	3	
19	PE	10	0	0	3	Role of freezing in the stability
20	PE	10	0	60	3	
21	PE	10	0	120	3	
22	PE	10	0	480	3	
23	PE	10	0	960	3	
24	PE	10	0	1440	3	
25	PTFE	10	0	20	3	
26	PTFE	10	0	40	3	
27	PTFE	10	0	60	3	
28	PTFE	10	0	80	3	
29	PTFE	10	0	100	3	
30	PU	10	0	0	3	
31	PU	10	0	60	3	
32	PU	10	0	120	3	
33	PU	10	0	480	3	
34	PU	10	0	960	3	
35	PU	10	0	1440	3	

5.1.3. MP Quantification and Characterization

The thawed MP dispersion was subjected to homogenization using a magnetic stirrer operating at 1000 rpm for a duration of 30 s, ensuring the uniform distribution of MP particles prior to measurement. Following the homogenization process, a 50 mL sample was extracted from the middle of the liquid, with the timing ranging immediately to 24 hours post-standing, depending on the experiment, in order to assess changes in MP concentration and particle size. The mean particle size, particle size distribution, and volume concentration of MPs were measured using laser in situ scattering and transmissometry (LISST-200X, Sequoia Scientific, Bellevue, USA) in conjunction with the laser diffraction (LD) method. Moreover, because the concentrations measured using the LD method can be affected by the presence of larger particles and thus have high accuracy for homogeneous samples (Perpetuo et al., 2022), the mass concentration of MPs was measured using a total-carbon-based quantitative method through employing an Elementar vario EL cube elemental analyzer (Langenselbold, Germany).

To quantify the MP in water, a total-carbon-based quantitative method was developed in this study employing an Elementar vario EL cube elemental analyzer. Samples of 30 mL were filtered through a 22 mm-diameter glass microfiber filter with a 1.6 μm pore size to capture all MPs on the filter medium. Subsequently, the filter was rinsed multiple times with DI water and alcohol to eliminate any residual surfactants that may have adsorbed onto the filter or onto MPs during the filtration process. Following this, the filters containing the MPs were subjected to drying in a vacuum oven at 50 °C for 12 h to remove any remaining moisture. The dried filters were then securely enclosed within 35×35 mm tinfoil and then introduced into an elemental analyzer operating at 1,100 °C. The calibration curve of total organic carbon analysis was built using potassium hydrogen phthalate solution and the carbon content of each MP sample was measured using the calibration curve to verify whether the polymer can be completely combusted in the analysis. The measured and theorical carbon content of each MP was provided in Table 5-2. All three polymer demonstrated a good recovery rate. Therefore, the MP mass concentration (C_{mp}) was thus calculated by the following equation:

$$C_{mp} = \frac{m_C}{V_{sample}CC_{mp}}$$

where m_C is the measured carbon mass (mg); V_{sample} is the volume of the sample (L); and TCC_{mp} is the percentage of carbon content of each type of MP.

Table 5-2. Measured and theorical carbon content of MPs

Polymer type	Measured carbon content (%)	Theorical carbon content (%)	Carbon recovery rate (%)
PE	86.88 ± 0.85	85.71	101.36 ± 0.99
PTFE	21.72 ± 0.38	24	90.51 ± 1.57
PU	62.11 ± 1.32	59.12	105.06 ± 2.23

The zeta potential of the MP dispersion was measured using a Malvern Zetasizer Nano ZS (Malvern, UK), while the pH was measured using a pH meter (AR15, Fisher Scientific). The water contact angles of MPs, finally, were measured using an optical goniometer with automatic calculation capability (AST Products, Inc., Billerica, USA). To investigate the potential impact of freezing on the physicochemical properties of MPs, a group of MPs at a concentration of 2000 mg/L was subjected to freezing for seven days, owing to the limited quantity of samples available in other experimental groups. For this process, 200 mg of each MP type was dispersed in 200 mL of water (DI and 35 PSU saline water) containing 1 mg/L Tween-20, using a high-speed homogenizer, and then placed in a freezer at –15 °C for seven days. Subsequently, the samples were filtered through a 1.6-µm pore size glass-fiber filter and rinsed with DI water. The frozen MPs were thereafter dried in a vacuum oven at 50 °C for 12 hours in preparation for water contact angle measurements. The MP powder was fixed on the glass slide using double-sided tape, and a 5 µL DI water was then dropped on the surface of the solid sample. The embedded software was able to automatically fit an ellipsoid to the curve of the sessile water droplet and determine the contact angles.

5.1.4. Theoretical Calculations

Theoretical calculations were employed to gain further insights into the experimental results. The theoretical settling and rising velocities of MPs were calculated using empirical equations developed by Dietrich (1982), which have been widely applied in previous studies to describe the motion of MPs in water (Waldschläger and Schüttrumpf, 2019; Wang et al., 2023). The settling/rising velocity of MPs was calculated using a modification of the Stokes equation (Dietrich, 1982; Kooi et al., 2017).

$$V_{SR} = -\left(\frac{\rho_{mp} - \rho_{water}}{\rho_{water}} g\omega_* v\right)$$

where ρ_{water} and ρ_{mp} are densities of water (1000 kg/m^3) and MPs (PE, PTFE, and PU have densities of 970, 2200, and 1050 kg/m^3); ω_* is the dimensionless velocity; and v is the kinematic viscosity. The value of ω_* can be calculated using the following equation:

$$\omega_* = 1.71 \times 10^{-4} D_*^2 \; for \; D_* < 0.05$$

$$\log \omega_* = -3.76715 + 1.92944 \log D_* - 0.09815(\log D_*)^2 - 0.00575 \log(D_*)^3$$
$$+ 0.00056 \log(D_*)^4 \; for \; 0.05 \geq D_* \geq 5 \times 10^9$$

where the dimensionless particle diameter, D_*, can be calculated from the equivalent spherical diameter, D_n (m):

$$D_* = \frac{\left|\rho_{mp} - \rho_{water}\right| g D_n^3}{\rho_{water} v}$$

Additionally, the Péclet number was utilized as an indicator of the relative significance of gravity versus diffusive forces. Péclet number can be calculated using the following equation (Dietrich, 1982; Waldschläger and Schüttrumpf, 2019; Wang et al., 2023):

$$Pe = \frac{2\pi g \left|\rho_{\mathrm{water}} - \rho_{\mathrm{mp}}\right| r^4}{3K_B T}$$

where Pe is Péclet number; g is gravity acceleration constant (9.81 m/s^2); r is the average radius of MPs; K_B is the Boltzmann constant (1.38×10^{-23} J/K); and T is the absolute temperature (298 K). It should be noted that a Péclet number less than 1 suggests that diffusive transport dominates particle motion in water, while a value greater than 1 indicates that settling or rising due to gravity governs particle motion (Kovalchuk and Starov, 2012).

Derjaguin, Landau, Verwey, and Overbeek (DLVO) theory has been extensively employed to explain the aggregation and stability of particles in a liquid medium, accounting for the van der Waals force and electrostatic repulsion forces between particles. In this study, a particle–particle model based on DLVO theory was used to characterize the interactions among MPs. In DLVO theory, the total interaction energy comprises van der Waals interaction energy and electrostatic interaction energy. (Derjaguin et al., 1987):

$$U_{total} = U_{132}^{vdw} + U_{132}^{el}$$

where U_{total} is the total interaction energy, U_{132}^{vdw} is van der Waals interaction energy; and U_{132}^{el} is electrostatic interaction energy.

The van der Waals interaction energy can be calculated using the formula:

$$U_{132}^{vdw} = \frac{-A_{132}a_1a_2}{6h(a_1 + a_2)}\left[\frac{1}{1 + \frac{11.12h}{\lambda_c}}\right]$$

where a_1 and a_2 are the radius of interacting particles 1 and 2, respectively (m); h is the separation distance between two interacting particles (nm); λ_c is the characteristic wavelength of the interaction, often assumed to be 100 nm; A_{131} is Hamaker constant for interacting between subject 1 in the medium 3, which can be calculated using the following formula:

$$A_{132} = \left(\sqrt{A_{11}} - \sqrt{A_{33}}\right)\left(\sqrt{A_{22}} - \sqrt{A_{33}}\right)$$

where A_{11} and $A_{22}$is the Hamaker constant of subject 1 and 2 in vacuum, because only interaction between same type of MPs was studied in this study, so same value was used for A_{11} and A_{22} to calculate the interaction energy for each type of MP; and A_{33} is the Hamaker constant of water (3.7×10^{-20}) (Feng et al., 2023).

The electrostatic interaction energy can be calculated by:

$$U_{132}^{el} = 4\pi\varepsilon\varepsilon_0\frac{a_1a_2}{(a_1 + a_2)}\left[\xi_1\xi_2\exp(2\kappa h) - \frac{1}{4}(\xi_1^2 + \xi_2^2)\exp(-2\kappa h)\right]$$

where ξ_1 and ξ_2 are zeta potential of particle 1 and 2, respectively; κ is inverse Debye length (m^{-1}), which can be calculated using following equation:

$$\kappa = \left(\frac{2N_Ae^2I}{\varepsilon\varepsilon_0k_BT}\right)^{1/2}$$

The Hamaker constant of a material in vacuum can be estimated based on their surface free energy using the equation:

$$A_{11} = 6\pi L^2 \gamma^d$$

where L is the separation distance; the value of $6\pi L^2$ was at about 1.44×10^{-18} m^2 for most materials (Luo et al., 2018); γ^d is dispersion component of the surface free energy. The value of surface free energy and Hamaker constant used in the calculation was provided in Table 5-3.

Table 5-3. Parameter used for DLVO calculations

Symbol	Parameter	MP type			Reference
		PE	PTFE	PU	
γ^d	Dispersion component of the surface free energy (J/m^2)	32.8	21.3	30.8	(Jańczuk et al., 1989; Owens and Wendt, 1969; Ryntz and Yaneff, 2003)
A_{11}	Hamaker constant of MP in vacuum	4.7×10^{-20}	2.5×10^{-20}	4.4×10^{-20}	
A_{132}	Hamaker constant of MP in water	1.2×10^{-21}	6.3×10^{-22}	3.3×10^{-22}	

5.2. Results and Discussion

5.2.1. Effects of Freezing Conditions on Microplastic Behavior

Studies have shown that large quantities of MPs become trapped in seasonal ice. It has been estimated, for instance, that the mass of MPs stored in sea ice is equal to that of MPs dispersed in the world's oceans (Kim et al., 2021). In the freshwater environment, MP abundance can be several times higher within the ice than in sub-ice water during the winter (Liu et al., 2023; Zhang et al., 2022). Moreover, the freezing process has the potential to alter the properties of MPs via physical compression or enhanced oxidation (Tian et al., 2022), but no studies have been implemented to investigate the freezing effect on MPs. Accordingly, in this study, MPs were characterized before and after freezing in order to observe the impact of freezing on MP behavior. Samples were extracted from the midst of the dispersions immediately following the magnetic stirrer homogenization process. The mean particle size and volume concentration of MPs, assessed using the LD method, are presented in Figure 5-1a, and 5-1b, respectively. Figure 5-1c, meanwhile, shows the mass concentration of MPs, determined through elemental analysis. To assess the influence of freezing conditions on MP behavior, two control groups were established: one evaluated immediately after sample preparation (Control-1) and the other after standing for 24 h (Control-2), thereby accounting for any potential effects of time.

All samples exhibited an increase in mean MP particle size after freezing relative to the control groups. The mean particle size of PE was 7.64 μm for Control-1, 8.07 μm for Control-2, and 11.14 μm for the freezing group. While being allowed to stand for 24 h (i.e., Control-2) did not significantly affect the mean particle size of PE, 24 h of freezing resulted in a 45.8% increase in mean particle size (i.e., for the freezing group relative to Control-1). This outcome underscores the impact of freezing, as opposed to mere prolonged standing, on PE particles. Freezing was also found to influence the mean particle size of PTFE, while Control-2 exhibited a significant increase in particle size compared to Control-1. This observation can be attributed to the unstable dispersion of PTFE in water, where the mean particle size of PTFE increased due to the aggregation of PTFE particles during extended standing. This behavior is consistent with the measured zeta potential of PTFE as presented in Figure 5-1d, (i.e., respective readings of −18.2 and −17.0 mV before and after freezing). Conversely, the change in mean particle size was not as pronounced in the case of the hydrophilic MP, aliphatic PU, as in the case of the two hydrophobic MPs. With a high zeta potential of −42.4 mV, the mean particle size differed only slightly between Control-1 and Control-2, pointing to the stability of PU during extended standing. Furthermore, the mean particle size of PU increased by only 9.0% for experimental group relative to Control-1, a significantly smaller increase compared to the other two MPs. This can be attributed to the hydrophilic surface of PU, which reduces hydrophobic interactions between particles, facilitating MP dispersion upon thawing after aggregation induced by physical compression from growing ice crystals.

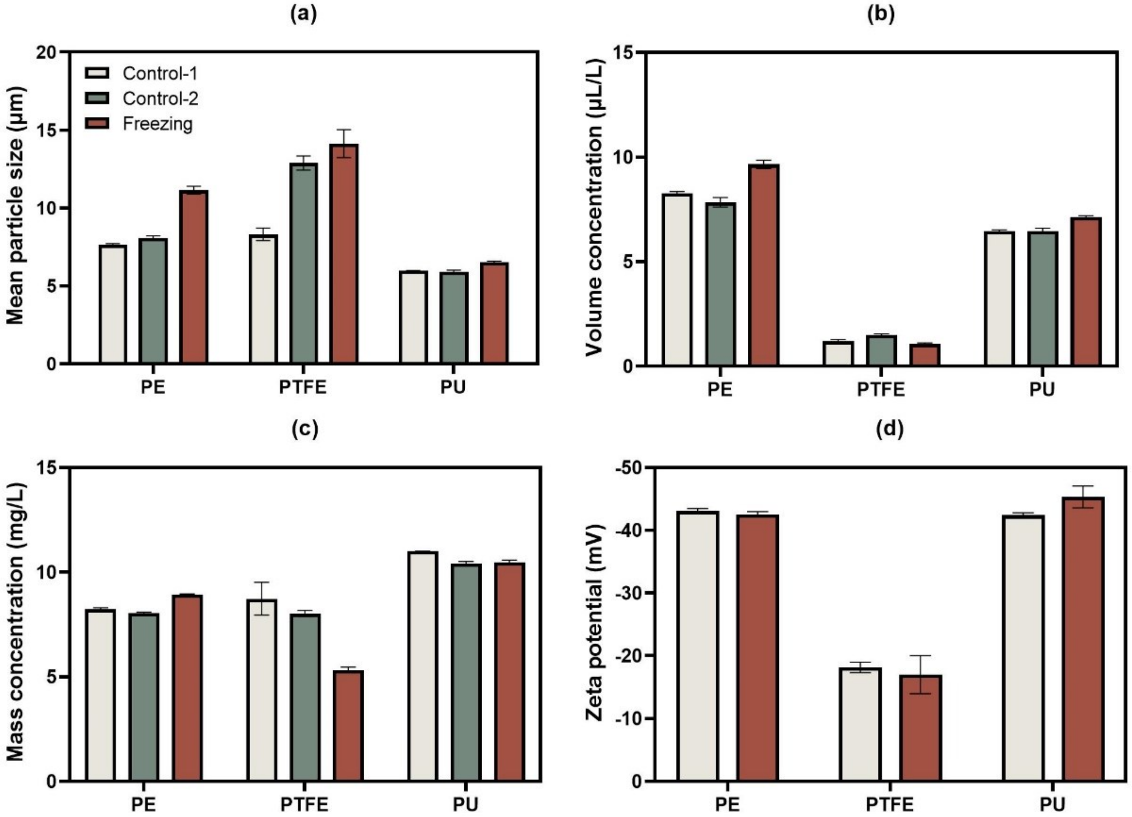

Figure 5-1. The (a) mean particle size, (b) volume concentration, and (c) mass concentration of MPs in both control groups and after freezing in freshwater. Control-1 represents the samples measured immediately following their preparation, while Control-2 denotes samples that were allowed to stand for 24 hours at 4 °C, corresponding to the duration of freezing in the experimental group.

The freezing of MPs can also alter the stability of MPs in water. As shown in Figure 5-1b and 5-1c, variations in MP concentration had differing effects after freezing depending on the type of MP. For instance, there were marked increases in both volume and mass concentrations of PE after freezing, in contrast to the two control groups. The volume concentrations for Control-1, Control-2, and the freezing group were 8.28, 7.84, and 9.66 µL/L, respectively, while the corresponding mass concentrations were 8.23, 8.04, and 8.93 mg/L. An increase in MP concentration after freezing was only observed in the case of PE, with no such increase observed for the other two polymer types. This rise in MP concentration after freezing can be attributed to the freezing-induced wetting transition of the hydrophobic surface (Lambley et al., 2023). PE-MPs do not easily become fully dispersed in water, even with the aid of Tween 20 surfactant and high-speed homogenization. As a result, some PE-MPs adsorb to the air/water interface due to the hydrophobicity of PE that has been allowed to stand for several minutes post-homogenization. Freezing can then result in the penetration of the water into the textured surface of the MP particles due to the pressure exerted by growing ice crystals, thereby promoting surface wetting (Lambley et al., 2023). In this study, the surfactant molecules expelled by the ice were compressed together with MPs, and enhanced the wetting process.

To simulate environmental conditions involving natural dissolved organic matter, sodium alginate was used to disperse the MPs, and then examined if the same phenomenon observed in the case of surfactant-assisted dispersion would occur (Figure 5-2). A similar trend was observed, where increased concentration and particle size were noted after freezing. However, it is important to note that the measured concentration remained lower compared to the dispersion prepared using Tween-20. This lower concentration, compared to surfactant-aided dispersion, is attributable to the less efficient dispersion achieved due to the relatively weak surface activity of sodium alginate.

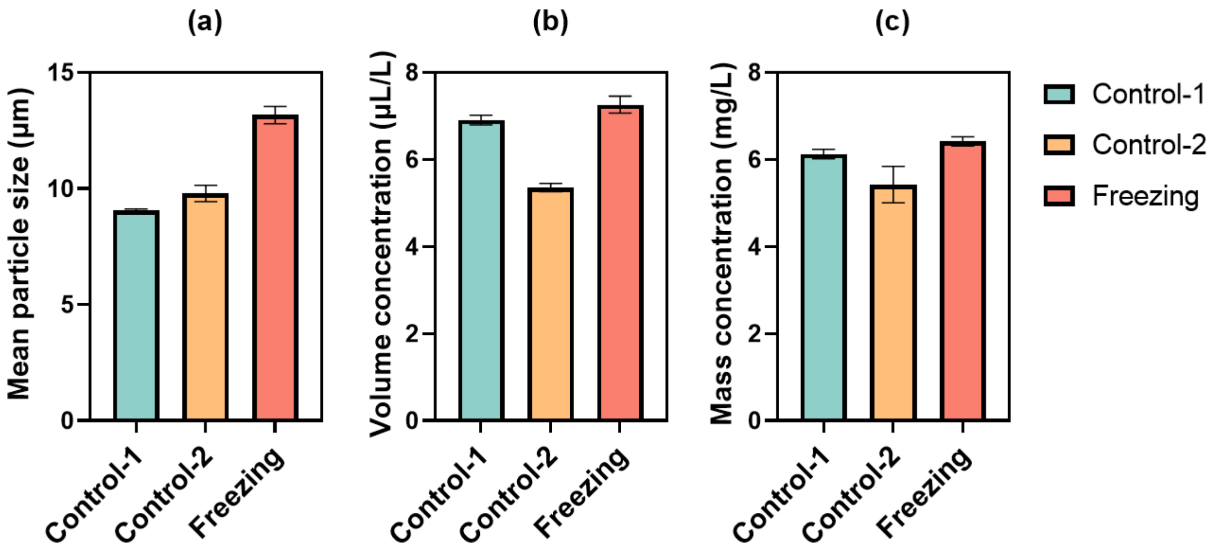

Figure 5-2. (a) Mean particle size, (b) volume concentration, and (c) mass concentration of PE-MPs dispersed with sodium alginate in control group and after freezing in freshwater.

PTFE was found to exhibit distinct behaviors after freezing, with the volume concentration and mass concentration of PTFE showing different trends. The volume concentration of PTFE was 1.21 μL/L for Control-1, 1.51 μL/L for Control-2, and 1.08 μL/L for the freezing group, while the corresponding mass concentrations were 8.74, 8.03, and 5.33 mg/L, respectively. The different trend between volume and mass concentration can also be attributed to the unstable dispersion of PTFE, leading to unreliable volume concentration readings when employing the LD method. The LD method, it should be noted, entails measuring the Brownian motion of particles in a solution and relating it to particle size. However, in an unstable particle dispersion, the Brownian motion is disrupted by the sedimentation of particles (Karmakar, 2019). In comparison, the mass concentration measured directly based on the total carbon analysis is more reliable in such cases.

A reduction in mass concentration of PTFE was accompanied by an increase in the mean particle size, driven by particle aggregation. This aggregation led to the gradual formation of flocs over time, with freezing exacerbating aggregation in comparison to the 24-h standing period. These formed flocs, owing to the substantial density of PTFE, resisted dispersion through magnetic stirrer homogenization and promptly settled following the stirring process. Also of note, the change in the behavior of the hydrophilic polymer, PU, after freezing was found to be relatively minor compared to that of the two hydrophobic MPs. Mean particle size presented a similar case, where freezing did not exert a significant influence on the stability of the PU-MP dispersion. The mass concentrations of PU were 11.00, 10.43, and 10.46 mg/L for Control-1, Control-2, and the freezing group, respectively.

The impact of freezing on the hydrophobicity of MPs was investigated by measuring the water contact angle of MPs before and after 7-day freezing in DI water and 35 practical salinity unit (PSU) saline water (**Figure 5-3**). There is no significant difference between control (Control-2 that standing for 24 h without freezing), freezing in DI water, and freezing in 35 PSU saline water, for PE and PTFE, but an increase in water contact angle was observed for PU; the figures were 64.9°, 86.5°, and 87.2° for control, freezing in DI water, and freezing in 35 PSU saline water, respectively. The results suggest that the freezing did not significantly affect the hydrophobicity of MPs.

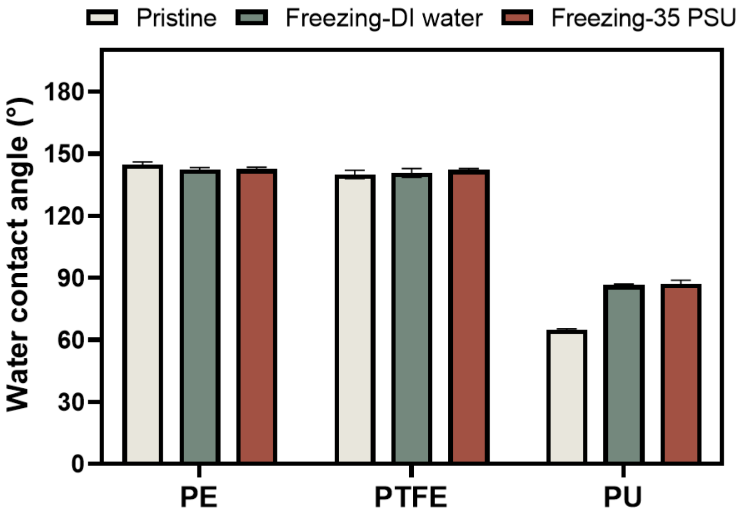

Figure 5-3. Water contact angles of pristine MPs, MPs following freezing in freshwater, and MPs after freezing in 35 PSU saline water.

The three polymers exhibited distinct behaviors when subjected to freezing after being released from thawing ice. Freezing increased the particle size of all the MP particles due to the physical compression within freshwater ice. However, the changes in concentration varied depending on the type of polymer. PE exhibited an increase in concentration after freezing, presumably attributable to enhanced surface wetting caused by ice crystal compression. In contrast, despite also being highly hydrophobic, PTFE exhibited a significant reduction in concentration after freezing. This reduction is attributable to PTFE's surface charge being too low to provide sufficient electrostatic repulsion between particles to keep them suspended, resulting in aggregated PTFE settling rapidly due to its high density. On the other hand, the hydrophilic MP—i.e., PU—exhibited relatively stable behavior before and after freezing. This stability can be attributed to its hydrophilic surface and neutral buoyancy, which allow the aggregated particles to disperse easily and maintain stable dispersion. In addition, the zeta potential and hydrophobicity of the MPs did not demonstrate a significant change before and after freezing, which suggests that freezing did not result in a significant change in the surface properties of the MPs.

5.2.2. Effects of Salinity on Behavior of Frozen Microplastics upon Release

Salinity plays a crucial role in governing the behavior of suspended particles in water by affecting the compression of the electrostatic double layer (Wang et al., 2023). The reduction in electrostatic repulsion due to increased salinity can accelerate particle aggregation and disrupt particle stability. Moreover, salinity influences the entrainment of MPs in ice, as the formation of brine channels between ice crystals creates narrow spaces in the ice in which for MP entrapment to occur (Chen et al., 2023d; Pradel et al., 2021b). Salinity levels in natural water bodies can range from less than 0.5 to 35 PSU, with estuarine regions experiencing particularly pronounced variations over short distances (Telesh and Khlebovich, 2010). Given the variability of salinity levels in natural environments, this study examined the impact of different salinity levels ranging from freshwater to seawater (35 PSU) as part of our investigation of the effects of freezing on MP behavior (Figure 5-4). As the results presented in the previous section demonstrate, little difference was observed between the Control-1 and Control-2 groups, the control group in the following sections are only Control-2 that standing for 24 h without freezing.

With the addition of NaCl in water, the behaviour of MPs before and after freezing changed very differently depending on the types of polymers. As discussed in previous section, the freshwater ice crystal compresses the particle together, resulting in the increase in mean particle size. However, the mean particle size of PE after freezing was dramatically dropped from 11.40 to 8.17 μm when increasing the salinity from 0 to 5 PSU. The freezing did not pose significant change in mean particle size at 5 PSU compared to the control group with mean particle size of 7.90 μm. The results indicate that the compression of particle mainly occur in freshwater ice and ice form in water with 5 PSU can generate space via brine network within ice structure, avoid the increase in the particle size via aggregation of particles.

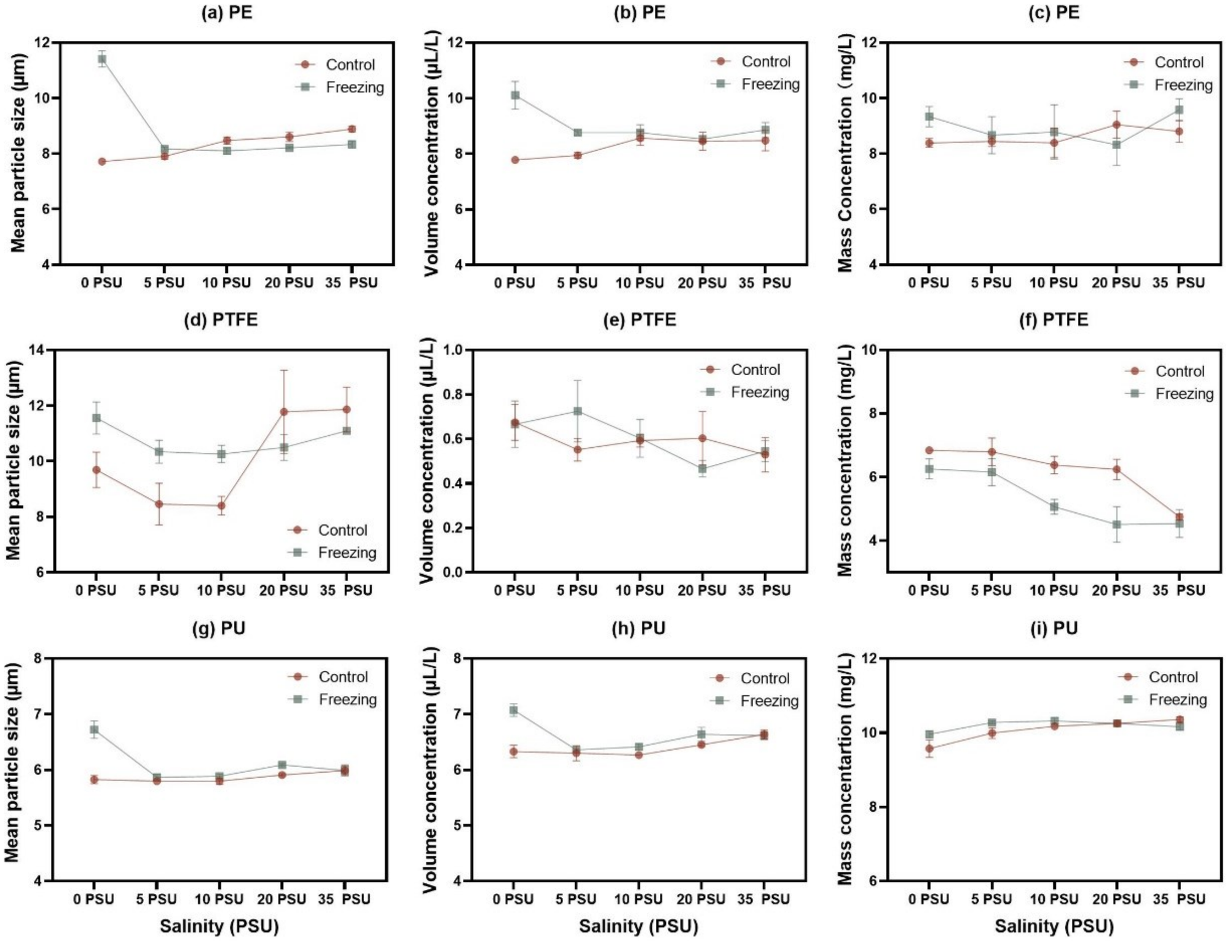

Figure 5-4. Change in mean particle size and concentration after freezing under different salinity. Mean particle size, volume concentration, and mass concentration for (a–c) PE, (d–e) PTFE, and (g–i) PU, respectively.

The effects of salinity on the behavior of MPs in ice has been observed in previous studies as well (Pradel et al., 2021b). For instance, Chen et al. (2023d) investigated the effects of salinity on the entrainment of MPs in ice, finding that a salinity of 2 PSU significantly increased the enrichment factor of PE-MPs in ice from 0.64 to 1.71, but that a further increase in salinity did not enhance the incorporation of MPs in ice. Similarly, in the present study, further increasing the salinity level beyond 5 PSU did not have a significant impact on the mean particle size, only causing a slight increase in the mean particle size of PE after freezing. However, there was an increasing trend in the mean particle size in the control group with rising salinity. This phenomenon can be attributed to the inhibitory effects of ionic strength on the electrostatic double layer, resulting in the aggregation of MPs. It is notable that the mean particle in the PE control group was greater than that of the freezing group at salinities of 10, 20, and 35 PSU. This observation can be attributed to the stabilizing effect of ice crystals within the brine channels, which provide ample space for the particles to immobilize without being compressed together. In contrast, the PE-MPs in the control group gradually aggregated over time due to limited electrostatic repulsion. This observation was substantiated by the increase in mean particle size as salinity levels increased in the case of the control group.

In terms of MP concentrations, the volume concentrations of PE demonstrated a similar trend under effect of salinity; consistent with the results for mean particle size, the difference in volume concentration of PE between the freezing and control groups were only significant in the case of the freshwater. However, the difference between the freezing and control groups in freshwater was more significant for volume concentrations compared to mass concentrations. This may be attributable to the augmentation in particle size resulting from aggregation induced by freezing, which can lead to an overestimation of volume concentrations when measured using the LD method

(Wang et al., 2023). As discussed in Section 5.2.1, the increase in PE concentration after a freezing–thawing cycle in freshwater can be attributed to wetting alterations enhanced by ice crystal compression. However, the introduction of salinity creates brine channels that mitigate the pressure generated by ice crystal growth. Consequently, the increased mean particle size and concentration due to the physical compression in freshwater freezing are eliminated after the addition of salt to the water.

The PTFE-MPs exhibited different behaviors than the PE-MPs after freezing under varying salinity levels. The mean particle size of PTFE in the freezing group was found to be larger than that in the control group across the 0–10 PSU range. However, when the salinity increased from 0 to 5 PSU, the mean particle size of PTFE in the freezing group only decreased by 11.8%, from 11.56 μm to 10.34 μm, whereas PE-MPs experienced a more significant drop of 47.9%. This difference can be attributed to differences in water stability between these two polymers: PTFE aggregates more rapidly than PE due to its lower surface charge. Some large PTFE aggregates may form before freezing, meaning that aggregation is primarily driven by surface charges rather than by the physical pressure of freezing in freshwater. Due to the instability of PTFE dispersion, the relatively large error bars in particle size measurements at 20 and 35 PSU demonstrate that the difference in mean particle size between the control and freezing groups was not significant (paired *t*-test, $p > 0.05$ for effect of freezing). Additionally, the mass concentration of PTFE suggests that freezing exacerbates particle instability by promoting aggregation. Within the 0–20 PSU range, the mass concentration was lower in the experimental groups than in the control group.

The effect of salinity under the impact of freezing was similar for PU-MPs to the effect observed in the case of PE-MPs. The increase in mean particle size under the impact of freezing observed in the case of freshwater ceased with the addition of salt. The increase in volume concentration after freezing in freshwater, meanwhile, is attributable to the overestimation of volume concentration due to the increased particle size when employing the LD method. The mass concentration of PU-MPs after freezing differed little from that that of the control group across salinity levels, indicating that the impact of freezing on PU-MPs is negligible.

In summary, the impacts of freezing on the behavior of MPs can primarily be attributed to accelerated aggregation caused by ice-formation-induced pressure. However, this compression is mitigated when salt is present in water, creating brine channels. Consequently, the impact of freezing on MP behavior can be significant in freshwater, but relatively minor in saltwater. It is worth noting that our study used a 24-h freezing time to assess the impact of freezing, whereas, in natural environments, frozen periods can extend for much longer durations. For instance, ice floes in the Arctic can endure for several months to years (Perovich and Richter-Menge, 2009). Under prolonged freezing, gravity drainage leads to the expulsion of brine from within the sea ice structure, progressively diminishing the salinity of ice over time. This process leads to modifications in the ice structure that can affect the physical characteristics of ice, including permeability, strength, and thermal conductivity (Hunke et al., 2011; Turner et al., 2013). These alterations may affect the MPs trapped within the sea ice.

5.2.3. Role of Freezing in the Stability of Microplastics

To further investigate the impact of freezing on the stability of MPs, an experiment was conducted to examine the settling and flotation of MPs over time (Figure 5-5). All experiments were conducted in freshwater conditions only, as the results in Section 5.2.2 indicate that freezing in saltwater conditions does not significantly alter the properties of MPs relative to those observed in freshwater conditions.

MPs naturally settle or float over time, depending on their density. Samples were extracted from the central section of the dispersion to assess alterations in mean particle size and concentration over time. All the dispersions exhibited a decrease in mean particle size and concentration over time due to settling and flotation processes. Larger particles are more influenced by gravity, leading to a higher settling/rising speed and, consequently, a gradual reduction in particle size within the dispersion's center. However, the mean particle size in the freezing group consistently exceeded that of the control group for all MPs. This observation further supports the assertion that aggregates forming during freshwater ice formation are not easily dispersed upon the introduction of turbulence in water.

Additionally, changes in particle size can have a physical impact on the stability of MPs in water. After freezing, the PE-MPs demonstrated higher concentrations compared to the control group during the early stages of the experiment. The freezing group consistently exhibited significantly higher volume concentrations throughout the 0 to 8-h period than the control group. Regarding mass concentration, the freezing group had a higher concentration than the control group from 0 to 4 h, although the difference was not statistically significant. The improvement in the dispersion of PE-MPs may be attributable to the wetting transition of MPs induced by freezing. However, freezing also increased the mean particle size, accelerating aggregation and thereby affecting the stability of PE-MPs. After 16 h, the concentration of PE in the control group exceeded that in the freezing group, indicating a rapid rising speed of PE-MPs in the freezing group due to their larger particle size.

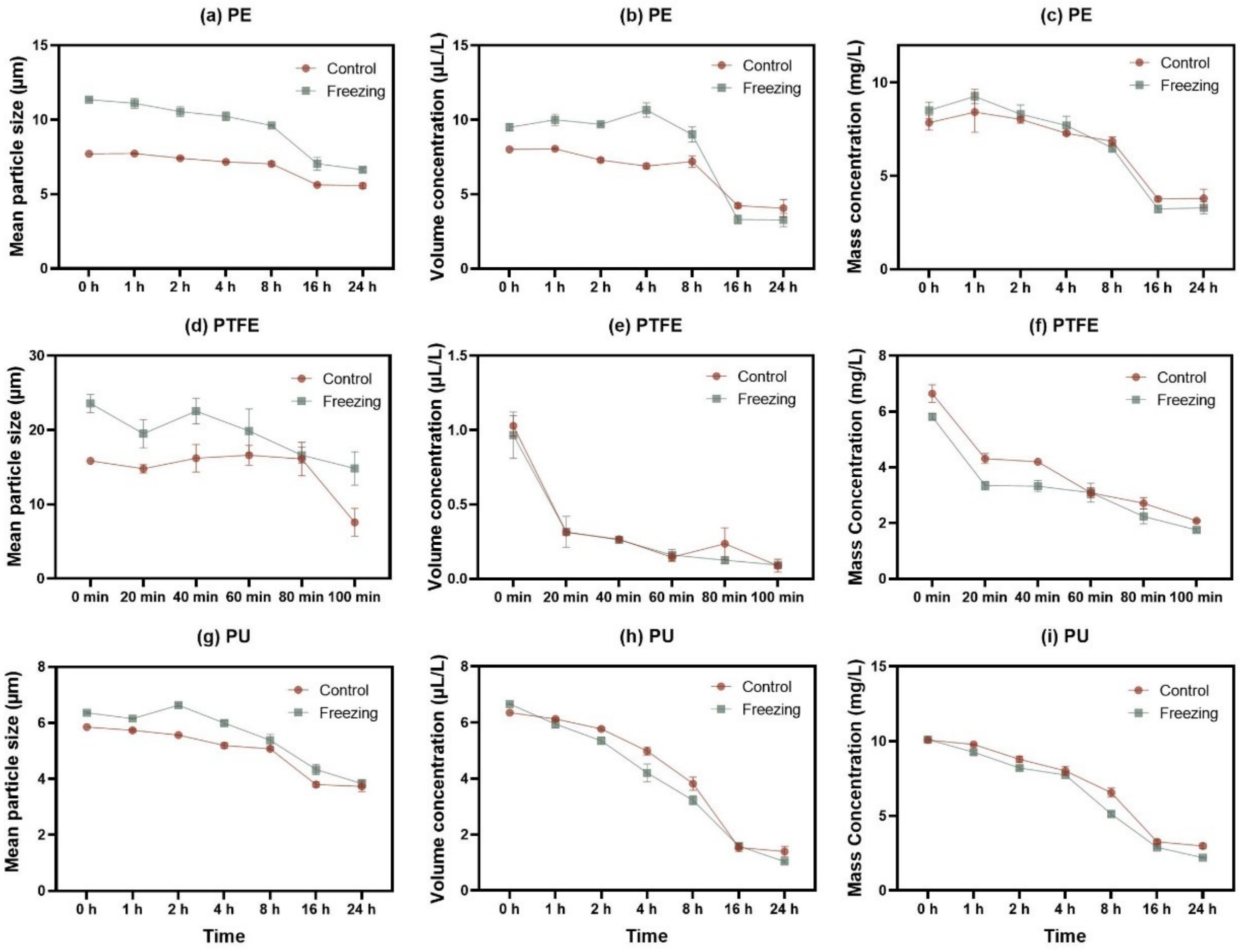

Figure 5-5. Change in mean particle size and concentration after freezing with time. Mean particle size, volume concentration, and mass concentration for (a–c) PE, (d–e) PTFE, and (g–i) PU, respectively. PTFE uses a different scale on the x-axis due to its rapid settling compared to the others.

PTFE, despite being a hydrophobic MP like PE, has a much higher density of 2.2 g/cm³. Additionally, compared to PE and PU, PTFE has a much lower absolute value of zeta potential, resulting in a significantly faster drop in concentrations in the middle of the dispersion. Therefore, only the first 100 minutes were studied for PTFE. The settling of PTFE demonstrated a consistent decline over time, but the concentration in the freezing group consistently remained higher than that in the control group during the 100-min period. Additionally, some PTFE-MPs were observed floating on the water surface in the control group, whereas this phenomenon was much less prevalent in the freezing group. A similar phenomenon was observed in the case of PE-MPs (Figure 5-6). However, unlike PE, PTFE did not exhibit a higher concentration in the freezing group than that in control group at the beginning of the experiment. This difference between these two polymers can be attributed to the rapid settlement of aggregated PTFE particles. The wetting alteration of PTFE particles induced by freezing caused more of them to move from the water surface into the water. Nevertheless, the aggregation process during freezing also accelerated the settling speed, which counteracted the expected increase in concentration resulting from enhanced wetting.

PU is a non-buoyant polymer with a density of 1.05 g/cm^3, slightly heavier than water. The increase in mean particle size in the freezing group was not as significant for the PU-MPs as for the two hydrophobic MPs due to the easy dispersion of aggregates resulting from its hydrophilic surface. Nevertheless, the increase in mean particle size also accelerated the settling of PU-MPs. The t-test analysis demonstrated that both the volume and mass concentrations were significantly lower in the freezing group than in the control group ($p < 0.05$).

The results of the settling/rising experiment demonstrate the impact of freezing on the stability of the MPs. Although the freezing in freshwater can enhance the wetting of hydrophobic MPs and result in more MPs dispersing in the water, the freezing-induced aggregation increases the size of MP particles and thus accelerates their settling/flotation, leading to less stability in the long term.

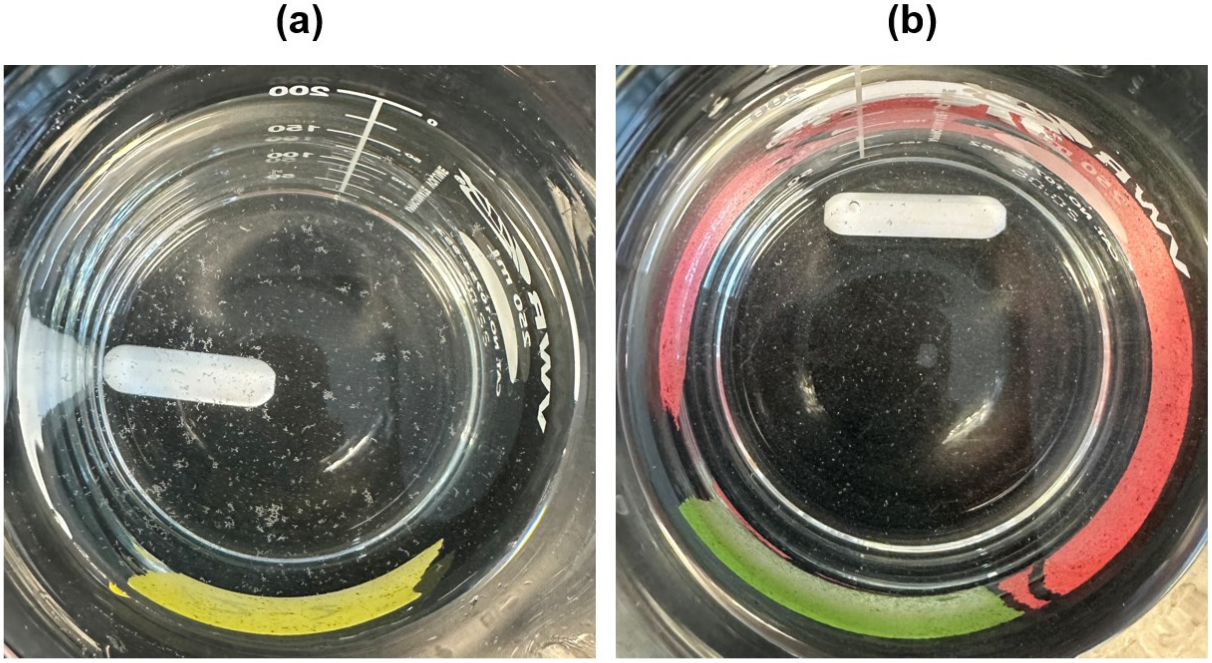

Figure 5-6. Comparative photographs of PE-MPs dispersion illustrating particle aggregation observed 30 minutes post-homogenization with a magnetic stirrer: (a) Control group without exposure to freezing, and (b) Sample subjected to freezing in freshwater.

5.2.4. Theoretical Explanations for the Effects of Freezing on MP Behaviors

To gain a deeper understanding of the mechanism underlying the behavioral alterations caused by freezing, theoretical calculations were conducted to analyze settling/rising velocities and interactions among the MPs. The theoretical settling/rising velocities and Péclet numbers of MPs before and after freezing are presented in Figure 5-7a and 5-7b. The Péclet number, it should be noted, is employed to assess the balance between buoyant forces acting on a particle and diffusive forces arising from Brownian motion. A Péclet number less than 1 indicates that Brownian motion is the dominant force affecting particle motion, while a Péclet number greater than 1 suggests that buoyant forces are governing particle behavior. The critical particle size at Péclet number of 1 is primarily influenced by the density difference between the particle and the surrounding medium.

In this study, PTFE exhibited the lowest critical particle size among the MPs (1.28 μm) due to its higher density compared to the other two polymers. The critical particle sizes for PE and PU when their Péclet number equaled 1 were 3.21 and 2.83 μm, respectively. However, it is important to note that all of the MPs used in this study had relatively large mean particle sizes, indicating that buoyant forces predominated their behavior in water. This is supported by the relatively rapid decrease in concentration in the central part of the dispersion within one day as observed in the experiment.

With the increase in particle size caused by freezing, the influence of buoyant force can increase, leading to acceleration in the settling/rising velocity. The predicted settling/rising velocity shown in Figure 5-7a is consistent with the experimental results described in Section 5.2.3 as part of the discussion of MP stability. The settling velocity of PTFE was observed to be several orders of magnitude higher than that of the other two polymers owing to the significant difference in density compared to the other two polymers. The predicted velocities for PE, PTFE, and PU in the control group were 0.08 m/day (rising), 14.22 m/day (settling), and 0.08 m/day (settling), respectively. Furthermore, the increase in particle size resulting from freezing in freshwater strengthened the dominance of buoyant forces acting on these MPs. The rising velocity of PE increased to 0.18 m/day, while the settling velocities of PTFE and PU increased to 37.05 and 0.10 m/day, respectively.

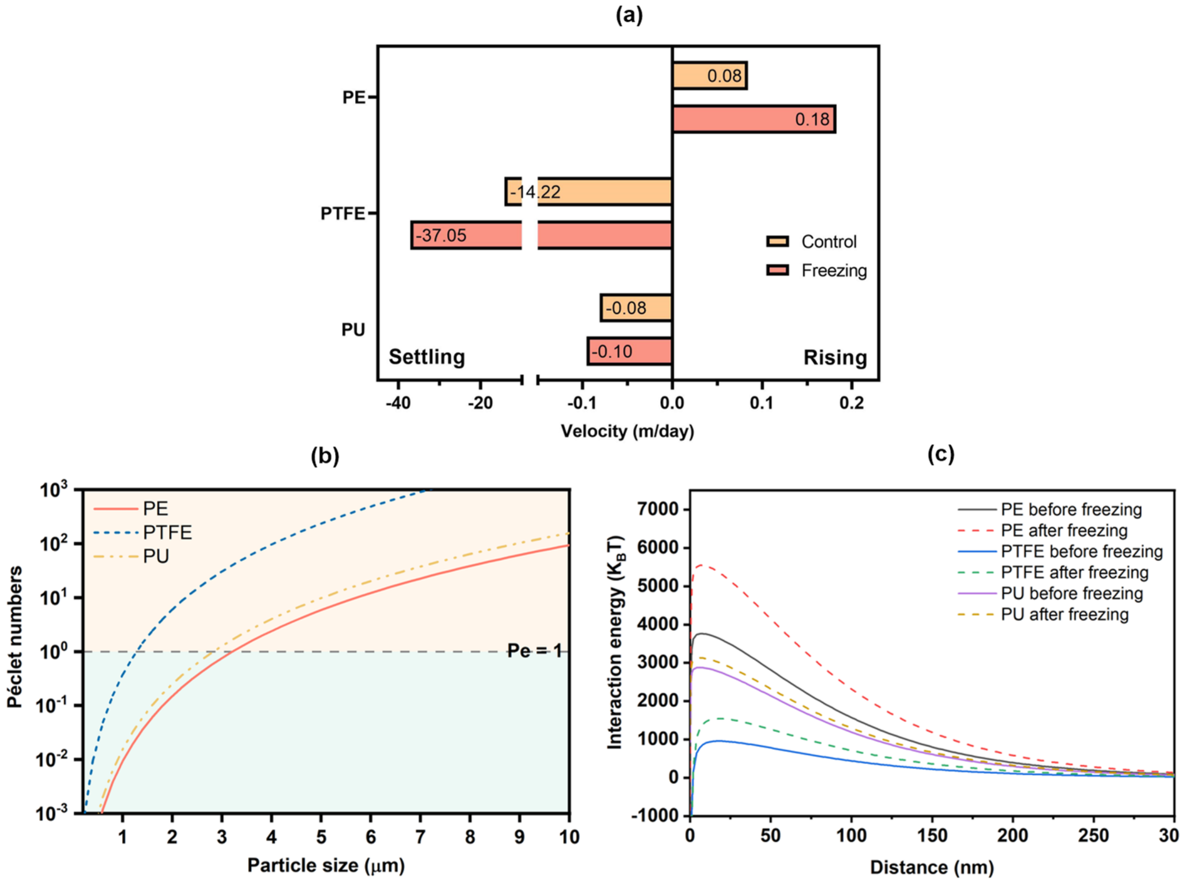

Figure 5-7. (a) Theoretical settling/rising velocity, (b) Péclet numbers, and (c) DLVO interaction energy of MPs before and after freezing.

DLVO analysis was employed to evaluate the aggregation and kinetic stability of MPs, with the results presented in Figure 5-7c. To investigate the effects of freezing in freshwater, an ionic strength of 0.02 mol/L was used in the DLVO analysis, given that the salinity in freshwater systems typically falls below 0.5 PSU. Due to the low ionic strength, all MPs exhibited energy barriers between particles, and for this reason they were subject to electrostatic repulsion resulting from the electrostatic double layer surrounding the particles. The magnitude of these energy barriers, which must be overcome for MP aggregation, varied depending on the polymer type, and the results of the DLVO analysis were consistent with the experimental findings. The energy barriers between MPs were strongest in the case of PE, followed by PU and then PTFE.

The influence of increased particle size on interaction energy was also examined. It was found that freezing did not affect the surface charges on the MP surface, but that it did result in an increased mean particle size for the MPs. The findings of the DLVO analysis indicate that the increased particle size could lead to a greater energy barrier between particles, hindering their aggregation. The theoretical explanation would be that this occurred because the increased particle size led to a more pronounced electrostatic repulsion force relative to the van der Waals force. However, the experimental results demonstrated that the MPs settled or rose at a faster rate after freezing. This discrepancy can be attributed to the fact that the DLVO analysis did not account for the influence of gravity, which becomes significant for colloidal particles larger than 1 μm.

In summary, the theoretical calculations effectively describe the changes in the stability of MPs observed before and after freezing in freshwater. The increase in settling/rising velocity of MPs after freezing is primarily attributable to the increased particle size, which strengthens the dominance of gravity over Brownian motion. While freezing does not alter the surface charges of the MPs, and they still exhibit substantial electrostatic repulsion, the prevailing gravitational forces cause the MPs to rapidly settle or rise based on their density. Hence, the stability changes brought about by freezing can significantly affect the environmental fate of MPs entrapped in ice and subsequently released during thawing.

5.2.5. Environmental Implications

The entrapment and enrichment of MPs in ice have been observed through environmental sampling in both freshwater and seawater contexts. Studies have shown that MPs can be several orders of magnitude more abundant in ice than in sub-ice water. MPs can be temporarily stored in the ice for durations ranging from months to years and then released back into the environment upon thawing. Although some studies have investigated the impacts of freezing on MPs in porous media and their transport, the influence of the freeze–thaw process on the behavior of MPs in aqueous environments has yet to be reported on in the literature (Koutnik et al., 2022; Li et al., 2023). Understanding the impact of freezing on MPs in aquatic environments can bridge the existing knowledge gap regarding the behavior of MPs, thereby facilitating the development of strategies to mitigate their threats in cold regions. This study thus examined the effect of freezing on the subsequent behavior of MPs (after thawing), with consideration given to polymer properties and salinity level.

Freezing of MPs in freshwater ice results in the aggregation of MP particles due to physical compression, leading to an increase in particle size once the MPs are released from the ice. In our experiment, aggregated MPs were not dispersed by high-speed homogenization using a magnetic stirrer, indicating that MP aggregates formed through freezing are resistant to turbulent flows in natural environments. Moreover, the particle size increase is more pronounced for hydrophobic

MPs (i.e., PE and PTFE) compared to hydrophilic MPs (i.e., PU), suggesting that hydrophobic interactions in water contribute to stronger aggregation, whereas hydrophilic particles are more readily dispersed once released back into the water. Additionally, the increase in particle size significantly affects the stability of MPs in water. Although freezing does not alter the MPs' surface charges, the freezing-induced aggregation enhances buoyancy effects, accelerating the settling/rising velocity of MPs in water. Furthermore, an increase in the concentration of PE in water post-freezing was observed. The hydrophobicity of hydrophobic MPs typically facilitates their attachment to the air/water interface, even for nonbuoyant hydrophobic MPs such as PTFE. Moreover, physical compression during the freezing process enhances the wetting of hydrophobic MPs, leading to improved dispersion in water and reduced surface affinity. This alteration in wetting due to freezing could significantly influence the environmental fate of MPs, increasing their mobility and potential ingestion by marine organisms, thus, enter in a food chain. Many studies have demonstrated the toxicity of MPs for benthic fauna, and the MPs in sediment can affect biogeochemical processes by reducing the bioturbation activities of benthic fauna due to their toxic effects (Green et al., 2017; Wazne et al., 2023).

The impact of freezing varies with salinity. While freezing in freshwater affects MP behavior, no significant impact on particle size and stability was observed in saline water compared to control groups in our experiment. Moreover, the presence of salt leads to the formation of a brine network within the ice structure due to brine rejection, providing space for, and reducing pressure on, MPs entrapped by growing ice crystals. It should be reiterated in this regard that our study only considered the impact of short-term freezing, whereas multi-year ice, common in natural environments, undergoes gravity drainage that gradually reduces ice salinity and redistributes particles within the porous ice structure, potentially altering particle properties and leading to the discharge of particles stored within ice (Johnston, 2017; Petrich and Eicken, 2010).

While this study examined the interactions and aggregation of MP particles under freezing conditions, aggregation between MPs and other naturally suspended particles in aqueous environments has been observed in several previous studies (Li et al., 2019; Yang et al., 2022b). The heterogeneous aggregation between MPs and other particles can be further intensified under freezing conditions, exerting a significant impact on the environmental fate of MPs by altering their density, size, and surface properties. Furthermore, recent studies have found that MPs trapped in sea ice may be ingested by ice algae and rapidly settle after melting (Bergmann et al., 2023). This indicates that freezing may accelerate the accumulation of MPs in the sediments of cold region waters, thereby impacting the polar ecosystems (Bergmann et al., 2023). MPs sequestered in seasonal or long-term ice may rapidly settle into sediments in polar and other cold region waters upon release. Our study provides a theoretical foundation for researching the behavior of MPs in cold regions. Against the backdrop of climate change, substantial quantities of MPs are being reintroduced into water, with the properties of entrapped MPs potentially undergoing complete alteration during freezing, yet there remains limited knowledge regarding the transport and behavior of MPs in cold regions, necessitating further exploration.

Chapter 6. Utilizing Electrosorption for Efficient Removal of Polyethylene Microplastics from Water: Critical Factors and Mechanistic Insights

6.1. Materials and Methods

6.1.1. Chemicals and Materials

Polyethylene (PE) with mean particle size ranging from 3–5 μm was used as model MP in this study. 5 mg MP was added into 1 L DI water with 5 μL 1:10 diluted Tween 20 to prepare 5 mg/L MP dispersion. The mixture was then homogenized with high-speed homogenizer at 14000 rpm to obtain the MP dispersion for the further MP removal tests. Graphite felt (GF) used for the electrodes were purchased from Tianwang Graphite Products Co., Ltd. (Dongguan, China). The reactor chamber is constructed from acrylic board and has internal dimensions of 45×60×125 mm. It includes 3 mm slots for electrodes, with a 3 mm distance between each slot. The inlet and outlet of the chamber are located on either side of the. Inlet and outlet can be closed when the water circulation system is not in use. The details of the reactor chamber are shown in the Figure 6-1.

This chapter is based on a manuscript that has been submitted to Water Research (Elsevier), Under Review, Manuscript ID: WR90562.

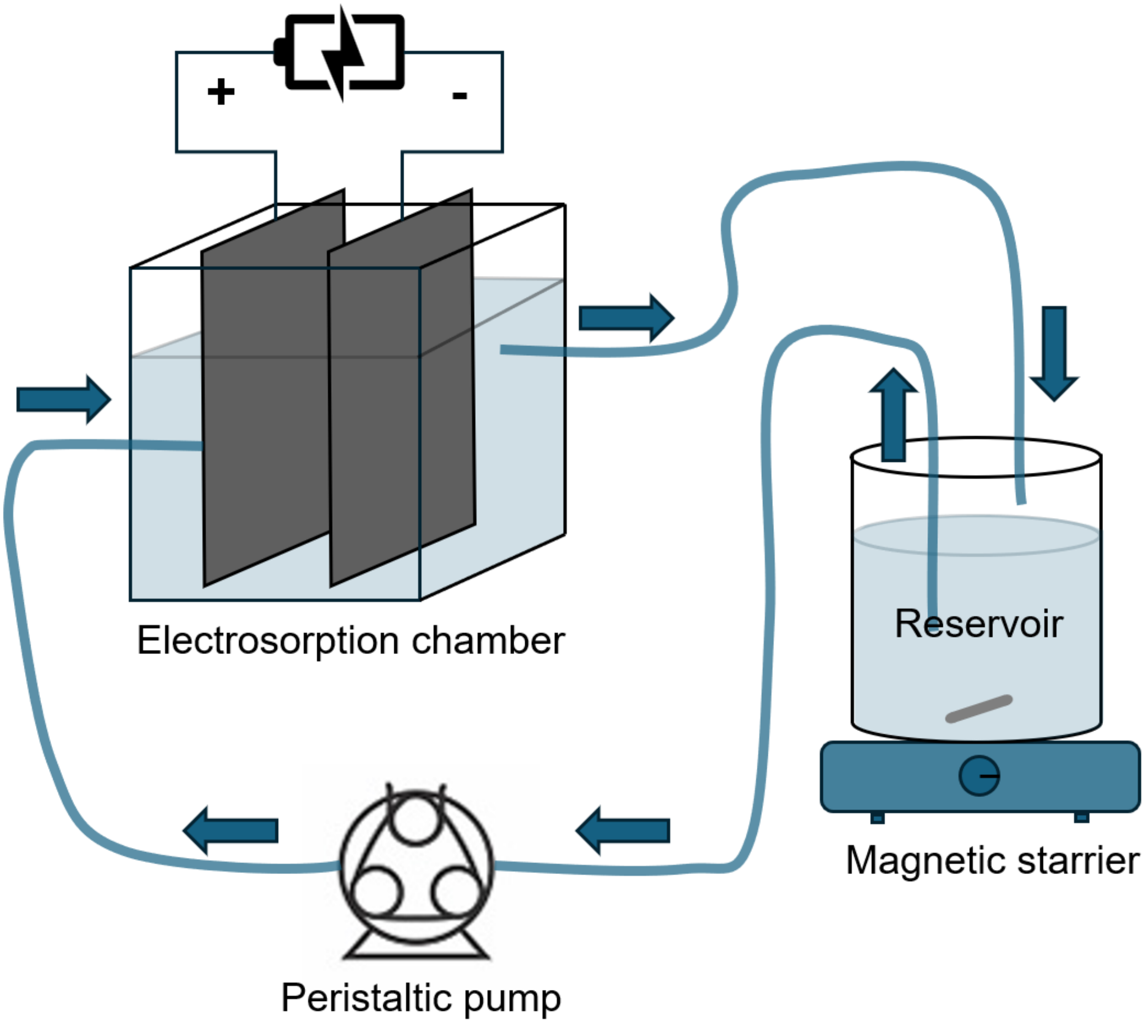

Figure 6-1. The schematic diagram of the ES system for MP removal with water.

6.1.2. Electrosorption Experiments

ES experiments aimed at removing MPs were conducted in a reactor chamber, using GF electrodes as both the cathode and anode. These experiments were performed under two conditions: with and without water circulation. In the setup without water circulation, 200 mL of MP dispersion was introduced into the chamber, with the electrodes spaced 30 mm apart. The ES experiments with a water circulation system used a peristaltic pump to facilitate water movement. A beaker containing 1 L of MP dispersion served as the reservoir, from which water was pumped into the reactor chamber at flow rates ranging from 15 to 80 mL/min before being returned to the reservoir. In this setup, the distance between the cathode and anode was reduced to 15 mm. For the setup with water circulation. 5–20 mM of KNO_3 was employed as electrolyte. To monitor the MP concentration, turbidity, and pH levels within the system, 15 mL samples were collected from both the reservoir and the outlet every 30 min. In the no-circulation setup, samples were taken from the middle of the reactor chamber every 30 min. The volume concentration and particle size of the MPs were measured using a LISST-200X (Sequoia Scientific, USA) via laser diffraction. The removal rate of MPs was calculated by dividing the post-treatment MP concentration by the pre-treatment concentration.

6.1.3. Experimental Design and Characterization

To investigate the factors influencing the removal rate of MPs in the ES system, a series of single-factor experiments were conducted for both the non-circulation and circulation systems. Factorial analysis is a statical method to determine the effects of multiple variables on a response, which has been widely applied in the experiment design (Chen et al., 2023b). A two-level full factorial design was employed to investigate the effects of various parameters—electric potential, flow rate, and electrolyte concentration—along with their interactions on the removal rate within the circulation system. Details of the experimental design are summarized in Table 6-1.

Table 6-1. Factorial design matrix and the corresponding removal efficiency.

Number	Coded levels			A	B	C	pH		Removal efficiency (%)
	A	B	C	Applied voltage (V)	Flow rate (mL/min)	Electrolyte concentration (mM)	Before treatment	After treatment	
1	−1	−1	−1	3	30	5	5.35	5.15	62.6
2	−1	−1	−1	3	30	5	5.41	6.3	80.8
3	−1	−1	−1	3	30	5	5.39	5.26	80.4
4	−1	−1	1	3	30	20	5.36	4.08	91.8
5	−1	−1	1	3	30	20	5.33	4.48	98.0
6	−1	−1	1	3	30	20	5.33	5.62	91.8
7	−1	1	−1	3	80	5	5.35	4.95	83.0
8	−1	1	−1	3	80	5	5.42	4.89	85.7
9	−1	1	−1	3	80	5	5.4	4.83	88.4
10	−1	1	1	3	80	20	5.36	4.84	98.3
11	−1	1	1	3	80	20	5.52	4.66	97.5
12	−1	1	1	3	80	20	5.3	4.99	96.4
13	1	−1	−1	6	30	5	5.48	6.28	66.1
14	1	−1	−1	6	30	5	5.22	5.28	82.5
15	1	−1	−1	6	30	5	5.48	5.38	69.1
16	1	−1	1	6	30	20	5.5	5.52	82.4
17	1	−1	1	6	30	20	5.48	5.77	95.3
18	1	−1	1	6	30	20	5.58	6.05	94.1
19	1	1	−1	6	80	5	5.33	5.6	95.4
20	1	1	−1	6	80	5	5.3	4.4	92.3
21	1	1	−1	6	80	5	5.48	3.82	93.9
22	1	1	1	6	80	20	5.31	6.1	98.5
23	1	1	1	6	80	20	5.51	6.25	98.5
24	1	1	1	6	80	20	5.33	5.63	94.9

The zeta potential of the MP dispersion was measured by Malvern Zetasizer Nano ZS (Malvern, UK). Scanning electron microscope (SEM; Hitachi S-3400N, Japan) equipped with energy dispersive X-ray spectroscopy (EDS) was used to observe the surface of both pristine and used electrodes to examine the adsorption of MPs onto the electrodes. The electrochemical characteristics of the system, including electrochemical impedance spectroscopy (EIS) and cyclic voltammetry (CV), were characterized by the Autolab workstation (Metrohm, Switzerland). The CV and EIS analysis were performed using the same cell as in the ES experiment, with 200 mL 5 mg/L PE MP at 5 or 20 mM KNO_3 without water circulation. EIS was measured with a fixed amplitude of 50 mV, and the frequency ranged from 0.01 to 10^5 Hz.

6.1.4. Theorical Calculations

Theoretical calculations were conducted to help explain the effect of electrochemical parameters on the removal efficiency of MPs observed in the experiments. The Derjaguin, Landau, Verwey, and Overbeek (DLVO) theory, which considers van der Waals and electrostatic forces between particles, is commonly used to elucidate the kinetic stability and coagulation behavior of colloidal systems (Feng et al., 2022b). In this study, the GF fiber has a diameter of approximately 9 μm, while the average particle size of the MPs is about 5 μm. Given the relatively small size difference between the fibers and particles, a particle-particle model was employed to examine the interaction energy between MP particles and between the electrode and MP particles. The total interaction energy is calculated as the sum of the van der Waals and electrostatic interaction energies (Butt et al., 2023; Chen et al., 2024). The van der Waals interaction energies are calculated using the following equation:

$$U_{132}^{vdw} = \frac{-A_{132}a_1a_2}{6h(a_1 + a_2)}\left[\frac{1}{1 + \frac{11.12h}{\lambda_c}}\right]$$

where a_1 and a_2 represent the radii of the interacting particles (m); h denotes the separation distance between the two interacting particles (m); λ_c is the characteristic interaction wavelength, typically assumed to be 100 nm (Wang et al., 2022a). The Hamaker constant A_{131}, which characterizes the interaction between material 1 in medium 3, can be determined using the following equation:

$$A_{132} = \left(\sqrt{A_{11}} - \sqrt{A_{33}}\right)\left(\sqrt{A_{22}} - \sqrt{A_{33}}\right)$$

where A_{11} and A_{22} represent the Hamaker constants for materials 1 and 2 in a vacuum, the values for PE and GF are 4.69 × 10^{-19} J and 8.80 × 10^{-20} J, respectively (Tsai et al., 1991). Additionally, A_{33} is the Hamaker constant for water, which is 3.7 × 10^{-20} J (Feng et al., 2023).

The electrostatic interaction energy can be determined using the following equation:

$$U_{132}^{el} = 4\pi\varepsilon\varepsilon_0\frac{a_1a_2}{(a_1 + a_2)}\left[\xi_1\xi_2\exp(-\kappa h) - \frac{1}{4}(\xi_1^2 + \xi_2^2)\exp(-2\kappa h)\right]$$

Here, ε_0 is permittivity of free space and ε is relative permittivity of water. ξ_1 and ξ_2 represent the surface potentials of subject 1 and 2, respectively (V). κ is inverse Debye length (m^{-1}), which can be calculated as:

$$\kappa = \left(\frac{2N_Ae^2I}{\varepsilon\varepsilon_0k_BT}\right)^{1/2}$$

where K_B is the Boltzmann constant (1.38×10^{-23} J/K); and T is the absolute temperature (298.15 K). The surface potential of the electrode can be estimated using the Grahame equation based on surface charge density (Butt et al., 2023):

$$\sigma = \sqrt{8c_0\varepsilon\varepsilon_0 k_B T}\,\sinh(\frac{e\varphi_0}{2k_BT})$$

where c_0 is bulk electrolyte concentration (n/m3) and e represents elementary charge (1.60218×10^{-19} C). σ is surface charge density (C/m2), which can be estimated by the integral area of the cyclic voltammogram.

6.2. Results and Discussion

6.2.1. MP Removal Using Electrosorption

A static water tank was initially used to investigate the influence of various factors on the efficiency of MP removal by ES technology. The removal efficiency of MP using ES technology and the change of turbidity of MP dispersion with treatment time are demonstrated in Figure 6-2. Turbidity was used as an additional indicator of MP concentration in the water, as MPs were the only particles present in the system. The trends in the turbidity reduction curves are consistent with the removal efficiency observed during the treatment. The removal efficiency of MPs was found to depend on the electrolyte concentration and the applied voltage. In the static water tank, higher removal efficiency is positively correlated with increasing KNO_3 concentration and voltage within the tested ranges. The highest removal efficiency achieved using ES was 89.0% at 20 mM KNO_3 and 12 V after 150 min of treatment. In contrast, at a lower electrolyte concentration (5 mM KNO_3), the removal efficiency remained relatively low across different applied voltages. After 150 min, the removal efficiencies of PE MP were 28.1%, 47.8%, and 59.4% for 3 V, 6 V, and 12 V, respectively. However, at 20 mM KNO_3, these efficiencies can be improved to 42.1%, 59.3%, and 89.0% for 3 V, 6 V, and 12 V, respectively.

The removal efficiencies exceed 80% at 12 V with both 10 and 20 mM KNO_3, achieving 84.0% and 89.0% respectively. However, the shapes of these two curves exhibit different trends. With 10 mM KNO_3 at 12 V, the increase in removal efficiency appears more linear, with values of 27.3%, 49.1%, 65.6%, and 83.0% at 30, 60, 90, and 120 min, respectively. In contrast, at 20 mM KNO3 and 12 V, most of the MP removal occurred within the first 60 min, with removal efficiencies of 51.3%, 77.5%, 81.5%, and 81.7% at 30, 60, 90, and 120 min, respectively. This indicates that while the maximum removal efficiency at 12 V is similar for both 10 and 20 mM KNO_3 concentrations, the higher salt concentration (20 mM KNO_3) accelerates the removal process.

The effect of KNO_3 concentration can be attributed to the interactive influences of electric double layer compression and increased solution conductivity. Higher ionic strength compresses the electric double layer on both the PE MP and electrode surfaces, reducing the distance over which electrostatic forces act (Jin et al., 2017; Torabi et al., 2023). This facilitates close proximity between MPs and the electrode surface, enhancing the removal. Additionally, the reduced electrostatic repulsion between MP particles promotes aggregation, making it easier for the aggregated particles to be trapped in the porous structure of the electrodes.

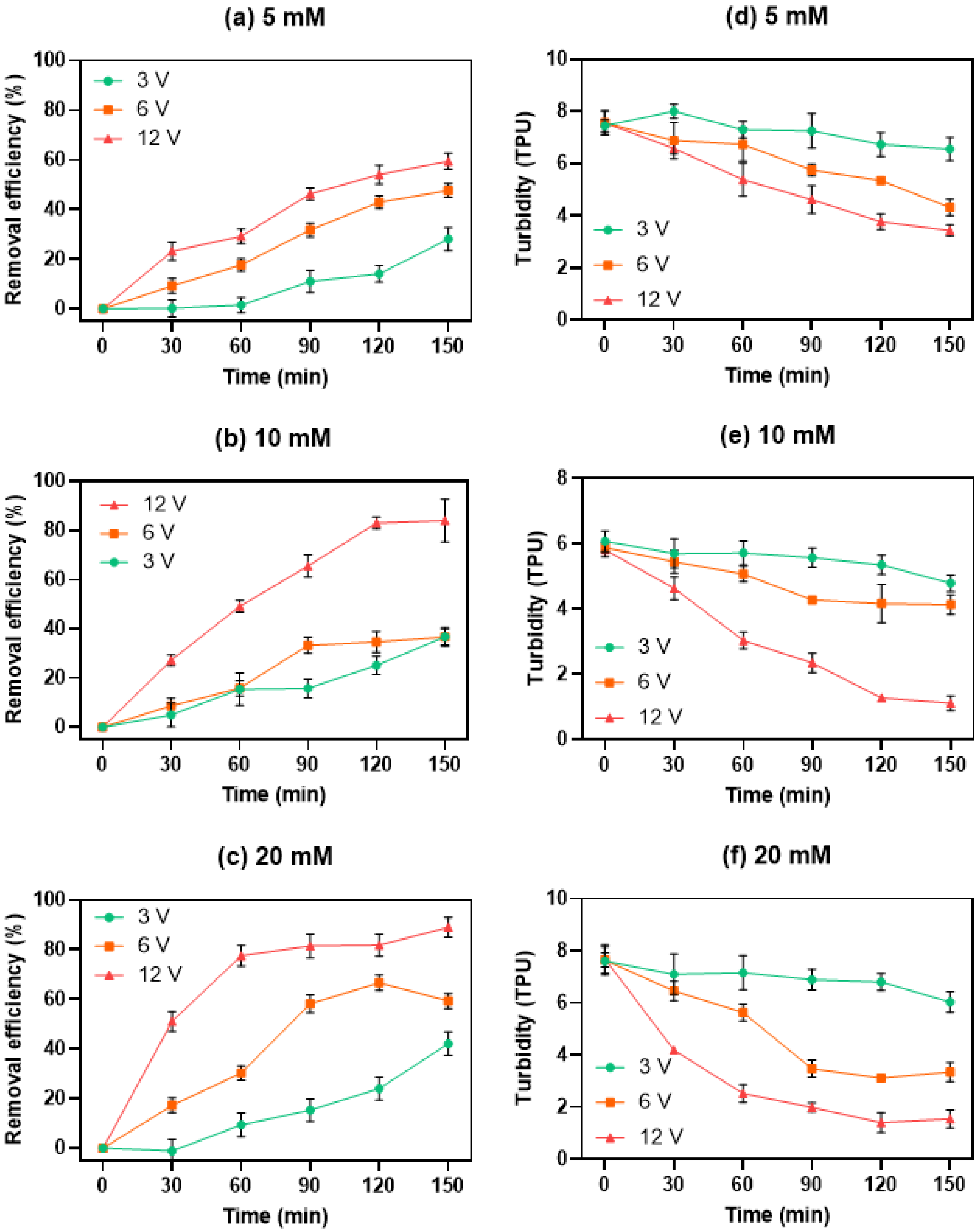

Figure 6-2. Removal efficiency and turbidity variation over treatment time using ES at 5, 10, and 20 mM KNO_3.

A similar trend has been observed in the removal of clay particles or organic pollutants using ES (Torabi et al., 2023; Xie et al., 2018). The mass of adsorbed solids on carbon felt electrodes during ES increased with salt concentration (NaCl, KCl, $CaCl_2$, and Na_2CO_3), although this increase peaked and subsequently declined with further salt additions (Xie et al., 2018). Torabi et al. (2023) found that using ES with carbon sheet electrodes for the removal of 4-chlorophenol achieved the highest removal rate at an ionic strength of 0.86 mM (adjusted with NaCl), which decreased with further increases in ionic strength. The decline in removal efficiency at higher ionic strengths can be attributed to the predominance of electrolysis reactions (Xie et al., 2018). Furthermore, high ionic strength can lead to the competitive adsorption between MP particle and ions (Lissaneddine et al., 2022). Although a decline in removal efficiency was not observed within the selected range of KNO_3 concentrations in this study, it is possible that further increases in ionic strength could result in such a decline. The threshold at which this decline occurs can vary depending on the type of electrolyte used.

6.2.2. Removal of Microplastics Through Electrosorption with Flow-Through Cell

Flow-through electrochemical cell is widely designed and used for the electrochemical treatment of water contaminants. The effect of hydraulic forces can be an important factor affecting the performance of ES. To explore this, a flow-through reactor with water circulation was developed to examine how flow rate influences the removal efficiency of MP using ES. The flow direction was firstly investigated to find the optimal direction for MP removal and the results are shown in Figure 6-3. It was found that flow from anode-to-cathode resulted in a significantly higher removal rate compared to flow from cathode-to-anode. This difference can be attributed to the electrostatic repulsion force between the negatively charged MPs and the cathode. When the flow direction is from cathode to anode, the cathode interferes with the movement of the MPs, hindering their adsorption onto the anode.

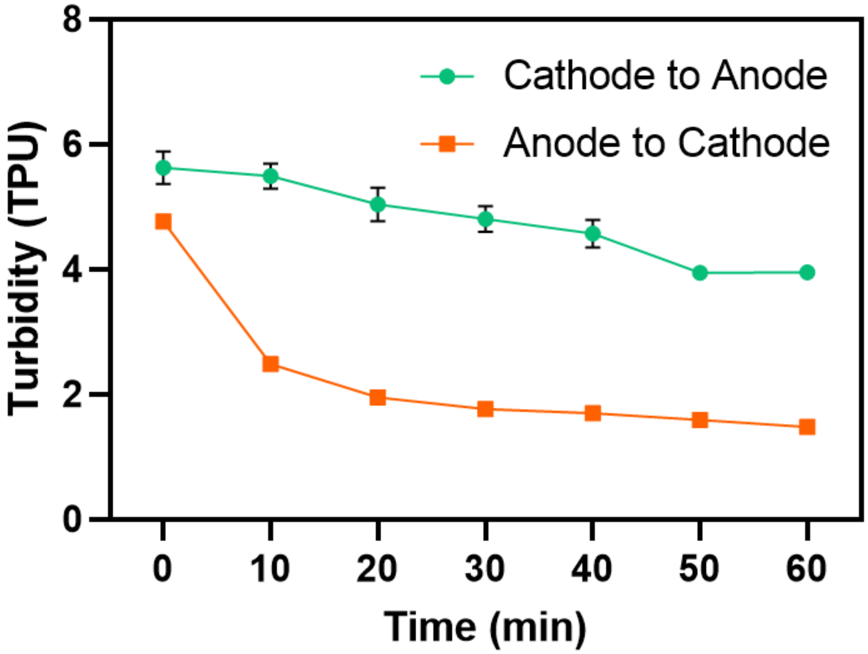

Figure 6-3. Comparison of the effect of flow direction on MP removal, measured by the change in turbidity over treatment time. Conditions: 6V, 10 mM KNO_3, and 30 mL/min flow rate.

The removal efficiency of MP was calculated based on samples collected from both the reservoir tank and the outlet water from reactor, with results shown in Figure 6-4. It can be found that flowing water can accelerate the removal of MP, with efficiencies of 34.4%, 85.3%, 93.9%, and 96.9% after 150 min of treatment at flow rates of 15, 30, 60, and 80 mL/min, respectively. This increased removal efficiency can be attributed to improved mass transfer associated with higher flow rates. A greater flow rate increases the frequency of contact between MP particles and the electrodes, thereby enhancing the likelihood of particle capture. Additionally, higher flow rates improve mixing, which reduces the thickness of the boundary layer adjacent to the electrode surface. This reduction facilitates the diffusion of MPs to the electrode surface for adsorption (García-López et al., 2023). Although this study did not observe a decline in removal efficiency within the tested flow rate range, other studies using ES for organic pollutant removal have indicated that the relationship between flow rate and removal performance is not linear (Bayram and Ayranci, 2012; Yang et al., 2021). In these studies, removal efficiencies declined after reaching a peak as flow rates continued to increase. Bayram and Ayranci (2012) investigated the effect of flow rate on ES performance for removing benzoic acid using activated carbon cloth electrode in a flow-through electrolytic cell. They found that optimal removal was achieved at 30 mL/min under their setup but continue increasing the concentration showed a slight decrease in the removal rate. Similar results were obtained in the study conducted by Yang et al. (2021) for the removal of Orange II using ES and peroxi-coagulation with flow-through cell. The decreased residence time due to the increased flow rate led to the decrease in the removal efficiency. The decrease in the residence time caused by increasing flow rates was compensated for by the water circulation in the ES system. However, further investigation is needed to determine the optimal flow rate for large-scale applications, aiming to maximize removal rates and efficiencies while minimizing energy consumption.

The removal efficiencies at 150 min are quite close for flow rate of 30, 60, and 80 mL/min despite showing significant differences at 30 min. At the high flow rate of 80 mL/min, the removal efficiency reached 88.1% after 30 min. However, additional treatment time at this flow rate did not result in a significant increase in removal efficiency; it rose to 94.6% at 90 min and 96.9% at 150 min, respectively. The removal efficiency improved from 88.8% at 90 min to 92.2% at 120 min, and finally to 93.9% at 150 min, respectively at 60 mL/min. In contrast, at the lower flow rate of 15 mL/min, the removal efficiency continued to increase throughout the 150 min treatment period, although the final efficiency (34.4%) was not as high as those achieved at higher flow rate condition.

This suggests that 150 min may not be sufficient for the low flow rate to reach equilibrium, and longer treatment time can further enhance removal efficiency under these conditions. Overall, while higher flow rates can accelerate the removal of MPs using ES, they may not significantly alter the maximum removal capacity of the system when using water circulation (Bayram and Ayranci, 2012).

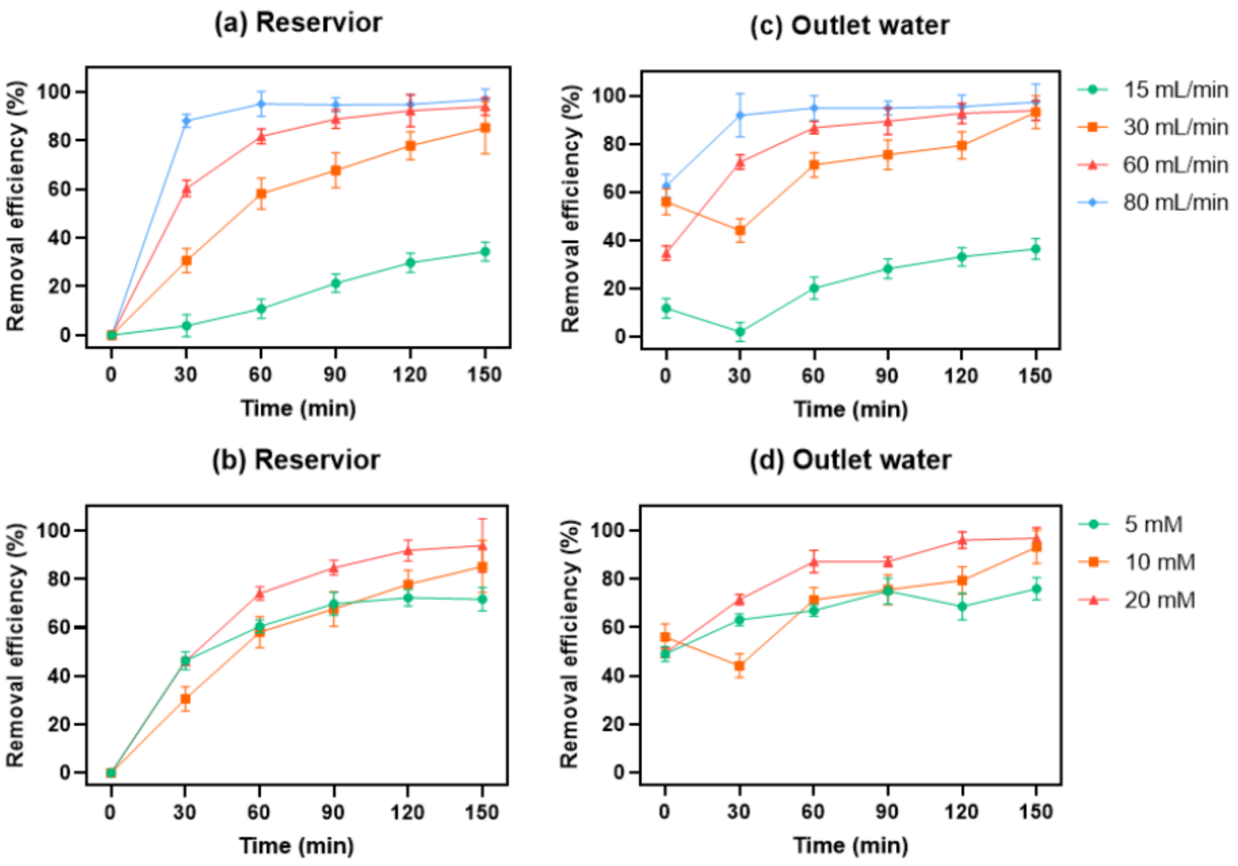

Figure 6-4. The removal efficiency of MP using ES at reservoir water and outlet water from reactor cell under different (a, c) flow rates (10 mM KNO_3) and (b, d) KNO_3 concentrations (30 mL/min flow rate).

The effect of electrolyte concentration was investigated at a voltage of 6 V and a flow rate of 30 mL/min. Under these conditions, the differences in in removal efficiency for MPs were relatively small. After 150 min of treatment, removal efficiencies were 71.7%, 85.3%, and 93.8% for 5, 10 and 20 mM KNO_3, respectively. These results are consistent with those from the static water tank experiments shown in Fig. 1; the increase in the electrolyte concentration can enhance removal efficiency via the compressed electric double layer and also the improved conductivity.

6.2.3. Factorial Analysis of Electrochemical Parameters Affecting Microplastic Removal

A 2^3 full factorial design was employed to statistically investigate the significance of various factors on removal efficiency and to assess their possible interactions. Three key parameters in the electrochemical system include the electrolyte concentration, flow rate, and voltage were selected to examine their effects on the removal efficiency of MPs using ES after 150 min treatment. Only main effects and two-way interactions were considered in the model, as higher order interactions have negligible impacts on the response, in accordance with the sparsity-of-effects principle. The results of the factorial analysis are demonstrated in Figure 6-5 and the analysis of variance (ANOVA) table is shown in **Table 6-2**.

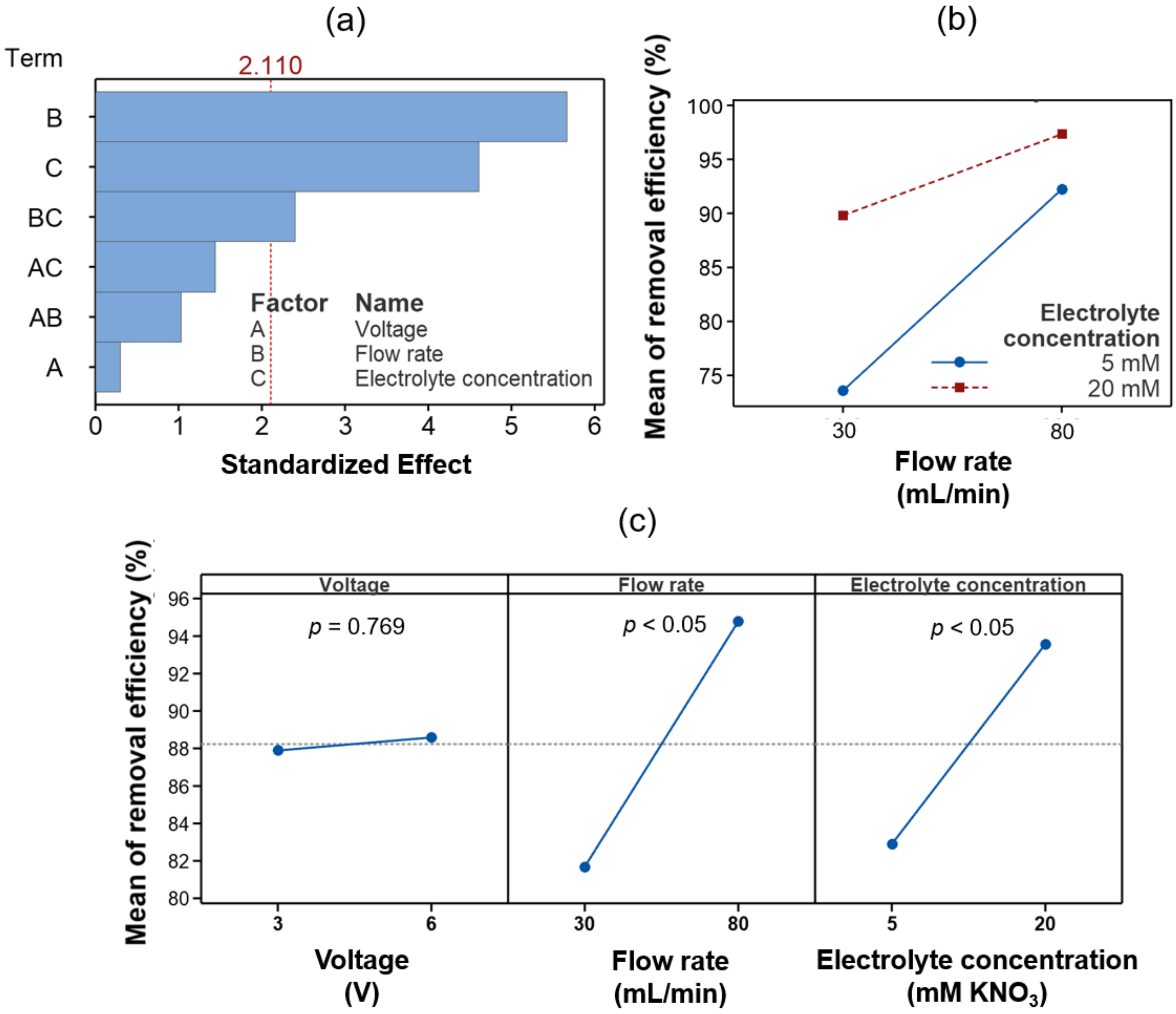

Figure 6-5. Results of factorial analysis. (a) Pereto chart f standardized effects ($\alpha = 0.05$); (b) two-way interaction plot with $p < 0.05$, and (c) main effect plot.

Table 6-2. ANOVA table for analysed factors and their two-way interactions.

Source	DF	Adj SS	Adj MS	F-Value	P-Value
Model	6	0.200259	0.033377	10.38	0.000
Linear	3	0.171597	0.057199	17.79	0.000
Voltage	1	0.000287	0.000287	0.09	0.769
Flow rate	1	0.103054	0.103054	32.06	0.000
Electrolyte concentration	1	0.068255	0.068255	21.23	0.000
2-Way Interactions	3	0.028662	0.009554	2.97	0.061
Voltage*Flow rate	1	0.003403	0.003403	1.06	0.318
Voltage*Electrolyte concentration	1	0.006681	0.006681	2.08	0.168
Flow rate*Electrolyte concentration	1	0.018577	0.018577	5.78	0.028
Error	17	0.054648	0.003215		
Lack-of-Fit	1	0.001831	0.001831	0.55	0.467
Pure Error	16	0.052818	0.003301		
Total	23	0.254907			

*DF: degree of freedom; Adj SS: adjusted sums of squares; Adj MS: adjusted mean squares.

The Pereto chart (Figure 6-5a) illustrates the relative importance of various factors in the removal efficiency of MPs, highlighting that flow rate, electrolyte concentration, and their interaction are statistically significant. The main effect plots in Figure 6-5c indicate that the mean removal efficiency improved from 81.7% to 94.8% when the flow rate was increased from 30 to 80 mL/min. This finding aligns with the results presented in Section 3.2., where a higher flow rate enhances mass transfer and increases the likelihood of particles being captured by the electrode within the selected flow rate range. Electrolyte concentration is the second most important factor in the model. The mean of MP removal efficiency increased from 82.9% to 93.6% as the electrolyte concentration was raised from 5 to 20 mM KNO_3. In contrast, the voltage used in the factorial analysis showed no statistically significant impact on removal efficiency at the level tested (3 and 6 V) with mean of removal efficiencies of 87.9% and 88.6%, respectively. While the effect of voltage with water circulation was not investigated in Section 3.2, it was studied in the static water tank, as noted in Section 3.1. In the static water tank, removal efficiencies were positively correlated with voltage, as shown in Figure 6-2a. However, in the ES treatment of MP with water circulation, no significant difference was observed between 3 and 6 V voltage. The differing effects of voltage on MP removal efficiency between the static water tank and the water circulation setup can be attributed to variations in hydraulic conditions. In a static water tank, MP adsorption on the electrodes primarily results from electrostatic attraction. Since the water is stationary, the adsorption rate depends on the potential created by the applied voltage. Additionally, increasing the voltage enhances the rate of water electrolysis, generating bubbles around the electrodes and introducing turbulence, which further increases the likelihood of particle capture. However, in the system with water circulation, the flowing water improves the mass transfer rate. Once the voltage is sufficient to capture MPs, further increases do not significantly enhance removal efficiency, as observed in the static water tank.

The only significant interaction identified in the model is the interactive effect of flow rate and electrolyte concentration, as shown in Figure 6-5b. The effect of flow rate is more pronounced at 5 mM KNO_3 compared to 20 mM KNO_3. Specifically, the mean removal efficiency was improved from 73.6% to 92.2% by increasing the flow rate from 30 to 60 mL/min. However, the mean removal efficiency was only slightly improved from 89.8% to 97.7% at 20 mM KNO_3. The more significant effect of flow rate on removal efficiency at 5 mM electrolyte concentration compared to 20 mM can be attributed to several factors related to mass transfer and electrostatic interactions. At lower ionic strength (5 mM), the dispersion of MPs is more stable due to a thicker electric double layer, which reduces effective electrostatic interactions between the electrodes and MP particles. This necessitates enhanced mass transfer (via higher flow rates) to achieve efficient removal. The higher ionic strength at 20 mM decreases the electrostatic repulsion between MPs, promoting their aggregation and enhancing their entrapment by the porous structure of the GF electrode. In this scenario, the process is less dependent on mass transfer because the electrostatic forces are already strong enough to facilitate efficient adsorption. Consequently, increasing the flow rate has a diminished effect on further improving removal efficiency.

Electrochemical processes are inherently complex, encompassing numerous factors that can significantly affect their performance. The factorial analysis conducted in this study is essential for systematically investigating the effects and interactions of multiple factors on the removal efficiency of the ES system. The insights gained from the factorial analysis are invaluable for optimizing the process parameters, enabling the achievement of optimal removal rates and efficiency with minimal energy consumption.

6.2.4. Characterization and Theoretical Calculation

Electrochemical characterizations and DLVO analysis were conducted to clarify the experimental results of ES for the removal of MPs. Figure 6-6 presents the CV curves and the calculated DLVO interaction energies. Figure 6-6a and 6-6b show the CV curves of the system within a voltage window from -1.6 V to 1.6 V at scan rates of 5, 10, and 20 mV/s for 5 and 20 mM KNO_3, respectively. Notably, no significant redox peaks are observed within this voltage range during the ES process. However, a higher current response is evident in the 20 mM KNO_3 solution compared to the 5 mM solution, which can be attributed to the reduced electrolyte resistance in the higher concentration solution.

To align with the voltage range used in the ES experiments, the voltage window was expanded from -3 V to 3 V, and the corresponding CV curves are shown in Figure 6-6c. Distinct peaks appear at approximately -1.5 V and +1.5 V, likely associated with the hydrogen evolution reaction and oxygen evolution reaction, respectively, due to the electrolysis of water. The appearance of these peaks confirms that the applied potential range exceeds the thresholds for water splitting, resulting in significant faradaic processes related to water electrolysis. These findings are consistent with observations from the ES experiments, where gas generation on the electrode was noted during the process.

The Nyquist plot in 5mM and 20 mM KNO_3 are shown in Figure 6-7. The absence of semicircle in both electrolyte concentrations suggests minimal charge transfer resistance (Zhou et al., 2022). Additionally , the steep slope of the plots indicates strong capacitive behavior, implying that ionic diffusion impedance is low and that the system is primarily governed by capacitive processes (Mei et al., 2018; Salehan et al., 2023). DLVO analysis was conducted to assess the interaction energies between MPs (MP-MP) and between MPs and the anode (MP-electrode) to better understand the electro-assisted sorption process. The surface potential of the electrode was calculated using the charge density estimated from the CV curve and the Grahame equation. Figure 6-6d presents the DLVO interaction energies for 5 mM and 20 mM KNO_3. The positive interaction energy between MPs in 5 mM KNO3 indicates electrostatic repulsion between the particles. However, in 20 mM KNO3, the sign of the MP-MP interaction energy changes, suggesting that the van der Waals attractive forces dominate the MP-MP interaction due to the screened double layer at higher ionic strength. Despite the decrease in electrostatic attraction between MPs and the electrode caused by double-layer shielding at higher ionic strengths, our experiments still demonstrated improved removal efficiency under these conditions (Figure 6-4 andFigure **6-5**). This suggests that the ES of MPs is influenced by both the interactions between colloidal particles and their electrostatic attraction to the electrode. Furthermore, the aggregation of MPs particles due to reduced electrostatic repulsion at higher ionic strengths likely increases particle size. The increased particle size of MPs, in turn, may enhance the attraction between the MPs and the electrode, and promote physical settling due to the reduced stability of the suspension, thereby improving the removal rate of MPs.

The interaction energies between the electrode and MPs at higher voltages were not calculated because Faradaic reactions become significant in this range. These reactions complicate the estimation of surface potential based solely on charge transfer, as the charge is consumed in chemical processes rather than contributing to the surface potential (as shown in Figure 6-6c). This observation aligns with our experimental findings: increasing the voltage beyond a certain threshold does not enhance the removal efficiency of MPs. Instead, the additional energy is primarily used for Faradaic processes, such as water electrolysis, rather than improving the electrostatic attraction between the particles and the electrode.

Furthermore, SEM characterization was performed on the cathode, anode, and the original GF electrode after the ES experiments (Figure 6-8). The SEM images reveal that the anode adsorbed more plastic particles compared to the cathode, which is consistent with the results of the DLVO analysis. This suggests that the adsorption of PE MPs primarily occurs on the anode due to the electrostatic attraction between negatively charged PE MP and the anode.

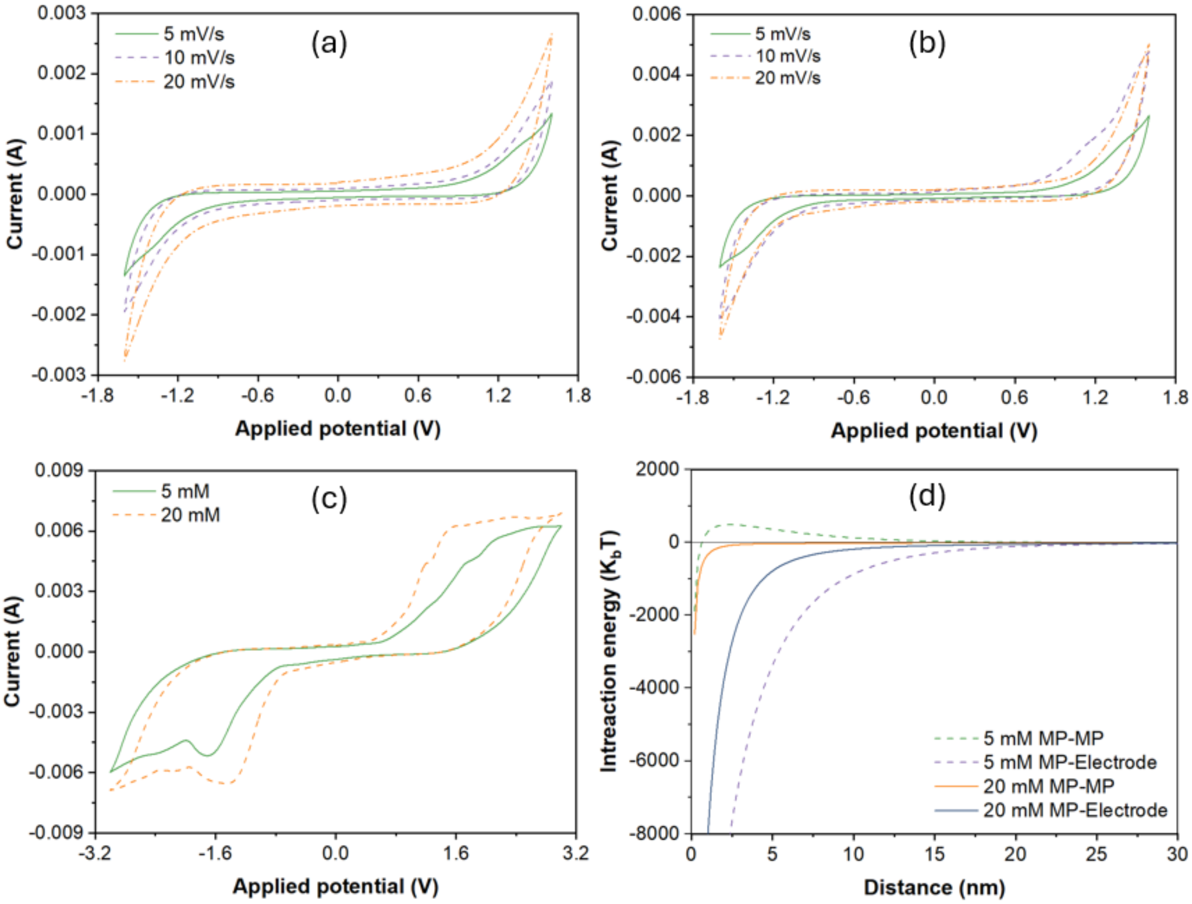

Figure 6-6. CV curves and DLVO interaction energies. (a) CV in 5 mM KNO3; (b) CV in 20 mM KNO_3, from -1.6 V to 1.6 V. (c) CV at 10 mV/s from -3 V to 3 V for 5 mM and 20 mM KNO_3. (d) DLVO interaction energy profiles between MPs (MP-MP) and between MP and the anode (MP-Electrode) at 1.6 V.

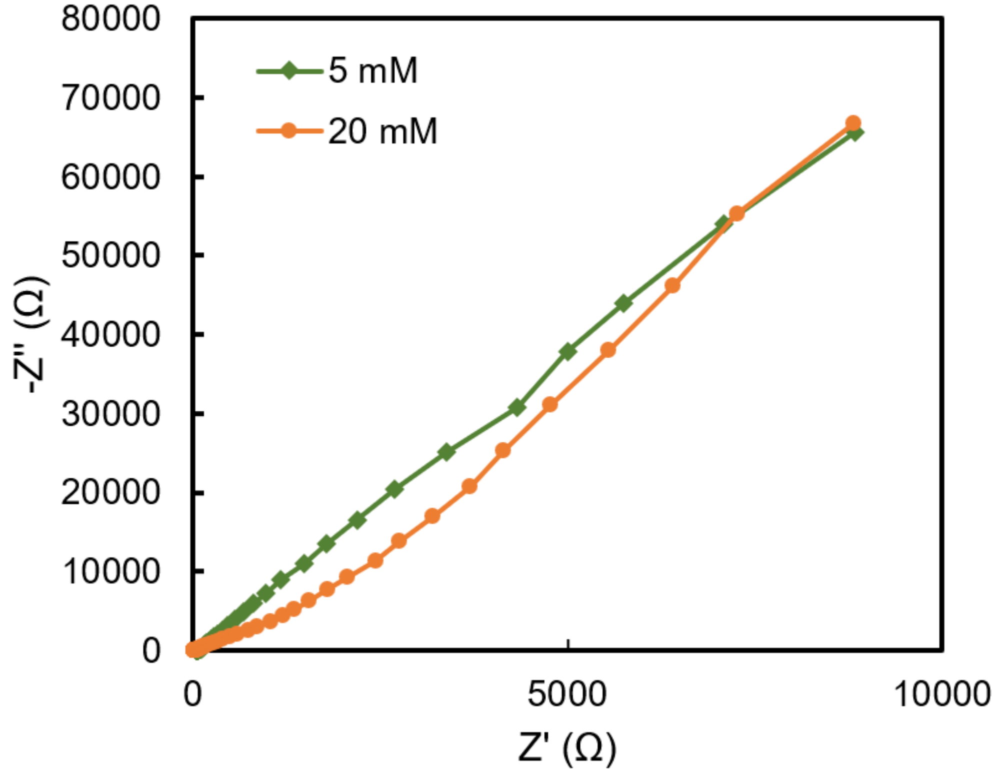

Figure 6-7. Nyquist plot of the ES system in static water tank at 5 and 20 mM KNO_3.

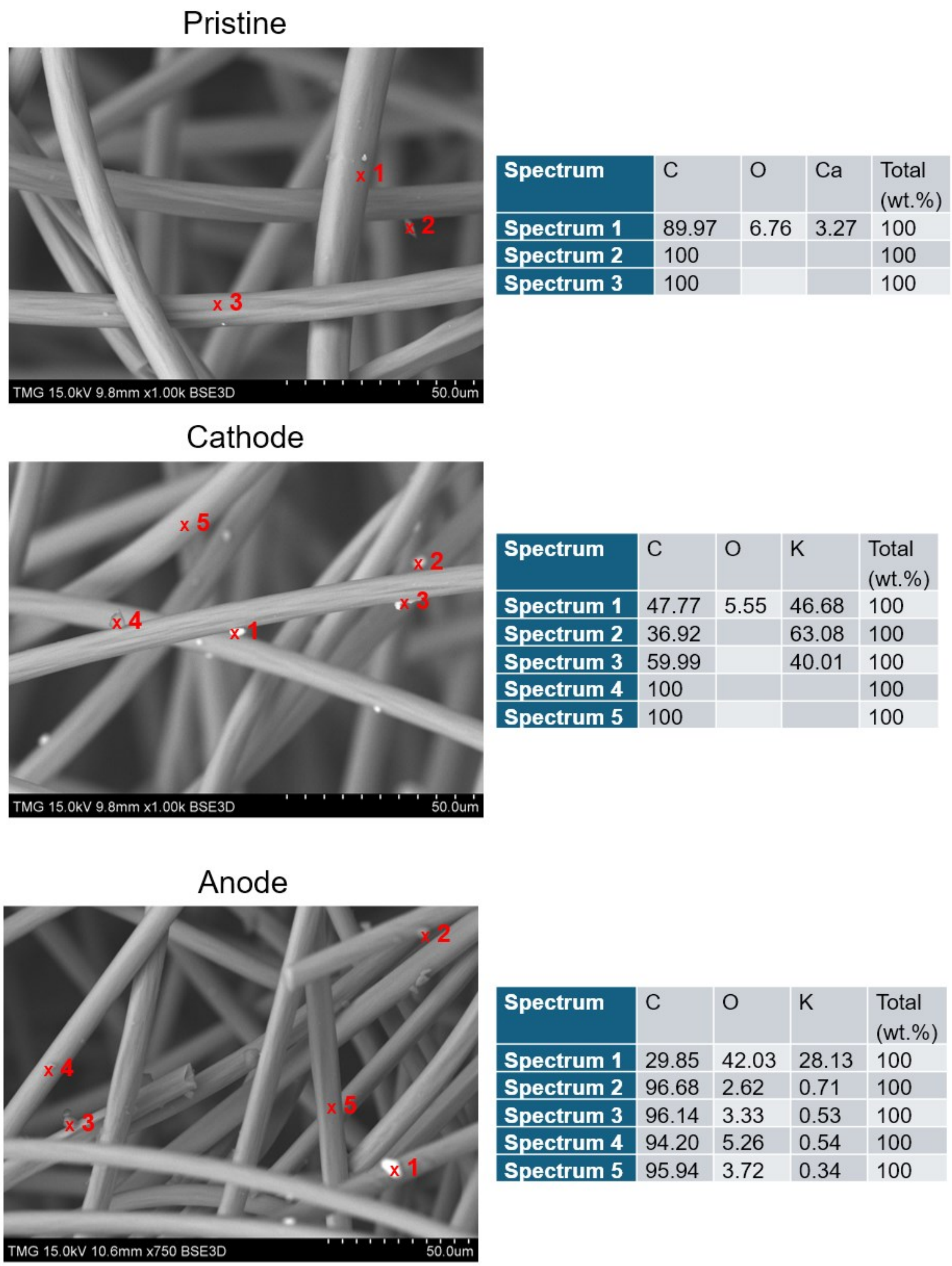

Spectrum	C	O	Ca	Total (wt.%)
Spectrum 1	89.97	6.76	3.27	100
Spectrum 2	100			100
Spectrum 3	100			100

Spectrum	C	O	K	Total (wt.%)
Spectrum 1	47.77	5.55	46.68	100
Spectrum 2	36.92		63.08	100
Spectrum 3	59.99		40.01	100
Spectrum 4	100			100
Spectrum 5	100			100

Spectrum	C	O	K	Total (wt.%)
Spectrum 1	29.85	42.03	28.13	100
Spectrum 2	96.68	2.62	0.71	100
Spectrum 3	96.14	3.33	0.53	100
Spectrum 4	94.20	5.26	0.54	100
Spectrum 5	95.94	3.72	0.34	100

Figure 6-8. SEM-EDS results of pristine, cathodic, and anodic GF. The lighter-colored particles on the electrodes are residual KNO_3 after drying. A greater number of MPs (particles with higher carbon content and darker color in the SEM image) attached to the GF surface after treatment.

6.2.5. Environmental Implications

The presence of MPs in natural waters and wastewater has been increasingly observed in recent years, largely due to the growing release of both primary and secondary MPs from human activities. Wastewater is a significant source of MPs in the natural aquatic environment. However, few studies have focused on separating MPs from water to prevent their discharge into the environment. Common wastewater treatment processes in WWTPs, such as filtration, air flotation, and flocculation, can partially remove larger MPs but are less efficient for smaller MPs, which pose greater environmental risks. In response to this challenge, this study develops an electrochemical treatment method using electro-assisted sorption with porous graphite fiber electrodes, investigating the effects of various electrochemical parameters and setups to preliminary optimize the system.

One of the key advantages of ES, compared to other chemical methods like electrocoagulation and chemical coagulation, is that it does not require the addition of external chemicals. Instead, it relies on applying an electric potential to porous electrodes, which causes charged MP particles to be physically adsorbed onto electrodes with opposite charges through electrostatic attraction. Removal efficiency can be influenced by factors such as applied voltage, electrolyte concentration in the water, and mass transfer efficiency. In a static ES system without water circulation, 150 min of treatment can effectively remove MPs from 200 mL of water, with removal efficiency positively correlated to both applied voltage and electrolyte concentration. However, mass transfer efficiency between the water and the electrode surface can limit MP removal via ES. Therefore, this study also investigated the removal efficiency of MPs under conditions with water circulation.

The results demonstrated that incorporating water circulation significantly enhanced both the rate and overall efficiency of MP removal through ES. After 150 min of treatment, MP removal rates ranged from 34.4% to 96.9%, depending on the electrolyte concentration and flow rate. A factorial analysis was conducted to further assess the impact of key electrochemical parameters in the ES system with water circulation. The analysis revealed that flow rate is the most critical factor influencing MP removal efficiency, suggesting that mass transfer may be the primary limitation for the adsorption of MPs onto the electrodes.

Electrolyte concentration also significantly improved removal efficiency within the range examined in the factorial analysis. A higher electrolyte concentration compresses the electric double layer around the MP particles, destabilizing their dispersion and promoting aggregation. This aggregation facilitates the capture of MP particles by the porous structure of the GF electrodes. Additionally, the gradually decreeing mean particle size of MPs over treatment time indicates that larger particles are easier to be captured by the porous structure. However, the factorial analysis showed no significant difference in removal efficiency between 3 V and 6 V, further supporting the conclusion that mass transfer is likely the primary limitation for MP adsorption onto the electrodes via ES. Moreover, increasing the voltage primarily contributes to Faradaic reactions rather than enhancing the surface potential of the electrodes. Although a consistent treatment time of 150 min was used throughout this study, under conditions of an 80 mL/min flow rate, 10 mM KNO_3 concentration, and 6V applied voltage, 88.1% of the MPs were removed in just about 30 min. This demonstrates that the system we developed is highly efficient in rapidly removing MPs.

This study demonstrates that ES is a highly promising technology for removing MPs, offering an efficient and cost-effective solution for separating MPs from wastewater, particularly in scenarios with high concentrations, such as laundry wastewater. Compared to conventional wastewater treatment methods, ES achieves high removal efficiency even for smaller MPs (PE particles with 3-5 µm mean particle size used in this study). Additionally, ES is a flexible technology that can be tailored to various scale requirements by adjusting the size of the electrode units, making it suitable for a wide range of applications—from removing MPs in washing machines to large-scale implementations in WWTPs.

This study investigated the potential of ES technology for MP removal, clearly highlighting its significant promise for further development. Compared to static conditions, water circulation in the reactor significantly improves the MP removal efficiency using ES treatment. A higher flow rate further enhances this efficiency, suggesting that mass transfer efficiency may be a limiting factor in MP removal. Additionally, higher electrolyte concentrations improve MP removal by increasing conductivity and compressing the electric double layer. By analyzing the influence of various parameters on MP removal efficiency and exploring the underlying mechanisms through DLVO theory, this study research establishes a foundation for future advancements in ES for MP removal. Future studies could focus on investigating the removal of MPs using ES in more complex, real-world environments. For example, research could explore how different types of MPs and the presence of other components in wastewater affect removal efficiency. Additionally, optimizing the system will be crucial not only to enhance removal performance but also to minimize energy consumption and operational costs, making it more practical for large-scale applications.

Chapter 7. Conclusions and Future Studies

7.1. Conclusions and Contributions of Thesis Research

- ***Analyzed the key factors influencing the entrainment of microplastics during ice formation processes.***

Ice formation results in the microplastic entrainment and enrichment, in which turbulence, environmental, and microplastic characteristics play important roles. This study aimed to explore the effect of various MP properties and environmental characteristics on the entrainment and enrichment of MPs in ice under varying turbulence conditions. It was found that high rotation speed in freshwater distinctively enhanced the entrainment of hydrophobic MPs in ice, this being attributable to the combined effects of frazil ice and air bubbles. The hydrophobic nature of these MPs caused them to be attracted to the water/air or water/ice interface. However, in saline water, high turbulence inhibited the entrainment of all of the MP types under study. The ice crystals formed a loose structure in saline water instead of congealing, and this allowed the exchange of MPs between ice and water, leading to the rapid expulsion of MPs from the ice. The enrichment factors of all the MPs under study increased in calm saline water compared to in calm freshwater. The results revealed that the entrainment and enrichment of MPs in ice can be critical pathways affecting their fate in cold regions.

- ***Investigated the role of aquatic dissolved organic matter in the entrainment of MPs under freezing conditions***

My study investigated the effects of aquatic dissolved organic matter on the properties of MPs through a 28-day interaction experiment conducted under both UV and dark conditions. The implications of the alteration in MP properties on their entrapment in ice were also explored in an ice formation experiment. The presence of aquatic organic matter on the MPs after the interactions was confirmed, but the interaction with aquatic organic matter had different impacts on the two types of MPs. Furthermore, the entrapment of MPs in ice was improved after their interaction with aquatic organic matter due to surface damage caused by physical abrasion and UV radiation. These findings underscore the critical role that the inherent properties of MPs play in determining their environmental behavior. These properties can significantly impact their interactions with other natural components in the environment, thereby influencing their behavior in a cold environment.

- ***Explored the freezing-induced alteration in MP behavior***

With changing temperatures, MPs stored in ice can be released back into the environment, while freezing conditions can alter the properties of MPs, ultimately affecting the fate of MPs in the environment. Freezing of MPs in freshwater ice results in the aggregation of MP particles due to physical compression, leading to an increase in particle size once the MPs are released from the ice. The freezing-induced aggregation enhances buoyancy effects, accelerating the settling/rising velocity of MPs in water. Additionally, freezing can lead to enhanced surface wetting alterations, thus improving the dispersion of hydrophobic MPs. The presence of salt in the water can mitigate the effect of freezing on MPs due to the formation of a brine network within the ice structure, which reduces the pressure on MPs entrapped by ice. In cold regions, numerous MPs undergo freezing and thawing, re-entering the water column.

- ***Developed a novel electrochemical treatment technology for MP removal***

A significant quantity of MPs still reaches the environment via wastewater treatment plant (WWTP) effluent because the techniques commonly used in WWTPs are not effective at removing MPs, especially smaller particles. Smaller MPs are particularly concerning as they can be transported over long distances and more easily enter the food chain, leading to heightened environmental impacts and potential health risks. To address this, an ES method was developed in this study to separate MPs from water using graphite felt electrodes. The effects and interactions of electrochemical factors, including flow rate in the flow-through cell, applied voltage and electrolyte concentration, on the removal efficiency of MPs using the ES system were preliminarily investigated using factorial experiments. Under optimal conditions, 96.9% of MPs were removed after 150 minutes of treatment. By analyzing the influence of various parameters on MP removal efficiency and exploring the underlying mechanisms through DLVO theory, this study research establishes a foundation for future advancements in ES for MP removal. Future studies could focus on investigating the removal of MPs using ES in more complex, real-world environments.

7.2. Future Studies

- MPs can undergo a variety of physical and chemical aging phenomena in the natural environment that alter their surface properties. The surface properties of MPs can also be changed by biofilms caused by microbial colonization and natural organic matter. The ice-trapped MPs may be redistributed through various means, including brine networks in sea ice or the freeze–thaw cycle. These can be important factors influencing the behavior of MPs in ice and need further investigation.

- While this study examined the interactions and aggregation of MP particles under freezing conditions, aggregation between MPs and other naturally suspended particles in aqueous environments has been observed in several previous studies. The heterogeneous aggregation between MPs and other particles can be further intensified under freezing conditions, exerting a significant impact on the environmental fate of MPs by altering their density, size, and surface properties. Furthermore, recent studies have found that MPs trapped in sea ice may be ingested by ice algae and rapidly settle after melting. The environmental fate of released MPs from melt ice and the effect of freezing on entrained MPs need to be further investigated.
- To further advance the ES treatment technology for MP removal, it is essential to investigate both the efficiency and energy consumption of ES in more complex environments. The removal efficiency for smaller MPs, or even nanoplastics, should be evaluated to assess its potential for large-scale applications. Additionally, a pilot prototype can be developed to verify its feasibility for engineering control of MPs in wastewater.

Peer-reviewed Journal Publications

1. ***Chen, Z.K.***, Elektorowicz, M., Ye, Z, Feng, Q., Wang, Z., Tian, X., Lyu, L., & An, C. (2024). Harnessing Electrosorption for High-Efficiency Removal of Polyethylene Microplastics from Water: Unveiling Key Influencing Factors and Underlying Mechanisms. Submitted to ***Water Research*** (*Elsevier*), Manuscript ID: WR90562.
2. ***Chen, Z.K.***, Elektorowicz, M., An, C., Tian, X., Wang, Z., Yang, X., & Lyu, L. (2024). Revealing the Freezing-induced Alteration in Microplastic Behavior and its Implication for the Microplastics Released from Seasonal Ice. ***Environmental Science & Technology*** (*ACS*), 58(30), 13529-13539.

   DOI: 10.1021/acs.est.4c05322
3. ***Chen, Z.K.***, Elektorowicz, M., An, C., & Tian, X. (2024). Seasonal ice encapsulation: the pivotal influence on microplastic transport and fate in cold regions. ***Environmental Science: Water Research & Technology*** *(RCS)*.

   DOI: 10.1039/D4EW00339J
4. ***Chen, Z.K.***, Elektorowicz, M., An, C., Tian, X., & Peng, H. (2024). Role of Aquatic Dissolved Organic Matter in the Entrainment of Microplastics under Freezing Conditions**.** ***ACS ES&T Water*** (ACS), 4(1), 256–267.

   DOI: 10.1021/acsestwater.3c00579
5. ***Chen, Z. K.***, Elektorowicz, M., An, C. & Tian, X. (2023). Entrainment and enrichment of microplastics in ice formation processes: Implications for the transport of microplastics in cold regions. ***Environmental Science & Technology*** (*ACS*), 57(8):3176-3186.

   DOI: 10.1021/acs.est.2c09340
6. ***Chen, Z. K.***, An, C., Elektorowicz, M., & Tian, X. (2022). Sources, behaviors, transformations, and environmental risks of organophosphate esters in the coastal

environment: A review, ***Marine Pollution Bulletin*** *(Elsevier)*, 180:113779.

DOI: 10.1016/j.marpolbul.2022.113779

7. ***Chen, Z. K.***, Feng, Q., Yue, R., Chen, Z., Moselhi, O., Soliman, A., Hammad, A. and An, C. (2022). Construction, renovation, and demolition waste in landfill: A review of waste characteristics, environmental impacts, and mitigation measures, ***Environmental Science and Pollution Research*** *(Springer)*, 29: 46509-46526.

   DOI: 10.1007/s11356-022-20479-5

8. ***Chen, Z. K.***, An, C., Wang, Y., Zhang, B., Tian, X., & Lee, K. (2022). A green initiative for oiled sand cleanup using chitosan/rhamnolipid complex dispersion with pH-stimulus response, ***Chemosphere*** *(Elsevier)*, 288:132628.

   DOI: 10.1016/j.chemosphere.2021.132628

9. ***Chen, Z. K.****,* An, C., et al. (2021) Spatiotemporal analysis of land use pattern and stream water quality in southern Alberta, Canada, ***Journal of Contaminant Hydrology*** *(Elsevier)*, 242:103852.

   DOI: 10.1016/j.jconhyd.2021.103852

10. Tian, X., Lu, C., Song, Z., An, C., Wan, S., Peng, H., An, Qi Feng & ***Chen, Z.K.*** (2024). Quantifying weather-induced unreliable public transportation service in cold regions under future climate model scenarios. ***Sustainable Cities and Society*** (*Elsevier*), 113:105660.

    DOI: 10.1016/j.scs.2024.105660

11. Wang, Z., Lee, K., Feng, Q., An, C., & ***Chen, Z.K.*** (2024). Effect of nanobubbles on the mobilization of microplastics in shorelines subject to seawater infiltration. ***Environmental Pollution*** (*Elsevier*), 349, 123950.

    DOI: 10.1016/j.envpol.2024.123950

12. Yang, X., Huang, G., ***Chen, Z.K.***, Feng, Q., An, C., Lyu, L., Bi, H., & Zhou, S. (2024). Spotlight on the vertical migration of aged microplastics in coastal waters. ***Journal of***

Hazardous Materials (*Elsevier*), 469, 134040.

DOI: 10.1016/j.jhazmat.2024.134040

13. Wang, Z., ***Chen, Z.K.***, & An, C. (2024). Improving solid waste management in remote First Nations communities through inventory-theory-based optimization. ***Canadian Journal of Civil Engineering*** (Canadian Science Publishing), 1(51).

    DOI: 10.1139/cjce-2023-0320

14. Peng, H., An, C., ***Chen, Z. K.***, Tian, X., & Sun, Y. (2023). Promoting cross-regional integration of maritime emission management: A Euro-American linkage of carbon markets. ***Environmental Science & Technology*** (ACS), 57(33), 12180-12190.

    DOI: 10.1021/acs.est.3c02529

15. Tian, X., Waygood, E. O. D., An, C., Chen, Z., & Peng, H. (2023). Achieving urban net-zero targets through regionalized electric bus penetration and energy transition. ***Transportation Research Part D: Transport and Environment*** *(Elsevier)*, 120, 103797.

    DOI: 10.1016/j.trd.2023.103797

16. Tian, X., An, C., and ***Chen, Z. K***, (2023). The role of clean energy in achieving decarbonization of electricity generation, transportation, and heating sectors by 2050: A meta-analysis review. ***Renewable and Sustainable Energy Reviews*** *(Elsevier)*, 182, 113404.

    DOI: 10.1016/j.rser.2023.113404

17. Wang, Z., ***Chen, Z. K.***, & An, C. (2022). A Review on Solid Waste Management in Canadian First Nations Communities: Policy, Practices, and Challenges. ***Cleaner Waste Systems*** *(Elsevier)*, 4:100074. doi: 10.1016/j.clwas.2022.100074

18. Chen, X., Bi, H., Yue, R., ***Chen, Z.K.***, & An, C. (2022) Effects of Oil Characteristics on the Performance of Shoreline Response Operations: A Review. ***Frontiers in Environmental Science*** (*Frontiers*), 2043.

DOI: 10.3389/fenvs.2022.1033909

19. Tian, X., An, C., Nik-Bakht, M., and ***Chen, Z. K.*** (2022). Assessment of reductions in NO2 emissions from thermal power plants in Canada based on the analysis of policy, inventory, and satellite data, ***Journal of Cleaner Production*** *(Elsevier)*, 341:130859.

    DOI: 10.1016/j.jclepro.2022.130859

20. Yue, R., An, C., Ye, Z., Bi, H., ***Chen, Z.K.***, Liu, X., Zhang, X., Lee, K. (2022). Cleanup of oiled shorelines using a dual responsive nanoclay/sodium alginate surface washing agent, ***Environmental Research*** *(Elsevier)*, 205:112531.

    DOI: 10.1016/j.envres.2021.112531

21. Tian, X., Huang, G., Song, Z., An, C., & ***Chen, Z.K.*** (2022). Impact from the evolution of private vehicle fleet composition on traffic related emissions in the small-medium automotive city. ***Science of The Total Environment*** *(Elsevier)*, 840, 156657.

    DOI: 10.1016/j.scitotenv.2022.156657

References

Abdurahman, A., Cui, K., Wu, J., Li, S., Gao, R., Dai, J., Liang, W., Zeng, F., 2020. Adsorption of dissolved organic matter (DOM) on polystyrene microplastics in aquatic environments: Kinetic, isotherm and site energy distribution analysis. Ecotoxicology and Environmental Safety 198110658.

Alimi, O.S., Farner, J.M., Tufenkji, N., 2021. Exposure of nanoplastics to freeze-thaw leads to aggregation and reduced transport in model groundwater environments. Water Research 189116533.

Alizadeh, A., Yamada, M., Li, R., Shang, W., Otta, S., Zhong, S., Ge, L., Dhinojwala, A., Conway, K.R., Bahadur, V., 2012. Dynamics of ice nucleation on water repellent surfaces. Langmuir 28(6), 3180-3186.

Amelia, T.S.M., Khalik, W.M.A.W.M., Ong, M.C., Shao, Y.T., Pan, H.-J., Bhubalan, K., 2021. Marine microplastics as vectors of major ocean pollutants and its hazards to the marine ecosystem and humans. Progress in Earth and Planetary Science 8(1), 1-26.

Anderson, Z.T., Cundy, A.B., Croudace, I.W., Warwick, P.E., Celis-Hernandez, O., Stead, J.L., 2018. A rapid method for assessing the accumulation of microplastics in the sea surface microlayer (SML) of estuarine systems. Scientific Reports 8(1), 1-11.

Andral, M., Roger, S., Montrejaud-Vignoles, M., Herremans, L., 1999. Particle size distribution and hydrodynamic characteristics of solid matter carried by runoff from motorways. Water Environment Research 71(4), 398-407.

Ardhuin, F., Jenkins, A.D., 2006. On the interaction of surface waves and upper ocean turbulence. Journal of Physical Oceanography 36(3), 551-557.

Asthana, R., Tewari, S., 1993. The engulfment of foreign particles by a freezing interface. Journal of Materials Science 285414-5425.

Aytan, U., Valente, A., Senturk, Y., Usta, R., Sahin, F.B.E., Mazlum, R.E., Agirbas, E., 2016. First evaluation of neustonic microplastics in Black Sea waters. Marine environmental research 11922-30.

Barber, D., Harasyn, M., Babb, D., Capelle, D., McCullough, G., Dalman, L., Matthes, L., Ehn, J., Kirillov, S., Kuzyk, Z., 2021. Sediment-laden sea ice in southern Hudson Bay: Entrainment, transport, and biogeochemical implications. Elem Sci Anth 9(1), 00108.

Barrette, P.D., 2021. Understanding frazil ice: The contribution of laboratory studies. Cold Regions Science and Technology 189103334.

Bayram, E., Ayranci, E., 2012. Electrosorption based waste water treatment system using activated carbon cloth electrode: Electrosorption of benzoic acid from a flow-through electrolytic cell. Separation and Purification Technology 86113-118.

Bergmann, M., Allen, S., Krumpen, T., Allen, D., 2023. High levels of microplastics in the Arctic sea ice alga Melosira arctica, a vector to ice-associated and benthic food webs. Environmental Science & Technology 57(17), 6799-6807.

Black, B.D., Harrington, G.W., Singer, P.C., 1996. Reducing cancer risks by improving organic carbon removal. Journal-American Water Works Association 88(6), 40-52.

Butt, H.J., Graf, K., Kappl, M., 2023. Physics and chemistry of interfaces. John Wiley & Sons.

Cai, M., Qi, Z., Guy, C., An, C., Chen, X., Wang, Z., Feng, Q., 2023. Insights into the abiotic fragmentation of biodegradable mulches under accelerated weathering conditions. Journal of Hazardous materials 454131477.

Cao, R., Liu, X., Duan, J., Gao, B., He, X., Bolan, N., Li, Y., 2022. Opposite impact of DOM on ROS generation and photoaging of aromatic and aliphatic nano-and micro-plastic particles. Environmental Pollution 315120304.

Chen, C.S., Le, C., Chiu, M.H., Chin, W.C., 2018a. The impact of nanoplastics on marine dissolved organic matter assembly. Science of the Total Environment 634316-320.

Chen, M., Yang, D., Guo, F., Deng, R., Nie, W., Li, L., Yang, X., Liu, S., Chen, Y., 2023a. Which sediment fraction mainly drives microplastics aging process: Dissolved organic matter or colloids? Journal of Hazardous materials 443130310.

Chen, W., Ouyang, Z.Y., Qian, C., Yu, H.Q., 2018b. Induced structural changes of humic acid by exposure of polystyrene microplastics: A spectroscopic insight. Environmental Pollution 2331-7.

Chen, X., Huang, C., Feng, R., Zhang, P., Wu, Y., Huang, W., 2023b. Multifunctional PVDF membrane coated with ZnO-Ag nanocomposites for wastewater treatment and fouling mitigation: Factorial and mechanism analyses. Journal of Environmental Informatics 41(1), 37-51.

Chen, Z.K., An, C., Tan, Q., Tian, X., Li, G., Zhou, Y., 2021. Spatiotemporal analysis of land use pattern and stream water quality in southern Alberta, Canada. Journal of Contaminant Hydrology 242103852.

Chen, Z., Wei, W., Liu, X., Ni, B.J., 2022a. Emerging electrochemical techniques for identifying and removing micro/nanoplastics in urban waters. Water Research 221118846.

Chen, Z.K., An, C., Elektorowicz, M., Tian, X., 2022b. Sources, behaviors, transformations, and environmental risks of organophosphate esters in the coastal environment: A review. Marine Pollution Bulletin 180113779.

Chen, Z.K., An, C., Wang, Y., Zhang, B., Tian, X., Lee, K., 2022c. A green initiative for oiled sand cleanup using chitosan/rhamnolipid complex dispersion with pH-stimulus response. Chemosphere 288132628.

Chen, Z.K., Elektorowicz, M., An, C., Tian, X., 2023c. Entrainment and enrichment of microplastics in ice formation processes: Implications for the transport of microplastics in cold regions. Environmental Science & Technology 57(8), 3176-3186.

Chen, Z.K., Elektorowicz, M., An, C., Tian, X., Peng, H., 2023d. Role of Aquatic Dissolved Organic Matter in the Entrainment of Microplastics under Freezing Conditions. ACS ES&T Water 4(1), 256-257.

Chen, Z.K., Elektorowicz, M., An, C., Tian, X., Wang, Z., Yang, X., Lyu, L., 2024. Revealing the Freezing-Induced Alteration in Microplastic Behavior and Its Implication for the Microplastics Released from Seasonal Ice. Environmental Science & Technology 58(30), 13529–13539.

Cheng, Y.L., Kim, J.-G., Kim, H.-B., Choi, J.H., Tsang, Y.F., Baek, K., 2021. Occurrence and removal of microplastics in wastewater treatment plants and drinking water purification facilities: A review. Chemical Engineering Journal 410128381.

Chubarenko, I., 2022. Physical processes behind interactions of microplastic particles with natural ice. Environmental Research Communications 4(1), 012001.

Chubarenko, I., Lazaryuk, A., Orlova, T., Lobchuk, O., Raguso, C., Zyubin, A., Lasagni, M., Saliu, F., 2022. Microplastics in the first-year sea ice of the Novik Bay, Sea of Japan. Marine Pollution Bulletin 185114236.

Derjaguin, B., Churaev, N., Muller, V., Derjaguin, B., Churaev, N., Muller, V., 1987. The Derjaguin—Landau—Verwey—Overbeek (DLVO) theory of stability of lyophobic colloids. Surface forces293-310.

Dethleff, D., Kempema, E., 2007. Langmuir circulation driving sediment entrainment into newly formed ice: Tank experiment results with application to nature (Lake Hattie, United States; Kara Sea, Siberia). Journal of Geophysical Research: Oceans 112(C2).

Dietrich, W.E., 1982. Settling velocity of natural particles. Water Resources Research 18(6), 1615-1626.

Fdez-Sanromán, A., Pazos, M., Rosales, E., Sanromán, M.Á., 2024. Advancing in wastewater treatment using sustainable electrosorbents. Current Opinion in Electrochemistry101450.

Feng, Q., An, C., Chen, Z., Wang, Z., 2023. New Perspective on the Mobilization of Microplastics through Capillary Fringe Fluctuation in a Tidal Aquifer Environment. Environmental Science & Technology 57(2), 929-938.

Feng, Q., An, C., Chen, Z., Yin, J., Zhang, B., Lee, K., Wang, Z., 2022a. Investigation into the impact of aged microplastics on oil behavior in shoreline environments. Journal of Hazardous materials 421126711.

Feng, Q., Chen, Z., Greer, C.W., An, C., Wang, Z., 2022b. Transport of Microplastics in Shore Substrates over Tidal Cycles: Roles of Polymer Characteristics and Environmental Factors. Environmental Science & Technology 56(12), 8187-8196.

Fitzner, M., Sosso, G.C., Cox, S.J., Michaelides, A., 2015. The many faces of heterogeneous ice nucleation: Interplay between surface morphology and hydrophobicity. Journal of the American Chemical Society 137(42), 13658-13669.

Forte, M., Iachetta, G., Tussellino, M., Carotenuto, R., Prisco, M., De Falco, M., Laforgia, V., Valiante, S., 2016. Polystyrene nanoparticles internalization in human gastric adenocarcinoma cells. Toxicology in Vitro 31126-136.

García-López, I., Arenas, L.F., Turek, T., Águeda, V.I., Garrido-Escudero, A., 2023. Mass transfer enhancement in electrochemical flow cells through 3D-printed biomimetic channels. Reaction Chemistry & Engineering 8(7), 1776-1784.

Geilfus, N., Munson, K., Sousa, J., Germanov, Y., Bhugaloo, S., Babb, D., Wang, F., 2019. Distribution and impacts of microplastic incorporation within sea ice. Marine Pollution Bulletin 145463-473.

Green, D.S., Boots, B., O'Connor, N.E., Thompson, R., 2017. Microplastics affect the ecological functioning of an important biogenic habitat. Environmental Science & Technology 51(1), 68-77.

Hall, D., Zvipriel, Oren, Y., Soffer, A., 1987. Purification of Aqueous Suspensions from Colloidal Particles by Electro-Adsorption on Porous Carbon Electrodes. Separation Science and Technology 22(2-3), 1017-1027.

Hashemi Safaei, S., Young, S., Samimi, Z., Parvizi, F., Shokrollahi, A., Baniamer, M., 2022. Technology development for the removal of Covid-19 pharmaceutical active compounds from water and wastewater: A review. Journal of Environmental Informatics 40(2), 141-156.

Hoffmann, L., Eggers, S.L., Allhusen, E., Katlein, C., Peeken, I., 2020. Interactions between the ice algae Fragillariopsis cylindrus and microplastics in sea ice. Environment International 139105697.

Hunke, E., Notz, D., Turner, A., Vancoppenolle, M., 2011. The multiphase physics of sea ice: a review for model developers. The Cryosphere 5(4), 989-1009.

Ito, M., Ohshima, K.I., Fukamachi, Y., Hirano, D., Mahoney, A.R., Jones, J., Takatsuka, T., Eicken, H., 2019. Favorable conditions for suspension freezing in an Arctic coastal polynya. Journal of Geophysical Research: Oceans 124(12), 8701-8719.

Iyer, S., Drushka, K., Rainville, L., 2021. Estimating turbulent kinetic energy dissipation rate using microstructure data from the ship-towed Surface Salinity Profiler. Journal of Atmospheric and Oceanic Technology 38(1), 77-89.

Jambeck, J.R., Geyer, R., Wilcox, C., Siegler, T.R., Perryman, M., Andrady, A., Narayan, R., Law, K.L., 2015. Plastic waste inputs from land into the ocean. Science 347(6223), 768-771.

Jańczuk, B., Białopiotrowicz, T., Wójcik, W., 1989. The components of surface tension of liquids and their usefulness in determinations of surface free energy of solids. Journal of Colloid and Interface Science 127(1), 59-66.

Jin, C., Zhao, W., Normani, S.D., Zhao, P., Emelko, M.B., 2017. Synergies of media surface roughness and ionic strength on particle deposition during filtration. Water Research 114286-295.

Johnston, M., 2017. Seasonal changes in the properties of first-year, second-year and multi-year ice. Cold Regions Science and Technology 14136-53.

Kanhai, L.D.K., Gardfeldt, K., Krumpen, T., Thompson, R.C., O'Connor, I., 2020. Microplastics in sea ice and seawater beneath ice floes from the Arctic Ocean. Scientific Reports 10(1), 1-11.

Karmakar, S., 2019. Particle size distribution and zeta potential based on dynamic light scattering: Techniques to characterize stability and surface charge distribution of charged colloids. Recent Trends Mater. Phys. Chem117-159.

Kelly, A., Lannuzel, D., Rodemann, T., Meiners, K., Auman, H., 2020. Microplastic contamination in east Antarctic sea ice. Marine Pollution Bulletin 154111130.

Kempama, E., Reimnitz, E., Barnes, P.W., 1989. Sea ice sediment entrainment and rafting in the Arctic. Journal of Sedimentary Research 59(2), 308-317.

Khadanga, M., Mishra, R., Sahu, B., 2022. Assessment of pollution and ecological risk index of heavy metals in the surface sediment of estuary and the coastal environment of Bay of Bengal. Journal of Environmental Informatics 39(1), 35-48.

Khan, N.A., Khan, A.H., López-Maldonado, E.A., Alam, S.S., López, J.R.L., Herrera, P.F.M., Mohamed, B.A., Mahmoud, A.E.D., Abutaleb, A., Singh, L., 2022. Microplastics: Occurrences, treatment methods, regulations and foreseen environmental impacts. Environmental Research 215114224.

Khatmullina, L., Isachenko, I., 2017. Settling velocity of microplastic particles of regular shapes. Marine Pollution Bulletin 114(2), 871-880.

Kholodov, V.A., Milanovskiy, E.Y., Konstantinov, A.I., Tyugai, Z.N., Yaroslavtseva, N.V., Perminova, I.V., 2018. Irreversible sorption of humic substances causes a decrease in wettability of clay surfaces as measured by a sessile drop contact angle method. Journal of Soils and Sediments 181327-1334.

Kim, S., Sin, A., Nam, H., Park, Y., Lee, H., Han, C., 2022. Advanced oxidation processes for microplastics degradation: A recent trend. Chemical Engineering Journal Advances 9100213.

Kim, S.K., Lee, H.J., Kim, J.S., Kang, S.H., Yang, E.J., Cho, K.H., Tian, Z., Andrady, A., 2021. Importance of seasonal sea ice in the western Arctic ocean to the Arctic and global microplastic budgets. Journal of Hazardous materials 418125971.

Kooi, M., Nes, E.H.v., Scheffer, M., Koelmans, A.A., 2017. Ups and downs in the ocean: effects of biofouling on vertical transport of microplastics. Environmental Science & Technology 51(14), 7963-7971.

Körber, C., Rau, G., Cosman, M., Cravalho, E., 1985. Interaction of particles and a moving ice-liquid interface. Journal of Crystal Growth 72(3), 649-662.

Koutnik, V.S., Leonard, J., Brar, J., Cao, S., Glasman, J.B., Cowger, W., Ravi, S., Mohanty, S.K., 2022. Transport of microplastics in stormwater treatment systems under freeze-thaw cycles: Critical role of plastic density. Water Research 222118950.

Kovalchuk, N., Starov, V., 2012. Aggregation in colloidal suspensions: Effect of colloidal forces and hydrodynamic interactions. Advances in Colloid and Interface Science 17999-106.

Kulovaara, M., 1996. Light-induced degradation of aquatic humic substances by simulated sunlight. International journal of environmental analytical chemistry 62(2), 85-95.

Kye, H., Kim, J., Ju, S., Lee, J., Lim, C., Yoon, Y., 2023. Microplastics in water systems: A review of their impacts on the environment and their potential hazards. Heliyon 9(3).

Lambley, H., Graeber, G., Vogt, R., Gaugler, L.C., Baumann, E., Schutzius, T.M., Poulikakos, D., 2023. Freezing-induced wetting transitions on superhydrophobic surfaces. Nature Physics1-7.

Lee, H., 2019. Effects of hydrophobic and hydrogen-bond interactions on the binding affinity of antifreeze proteins to specific ice planes. Journal of Molecular Graphics and Modelling 8748-55.

Li, M., He, L., Hsieh, L., Rong, H., Tong, M., 2023. Transport of plastic particles in natural porous media under freeze–thaw treatment: Effects of porous media property. Journal of Hazardous materials 442130084.

Li, Y., Wang, X., Fu, W., Xia, X., Liu, C., Min, J., Zhang, W., Crittenden, J.C., 2019. Interactions between nano/micro plastics and suspended sediment in water: Implications on aggregation and settling. Water Research 161486-495.

Lipp, G., Körber, C., Rau, G., 1990. Critical growth rates of advancing ice-water interfaces for particle encapsulation. Journal of Crystal Growth 99(1-4), 206-210.

Lissaneddine, A., Pons, M.N., Aziz, F., Ouazzani, N., Mandi, L., Mousset, E., 2022. A critical review on the electrosorption of organic compounds in aqueous effluent–Influencing factors and engineering considerations. Environmental Research 204112128.

Liu, F., Olesen, K.B., Borregaard, A.R., Vollertsen, J., 2019. Microplastics in urban and highway stormwater retention ponds. Science of the Total Environment 671992-1000.

Liu, J., Zhu, C., Liu, K., Jiang, Y., Song, Y., Francisco, J.S., Zeng, X.C., Wang, J., 2017. Distinct ice patterns on solid surfaces with various wettabilities. Proceedings of the National Academy of Sciences of the United States of America 114(43), 11285-11290.

Liu, Y., Shi, X., Zhang, S., Lu, J., Li, W., Sun, B., Zhao, S., Yao, D., Huotari, J., 2023. The spatial distribution and abundance of microplastics in lake waters and ice during ice-free and ice-covered periods. Environmental Pollution 323121268.

Lu, M., Gao, X., Liu, P., Tang, H., Wang, F., Ding, Y., Zhang, S., Yang, M., 2017. Photo-and thermo-oxidative aging of polypropylene filled with surface modified fumed nanosilica. Composites Communications 351-58.

Luo, H., Liu, C., He, D., Sun, J., Zhang, A., Li, J., Pan, X., 2022. Interactions between polypropylene microplastics (PP-MPs) and humic acid influenced by aging of MPs. Water Research 222118921.

Luo, Y., Gao, X., Tian, R., Li, H., 2018. Approach to estimation of hamaker constant as taking hofmeister effects into account. Journal of Physical Chemistry C 122(17), 9432-9440.

Lv, J., Chen, R., Wu, Z., Bai, Y., Song, H., Tian, C., Wang, M., Lin, Z., 2023. Freezing-induced microplastic degradation in an anoxic Fe (ii)-containing solution: the key role of Fe (iv) and· OH. Environmental Science: Nano 10(10), 2744-2753.

Malli, A., Corella-Puertas, E., Hajjar, C., Boulay, A.-M., 2022. Transport mechanisms and fate of microplastics in estuarine compartments: A review. Marine Pollution Bulletin 177113553.

Mei, B.A., Munteshari, O., Lau, J., Dunn, B., Pilon, L., 2018. Physical interpretations of Nyquist plots for EDLC electrodes and devices. Journal of Physical Chemistry C 122(1), 194-206.

Menzel, T., Meides, N., Mauel, A., Mansfeld, U., Kretschmer, W., Kuhn, M., Herzig, E.M., Altstädt, V., Strohriegl, P., Senker, J., 2022. Degradation of low-density polyethylene to nanoplastic particles by accelerated weathering. Science of the Total Environment 826154035.

Mintenig, S.M., Int Veen, I., Löder, M.G., Primpke, S., Gerdts, G., 2017. Identification of microplastic in effluents of waste water treatment plants using focal plane array-based micro-Fourier-transform infrared imaging. Water Research 108365-372.

Mountford, A.S., Morales Maqueda, M.A., 2021. Modeling the accumulation and transport of microplastics by sea ice. Journal of Geophysical Research: Oceans 126(2), e2020JC016826.

Obbard, R.W., 2018. Microplastics in polar regions: The role of long range transport. Current Opinion in Environmental Science & Health 124-29.

Owens, D.K., Wendt, R., 1969. Estimation of the surface free energy of polymers. Journal of Applied Polymer Science 13(8), 1741-1747.

Oziel, L., Massicotte, P., Randelhoff, A., Ferland, J., Vladoiu, A., Lacour, L., Galindo, V., Lambert-Girard, S., Dumont, D., Cuypers, Y., 2019. Environmental factors influencing the seasonal dynamics of spring algal blooms in and beneath sea ice in western Baffin Bay. Elementa: Science of the Anthropocene 7.

Paço, A., Duarte, K., da Costa, J.P., Santos, P.S., Pereira, R., Pereira, M., Freitas, A.C., Duarte, A.C., Rocha-Santos, T.A., 2017. Biodegradation of polyethylene microplastics by the marine fungus Zalerion maritimum. Science of the Total Environment 58610-15.

Peeken, I., Primpke, S., Beyer, B., Gütermann, J., Katlein, C., Krumpen, T., Bergmann, M., Hehemann, L., Gerdts, G., 2018. Arctic sea ice is an important temporal sink and means of transport for microplastic. Nature Communications 9(1), 1-12.

Perovich, D.K., Richter-Menge, J.A., 2009. Loss of sea ice in the Arctic. Annual Review of Marine Science 1417-441.

Perpetuo, L., Ferreira, R., Thongboonkerd, V., Guedes, S., Amado, F., Vitorino, R., 2022. Urinary exosomes: diagnostic impact with a bioinformatic approach. Adv Clin Chem 11169-99.

Petrich, C., Eicken, H., 2010. Growth, structure and properties of sea ice. Sea ice 223-77.

Peydayesh, M., Suta, T., Usuelli, M., Handschin, S., Canelli, G., Bagnani, M., Mezzenga, R., 2021. Sustainable removal of microplastics and natural organic matter from water by coagulation–flocculation with protein amyloid fibrils. Environmental Science & Technology 55(13), 8848-8858.

Pfirman, S., Eicken, H., Bauch, D., Weeks, W., 1995. The potential transport of pollutants by Arctic sea ice. Science of the Total Environment 159(2-3), 129-146.

Philippe, A., Schaumann, G.E., 2014. Interactions of dissolved organic matter with natural and engineered inorganic colloids: a review. Environmental Science & Technology 48(16), 8946-8962.

Pradel, A., Ferreres, S., Veclin, C., El Hadri, H., Gautier, M., Grassl, B., Gigault, J., 2021a. Stabilization of fragmental polystyrene nanoplastic by natural organic matter: insight into mechanisms. ACS ES&T Water 1(5), 1198-1208.

Pradel, A., Maud, G., Dominique, B., Julien, G., 2021b. Micro-and nanoplastic transfer in freezing saltwater: implications for their fate in polar waters. Environmental Science: Processes & Impacts 23(11), 1759-1770.

Prata, J.C., 2018. Microplastics in wastewater: State of the knowledge on sources, fate and solutions. Marine Pollution Bulletin 129(1), 262-265.

Qiu, X., Ma, S., Zhang, J., Fang, L., Guo, X., Zhu, L., 2022. Dissolved organic matter promotes the aging process of polystyrene microplastics under dark and ultraviolet light conditions: the crucial role of reactive oxygen species. Environmental Science & Technology 56(14), 10149-10160.

Rajala, K., Grönfors, O., Hesampour, M., Mikola, A., 2020. Removal of microplastics from secondary wastewater treatment plant effluent by coagulation/flocculation with iron, aluminum and polyamine-based chemicals. Water Research 183116045.

Ruiz, J.A.R., Pedros, M., Tallon, J.M., Dumon, M., 2011. Micro and nano cellular amorphous polymers (PMMA, PS) in supercritical CO2 assisted by nanostructured CO2-philic block copolymers–one step foaming process. Journal of Supercritical Fluids 58(1), 168-176.

Ryntz, R.A., Yaneff, P.V., 2003. Coatings of polymers and plastics. CRC Press.

Salehan, P., Ensafi, A.A., Andikaey, Z., Rezaei, B., 2023. H-CoNiSe2/NC dodecahedral hollow structures for high-performance supercapacitors. Scientific Reports 13(1), 2070.

Schuster-Wallace, C., Dickson-Anderson, S., Papalexiou, S., Ganzouri, A.E., 2022. Design and application of the tank simulation model (TSM): Assessing the ability of rainwater harvesting to meet domestic water demand. Journal of Environmental Informatics 40(1), 16-29.

Serreze, M.C., McLaren, A.S., Barry, R.G., 1989. Seasonal variations of sea ice motion in the Transpolar Drift Stream. Geophysical Research Letters 16(8), 811-814.

Sharma, V.K., Ma, X., Guo, B., Zhang, K., 2021. Environmental factors-mediated behavior of microplastics and nanoplastics in water: a review. Chemosphere 271129597.

Shi, X., Chen, Z., Liu, X., Wei, W., Ni, B.-J., 2022. The photochemical behaviors of microplastics through the lens of reactive oxygen species: Photolysis mechanisms and enhancing photo-transformation of pollutants. Science of the Total Environment 846157498.

Smedsrud, L.H., 2001. Frazil-ice entrainment of sediment: large-tank laboratory experiments. Journal of Glaciology 47(158), 461-471.

Smedsrud, L.H., 2002. A model for entrainment of sediment into sea ice by aggregation between frazil-ice crystals and sediment grains. Journal of Glaciology 48(160), 51-61.

Sommer, F., Dietze, V., Baum, A., Sauer, J., Gilge, S., Maschowski, C., Gieré, R., 2018. Tire abrasion as a major source of microplastics in the environment. Aerosol and Air Quality Research 18(8), 2014-2028.

Stevenson, F.J., 1994. Humus chemistry: genesis, composition, reactions, 2nd Edition ed. John Wiley & Sons.

Sun, J., Dai, X., Wang, Q., Van Loosdrecht, M.C., Ni, B.-J., 2019. Microplastics in wastewater treatment plants: Detection, occurrence and removal. Water Research 15221-37.

Sun, X., Liang, J., Zhu, M., Zhao, Y., Zhang, B., 2018. Microplastics in seawater and zooplankton from the Yellow Sea. Environmental Pollution 242585-595.

Swart, B., Pihlajamäki, A., Chew, Y.J., Wenk, J., 2022. Microbubble-microplastic interactions in batch air flotation. Chemical Engineering Journal 449137866.

Talvitie, J., Mikola, A., Setälä, O., Heinonen, M., Koistinen, A., 2017. How well is microlitter purified from wastewater?–A detailed study on the stepwise removal of microlitter in a tertiary level wastewater treatment plant. Water Research 109164-172.

Telesh, I.V., Khlebovich, V.V., 2010. Principal processes within the estuarine salinity gradient: a review. Marine Pollution Bulletin 61(4-6), 149-155.

Tian, C., Lv, J., Zhang, W., Wang, H., Chao, J., Chai, L., Lin, Z., 2022. Accelerated degradation of microplastics at the liquid interface of ice crystals in frozen aqueous solutions. Angewandte Chemie International Edition 61(31), e202206947.

Tobias, H., Taragan, E., Oren, Y., Soffer, A., 1987. Removal of suspended alumina particles from heavy water by electroadsorption on fibrous carbon electrodes. Nuclear Technology 77(1), 46-49.

Torabi, E., Taheri, E., Pourzamani, H., Fatehizadeh, A., Rtimi, S., Aminabhavi, T.M., 2023. Electrosorption of phenolic compounds by carbon sheet electrode from zinc chloride functionalized activated carbon from pomegranate husk. Chemical Engineering Journal 455140800.

Tsai, C.J., Pui, D.Y., Liu, B.Y., 1991. Elastic flattening and particle adhesion. Aerosol Science and Technology 15(4), 239-255.

Turner, A.K., Hunke, E.C., Bitz, C.M., 2013. Two modes of sea-ice gravity drainage: A parameterization for large-scale modeling. Journal of Geophysical Research, Oceans 118(5), 2279-2294.

Urdiales, C., Sandoval, M.P., Escudey, M., Pizarro, C., Knicker, H., Reyes-Bozo, L., Antilén, M., 2018. Surfactant properties of humic acids extracted from volcanic soils and their applicability in mineral flotation processes. Journal of Environmental Management 227117-123.

Ushio, S., Wakatsuchi, M., 1993. A laboratory study on supercooling and frazil ice production processes in winter coastal polynyas. Journal of Geophysical Research: Oceans 98(C11), 20321-20328.

Voermans, J., Babanin, A., Thomson, J., Smith, M., Shen, H., 2019. Wave attenuation by sea ice turbulence. Geophysical Research Letters 46(12), 6796-6803.

Volikov, A.B., Kholodov, V.A., Kulikova, N.A., Philippova, O.I., Ponomarenko, S.A., Lasareva, E.V., Parfyonova, A.M., Hatfield, K., Perminova, I.V., 2016. Silanized humic substances act as hydrophobic modifiers of soil separates inducing formation of water-stable aggregates in soils. Catena 137229-236.

von Friesen, L.W., Granberg, M.E., Pavlova, O., Magnusson, K., Hassellöv, M., Gabrielsen, G.W., 2020. Summer sea ice melt and wastewater are important local sources of microlitter to Svalbard waters. Environment International 139105511.

Von Wandruszka, R., 2000. Humic acids: Their detergent qualities and potential uses in pollution remediation. Geochemical Transactions 1(1), 1-6.

Waldschläger, K., Schüttrumpf, H., 2019. Effects of particle properties on the settling and rise velocities of microplastics in freshwater under laboratory conditions. Environmental Science & Technology 53(4), 1958-1966.

Wang, J., Guo, X., Xue, J., 2021a. Biofilm-developed microplastics as vectors of pollutants in aquatic environments. Environmental Science & Technology 55(19), 12780-12790.

Wang, Y., Li, Y.n., Tian, L., Ju, L., Liu, Y., 2021b. The removal efficiency and mechanism of microplastic enhancement by positive modification dissolved air flotation. Water Environment Research 93(5), 693-702.

Wang, Y., Xu, L., Chen, H., Zhang, M., 2022a. Retention and transport behavior of microplastic particles in water-saturated porous media. Science of the Total Environment 808152154.

Wang, Z., An, C., Chen, X., Lee, K., Zhang, B., Feng, Q., 2021c. Disposable masks release microplastics to the aqueous environment with exacerbation by natural weathering. Journal of Hazardous materials 417126036.

Wang, Z., An, C., Lee, K., Chen, X., Zhang, B., Yin, J., Feng, Q., 2022b. Physicochemical change and microparticle release from disposable gloves in the aqueous environment impacted by accelerated weathering. Science of the Total Environment 832154986.

Wang, Z., An, C., Lee, K., Feng, Q., 2023. Overlooked Role of Bulk Nanobubbles in the Alteration and Motion of Microplastics in the Ocean Environment. Environmental Science & Technology 57(30), 11289-11299.

Wang, Z., Sedighi, M., Lea-Langton, A., 2020. Filtration of microplastic spheres by biochar: removal efficiency and immobilisation mechanisms. Water Research 184116165.

Wang, Z., Wang, P., Wang, C., Zhang, S., Hou, J., Ao, Y., 2022c. Statistical optimization of microcystis growth and microcystin production in natural phytoplankton community using microcosm bioassays. Journal of Environmental Informatics 40(1), 1-15.

Wazne, M., Mermillod-Blondin, F., Vallier, M., Hervant, F., Dumet, A., Nel, H.A., Kukkola, A., Krause, S., Simon, L., 2023. Microplastics in freshwater sediments impact the role of a main bioturbator in ecosystem functioning. Environmental Science & Technology 57(8), 3042-3052.

Weithmann, N., Möller, J.N., Löder, M.G., Piehl, S., Laforsch, C., Freitag, R., 2018. Organic fertilizer as a vehicle for the entry of microplastic into the environment. Science Advances 4(4), eaap8060.

Wu, L.M., Tong, D.S., Zhao, L.Z., Yu, W.H., Zhou, C.H., Wang, H., 2014. Fourier transform infrared spectroscopy analysis for hydrothermal transformation of microcrystalline cellulose on montmorillonite. Applied Clay Science 9574-82.

Xie, S., Ren, W., Qiao, C., Tong, K., Sun, J., Zhang, M., Liu, X., Zhang, Z., 2018. An electrochemical adsorption method for the reuse of waste water-based drilling fluids. Natural Gas Industry B 5(5), 508-512.

Yang, M., Zhang, B., Xin, X., Liu, B., Zhu, Z., Dong, G., Zhao, Y., Lee, K., Chen, B., 2022a. Microplastic-oil-dispersant agglomerates in the marine environment: Formation mechanism and impact on oil dispersion. Journal of Hazardous materials 426127825.

Yang, W., Zhou, M., Ma, L., 2021. A continuous flow-through system with integration of electrosorption and peroxi-coagulation for efficient removal of organics. Chemosphere 274129983.

Yang, X., An, C., Feng, Q., Boufadel, M., Ji, W., 2022b. Aggregation of microplastics and clay particles in the nearshore environment: Characteristics, influencing factors, and implications. Water Research 224119077.

Yao, R., Yang, J., Wang, X., Zhao, Y., Li, H., Gao, P., Xie, W., Zhang, X., 2022. Improving soil salinity simulation by assimilating electromagnetic induction data into HYDRUS model using ensemble Kalman filter. Journal of Environmental Informatics 39(2), 81-96.

Yemmou, M., Brierre, A., Azouni, M., 1991. Rejection and capture of solid particles by ice. Advances in Space Research 11(7), 327-330.

Yuan, F., Li, X., Yu, W., Du, J., Wang, D., Yang, X., Zhou, C., Wang, J., Yuan, H., 2022. A high-efficiency mini-hydrocyclone for microplastic separation from water via air flotation. Journal of Water Process Engineering 49103084.

Yuan, Y., Teja, A.S., 2011. Quantification of specific interactions between CO2 and the carbonyl group in polymers via ATR-FTIR measurements. The Journal of Supercritical Fluids 56(2), 208-212.

Zhang, B., Xu, D., Wan, X., Wu, Y., Liu, X., Gao, B., 2022. Comparative analysis of microplastic organization and pollution risk before and after thawing in an urban river in Beijing, China. Science of the Total Environment 828154268.

Zhang, D., Cui, Y., Zhou, H., Jin, C., Yu, X., Xu, Y., Li, Y., Zhang, C., 2020. Microplastic pollution in water, sediment, and fish from artificial reefs around the Ma'an Archipelago, Shengsi, China. Science of the Total Environment 703134768.

Zhang, W., Zhang, S., Wang, J., Wang, Y., Mu, J., Wang, P., Lin, X., Ma, D., 2017. Microplastic pollution in the surface waters of the Bohai Sea, China. Environmental Pollution 231541-548.

Zhang, Y., Jiang, H., Bian, K., Wang, H., Wang, C., 2021. Is froth flotation a potential scheme for microplastics removal? Analysis on flotation kinetics and surface characteristics. Science of the Total Environment 792148345.

Zhao, N., Li, M., Gong, H., Bai, H., 2020. Controlling ice formation on gradient wettability surface for high-performance bioinspired materials. Science Advances 6(31), eabb4712.

Zhou, J., Zhang, Y., Balda, M., Presser, V., Kopinke, F.D., Georgi, A., 2022. Electro-assisted removal of polar and ionic organic compounds from water using activated carbon felts. Chemical Engineering Journal 433133544.